PNNL-16628

Pacific Northwest
National Laboratory
Operated by Battelle for the
U.S. Department of Energy

Nondestructive and Destructive Examination Studies on Removed from-Service Control Rod Drive Mechanism Penetrations

S. E. Cumblidge
S. R. Doctor
G. J. Schuster
R. V. Harris
S. L. Crawford
R. J. Seffens
M. B. Toloczko
S. M. Bruemmer

May 2007

Prepared for the U.S. Department of Energy
under Contract DE-AC05-76RL01830

DISCLAIMER

PACIFIC NORTHWEST NATIONAL LABORATORY
operated by
BATTELLE
for the
UNITED STATES DEPARTMENT OF ENERGY
under Contract DE-AC05-76RL01830

Printed in the United States of America

Available to DOE and DOE contractors from the
Office of Scientific and Technical Information,
P.O. Box 62, Oak Ridge, TN 37831-0062;
ph: (865) 576-8401
fax: (865) 576-5728
email: reports@adonis.osti.gov

Available to the public from the National Technical Information Service,
U.S. Department of Commerce, 5285 Port Royal Rd., Springfield, VA 22161
ph: (800) 553-6847
fax: (703) 605-6900
email: orders@ntis.fedworld.gov
online ordering: http://www.ntis.gov/ordering.htm

This document was printed on recycled paper.
(8/00)

PNNL-16628

Nondestructive and Destructive Examination Studies on Removed-from-Service Control Rod Drive Mechanism Penetrations

S. E. Cumblidge
S. R. Doctor
G. J. Schuster
R. V. Harris
S. L. Crawford
R. J. Seffens
M. B. Toloczko
S. M. Bruemmer

May 2007

Prepared for the
U.S. Nuclear Regulatory Commission
Division of Fuel, Engineering and Radiological Research
Office of Nuclear Regulatory Research
under U.S. Department of Energy
Contract DE-AC05-76RL01830

Pacific Northwest National Laboratory
Richland, Washington 99352

Abstract

Studies conducted at the Pacific Northwest National Laboratory (PNNL) in Richland, Washington, focused on assessing the effectiveness of nondestructive examination (NDE) techniques for inspecting control rod drive mechanism (CRDM) nozzles and J-groove weldments. The primary objectives of this work are to provide information to the U.S. Nuclear Regulatory Commission (NRC) on the effectiveness of NDE methods as related to the in-service inspection of CRDM nozzles and J-groove weldments and to enhance the knowledge base of primary water stress corrosion cracking (PWSCC) through destructive characterization of the CRDM assemblies.

Two CRDM assemblies were removed from service, decontaminated, and then used in a series of NDE and destructive examination (DE) measurements; this report addresses the following questions: 1) What did each NDE technique detect? 2) What did each NDE technique miss? 3) How accurately did each NDE technique characterize the detected flaws? 4) Why did the NDE techniques perform or not perform? Two CRDM assemblies including the CRDM nozzle, the J-groove weld, buttering, and a portion of the ferritic head material were selected for this study. This report focuses on a CRDM assembly that contained suspected PWSCC, based on in-service inspection data and through-wall leakage.

The NDE measurements used to examine the CRDM assembly followed standard industry techniques for conducting in-service inspections of CRDM nozzles and the crown of the J-groove welds and buttering. These techniques included eddy current testing (ET), time-of-flight diffraction ultrasound, and penetrant testing. In addition, laboratory-based NDE methods were employed to conduct inspections of the CRDM assembly with particular emphasis on inspecting the J-groove weld and buttering. These techniques included volumetric ultrasonic inspection of the J-groove weld metal and visual testing via replicant material of the J-groove weld. The results from these NDE studies were used to guide the development of the destructive characterization plan.

The NDE studies found several crack-like indications. The NDE and DE studies determined that one of these was a through-weld, radially oriented PWSCC crack in the wetted surface of the J-groove weld, located at the transition point between the weld and the buttering. The crack was 6 mm long on the surface and quickly grew to 25 mm long at a depth of 8 mm, covering the length of the weld between the penetration tube and the carbon steel.

The NDE studies found that only ET was able to detect the through-weld crack. The crack was oriented poorly for the ultrasonic testing and was too tight for accurate dye penetrant testing or visual testing. The ET voltage response of the through-wall crack was 30% of the response from a deep electrical discharge machined notch.

Destructive examination showed the crack is PWSCC and that it initiated on the wetted surface, grew and expanded through the weld metal, and exited into the annulus. The crack was branched and discontinuous along its length.

Summary

Studies conducted at the Pacific Northwest National Laboratory (PNNL) in Richland, Washington, focused on assessing the effectiveness of nondestructive examination (NDE) techniques for inspecting control rod drive mechanism (CRDM) nozzles and J-groove weldments. The primary objectives of this work are to provide information to the U.S. Nuclear Regulatory Commission (NRC) on the effectiveness of NDE methods as related to the in-service inspection of CRDM nozzles and J-groove weldments and to enhance the knowledge base of primary water stress corrosion cracking (PWSCC) through destructive characterization of the CRDM assemblies. Two CRDM assemblies were removed from service, decontaminated, and then used in a series of NDE and destructive examination (DE) measurements; this report addresses the following questions: 1) What did each NDE technique detect? 2) What did each NDE technique miss? 3) How accurately did each NDE technique characterize the detected flaws? 4) Why did the NDE techniques perform or not perform? 5) What was the type and extent of the degradation present in the CRDMs? Two CRDM assemblies including the CRDM nozzle, the J-groove weld, buttering, and a portion of the ferritic head material were selected for this study. This report focuses on a CRDM assembly that contained suspected PWSCC, based on in-service inspection data and through-wall leakage.

Nondestructive Testing of CRDM Nozzle 59

The penetration tube of Nozzle 59 was examined using eddy current testing (ET), time-of-flight diffraction (TOFD), and visual testing (VT) via Microset replicant. One would expect that a crack that penetrates into the tube from the inner surface should show up in each NDE method, while innocuous features are less likely to appear on all three techniques. The examinations of the penetration tube yielded some areas of interest but no confirmed cracking. The penetration tube was considered to be a lower priority than the J-groove weld of Nozzle 31.

The J-groove weld and buttering were inspected volumetrically using ultrasound, and the surface was examined using visual testing via replicant. No large crack-like indications were found in the J-groove weld using direct VT and VT using replicant, and the immersion ultrasonic testing (UT) indications appear to be embedded welding defects. The Microset replica and VT did reveal several small crack-like indications, but no indication was longer than 1 cm.

Although a series of UT signals coincident with the locations of the small cracks was found via VT at 90–135 degrees, the UT data in this area look a great deal like a string of fabrication flaws. This area is the most interesting for possible future DE work, but with no confirmed cracking in the area and no confirmation of nozzle leakage based on boric acid deposits, this weld was designated a lower priority than the weld on Nozzle 31.

Nondestructive Testing of CRDM Nozzle 31

The NDE examinations on the penetration tube of Nozzle 31 found the penetration tube to be free of significant surface-breaking defects. The penetration tube in Nozzle 31 contained no strong ET indications; only weak (<1-V) scratch-like indications were detectable. The only TOFD indications that

were found were determined to be embedded in the tube and not surface-breaking, as no break in the lateral wave was seen.

As TOFD and ET agreed that the penetration tube was not likely to be cracked, the penetration tube of Nozzle 31 was considered the lowest priority for DE. This is interesting, as Nozzle 31 was considered to be leaking based on the presence of boric acid on the pressure vessel head. If Nozzle 31 had leaked, it must have done so through the J-groove weld.

The J-groove weld of Nozzle 31 was found to be cracked by bare metal VT, ET, and PT. The cracking was not detectable using the volumetric UT inspection, but UT inspection did reveal what appeared to be areas with fabrication flaws. Sixteen crack-like indications were found by ET in four distinct areas. Seven small crack-like indications were found clustered around 60 degrees; five were found clustered around 150 degrees; three were found clustered around 210 degrees; and one was found at 255 degrees. The ET indications at 200 and 225 degrees were confirmed using PT and bare metal VT. It is not known how deep these crack-like indications penetrate into the weld, however. Future work will involve destructively analyzing these cracks to determine their depth.

A crack-like indication was found using both PT and ET at 215 degrees. This indication is unusual for two reasons—the indication is circumferential, not axial like the other crack-like indications, and the ET response is relatively weak at 1.8 V with a 15 dB gain setting. Because of this indication, all ET responses larger than 1.8 V were considered crack-like for this analysis.

Destructive Testing of CRDM Nozzle 31

Cutting Nozzle 31 revealed the through-weld crack to start at 155 degrees on the wetted surface at the weld-buttering interface and end at 135 degrees above the triple point. The cutting of this section also revealed two nearby cracks that had penetrated 8 mm into the material.

The metallographic characterization of the serial sections effectively mapped the cracks from the their initiation in Alloy 182 weld metal on the pressurized water reactor (PWR) primary water surface to their end, either when intersecting with low-alloy steel, entering the Alloy 600 CRDM tube, or exiting at the interference-fit gap above the J-groove weld. Cracking in Alloy 182 weld metal is interdendritic or intergranular and clearly has propagated because of stress corrosion cracking (SCC). No evidence for hot cracking in the weld was observed. Initiation appears to result from SCC near the fusion line between the butter passes and the J-groove weld. Surface damage and defects in the near-surface region may have promoted crack nucleation, but additional examinations will be needed to determine this.

The main crack is observed at a length of ~6 mm on the PWR primary water surface and expands to a lateral length of ~25 mm across the Alloy 182 weld metal within 8 millimeters below the surface. At this depth, the crack has already reached the low-alloy steel plate material on one side and remains in the alloy 182 J-groove weld on the other. The main crack path length from the PWR primary water surface initiation site to the gap exit surface is estimated at ~25 mm. Based on laboratory tests in simulated PWR primary water, typical crack-growth rates can range from $\sim 3 \times 10^{-8}$ to $\sim 3 \times 10^{-7}$ mm/s for as-welded Alloy 182 at 290 to 320°C. This results in an estimated time of ~2.5 to 25 years for the crack to propagate through-wall after initiation. Because crack initiation normally accounts for some important fraction of life and through-wall cracking occurred at some time before its full 20-year life, the SCC crack-growth

rate experienced in service was probably closer to the high end for measured propagation rates in the laboratory.

Conclusions

PNNL found, removed, and destructively characterized a through-weld PWSCC crack in the J-groove weld of North Anna 2 CRDM Nozzle 31. The purpose of this report is to provide this information quickly because of the importance of this issue. A full NUREG/CR with additional work will be published in FY 08.

- Visual testing via replicant and high-resolution photography was ineffective at finding the cracks because the cracks were very tight and short, and the surface conditions were not conducive to an effective visual test. It is possible that the replicant would have produced better results if the replicant had been examined using scanning electron microscopy.

- Bare metal visual testing via high-resolution photography was ineffective at finding most of the cracks because the geometry prevented a complete inspection, the surface conditions were poor, and the cracks were both very short and very tight. The through-weld crack was not clearly visible on the wetted surface of the J-groove weld even when placed in an optical microscope. Bare metal VT was useful in characterizing the crack-like indications found at 200 and 225 degrees.

- Volumetric inspection of the J-groove weld using zero-degree ultrasound of frequencies ranging from 5 MHz to 500 kHz found many fabrication flaws but was not able to detect the through-weld crack as the crack was axially oriented and presented almost no surface area to the ultrasonic beam.

- Penetrant testing was ineffective at finding the through-weld crack because the crack was too tight to allow the penetrant dye into the crack in sufficient amounts to produce a visible indication. Penetrant testing was useful in finding other crack-like indications and in following up the visual testing via replicant.

- Eddy current testing was able to detect the through-weld crack, all crack-like indications detected using PT and verified with VT, and others that were only detectable with ET. Eddy current testing was the most useful NDE technique for finding PWSCC on the J-groove weld and showed much higher sensitivity than any of the other NDE techniques.

- It would be very useful for a volumetric technique, such as TOFD, to be developed and deployed on the J-groove weld to verify ET results, as currently only ET provides good sensitivity for inspecting the J-groove weld metal but ET is incapable of depth-sizing flaws.

- A detailed characterization of ET noise levels and ET responses to fabrication flaws in J-groove welds would be helpful in discriminating between the possibly small and low-voltage, service-induced PWSCC and innocuous indications.

Acknowledgments

The work described in this report was sponsored by the U.S. Nuclear Regulatory Commission under NRC Job Code Numbers Y6867, Y6534, and N6329. Mr. Wallace Norris, Ms. Carol E. Moyer, and Iouri Prokofiev were the NRC program monitors. Thanks also goes to William Cullen for his support and ideas.

This work was performed in cooperation with the Electric Power Research Institute. The CRDMs were cut from the pressure vessel head by EPRI, important decontamination equipment was paid for by EPRI, and the CRDMs are to be disposed of by EPRI as well. Thanks go to Al Aluwhalia and Robert Barnes for their work in making this project a success.

Abbreviations, Acronyms, and Initialisms

BSE	backscatter-electron
CCW	counterclockwise
COD	crack opening dimension
CRDM	control rod drive mechanism
DE	destructive evaluation
dpm	decays per minute
EDM	electrical discharge machined
EPRI	Electric Power Research Institute
ET	eddy current testing
ID	inner diameter
IDSCC	interdendritic stress corrosion cracking
MDA	minimum detectable activity
NDE	nondestructive evaluation
NRC	Nuclear Regulatory Commission
OD	outer diameter
PNNL	Pacific Northwest National Laboratory
PT	penetrant testing
PV	Pressure Vessel
PWR	pressurized water reactor
PWSCC	primary water stress corrosion cracking
RPL	Radiochemical Processing Laboratory
RPV	reactor pressure vessel
SAFT	synthetic aperture focusing technique
SCC	stress-corrosion cracking
SEM	scanning electron microscopy
TOF	Time of Flight
TOFD	time-of-flight diffraction
UT	Ultrasonic Testing
VT	visual testing

Contents

Figures

Tables

1.0 Introduction

Significant degradation has been found in welded assemblies that contain nickel-based alloys (Buisine et al. 1993; Embring and Pers-Anderson 1994; Faidy et al. 1994; Champigny et al. 2002; Lang 2003). Control rod drive mechanism (CRDM) nozzle assemblies with primary water stress corrosion cracking (PWSCC) have been identified and removed from service in light water reactors. Some of these CRDM nozzle assemblies are being studied at the Pacific Northwest National Laboratory (PNNL) in Richland, Washington.

Figure 1.1 is a diagram of a CRDM penetration-nozzle assembly showing the pressure vessel head, the penetration tube, and the J-groove weld. A description of these product forms can be found in Doctor et al. (2004). Most of the interface between the penetration tube and the vessel head is a simple interference fit and is not watertight. When a pressurized water reactor (PWR) is at operating pressures and temperatures, the pressure vessel head is slightly deformed, further opening the interference fit in some regions. The only barriers between the primary coolant and the outside are the J-groove weld, buttering, and the penetration tube above the weld. Any cracks that propagate through either of these sections can lead to leakage.

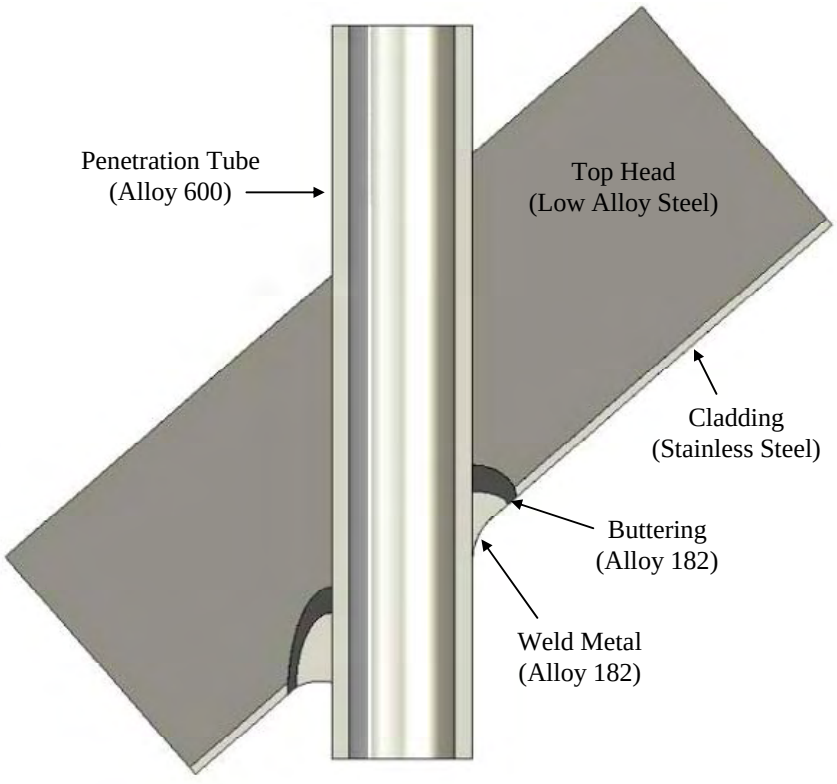

Figure 1.1. Control Rod Drive Mechanism Penetration-Nozzle Assembly

One objective of this work is to provide information to the U.S. Nuclear Regulatory Commission (NRC) on the effectiveness of NDE methods as related to the in-service inspection of CRDM nozzles and J-groove welds. The selected NDE measurements follow standard industry techniques for conducting in-service inspections of CRDM nozzles and the crown of the J-groove welds and buttering. In addition, laboratory-based NDE methods were employed to conduct inspections of the CRDM assemblies, with particular emphasis on inspecting the J-groove weld and buttering. Two CRDM assemblies that were removed from the discarded North Anna 2 reactor pressure vessel (RPV) head were selected for this study. One CRDM, Nozzle 31, contained suspected PWSCC, based on in-service inspection data and through-wall leakage; the other, Nozzle 59, contained evidence suggesting through-wall leakage, but this was unconfirmed by the in-service inspection data.

A secondary objective is to enhance the knowledge base for PWSCC through destructive characterization of the CRDM assemblies. Project efforts used the results from the NDE studies to guide the destructive examination (DE) of the CRDMs. The purpose of the destructive analysis was to reveal the flaw morphology compared with NDE responses, to determine what each NDE method detected or missed, and how accurately each NDE technique characterized the detected flaws.

Figure 1.2 shows the program concept. Nondestructive evaluation will be made of the surfaces and volumes for the various product forms in the CRDM nozzle assemblies. Nickel-based alloy product forms are the forms that typically contain PWSCC. Four nondestructive testing modalities were used at PNNL on two CRDM nozzle assemblies removed from service—eddy current (ET), time-of-flight diffraction (TOFD), immersion ultrasonic testing (UT), and visual testing (VT). The NDE inspections were conducted in a laboratory environment using very high sensitivity to optimize flaw detection but were not performed to meet existing codes and standards.

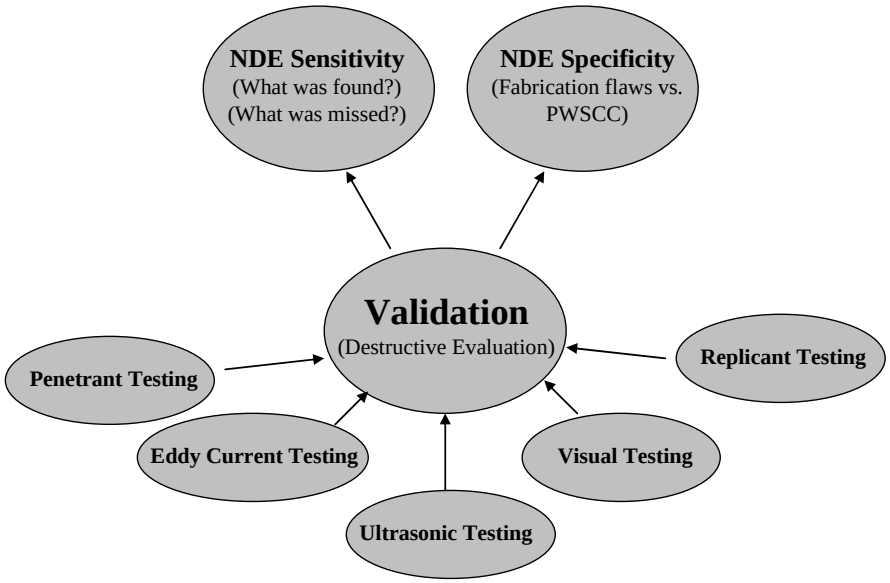

Figure 1.2. NDE Studies of CRDM Nozzle Assemblies Removed from Service

The NDE data from all of the inspections were combined or fused into an assessment of degradation. This assessment was used to guide the development of a DE plan with subsequent sectioning and metallurgical study of the two CRDM nozzle assemblies.

Metallographic techniques, including micro-polishing and etching, were used on some materials removed from the two CRDM nozzle assemblies. Also, photographs and micrographs from an optical microscope were combined with electron images of exposed degradation from a scanning electron microscope (SEM). Atomic elemental composition of PWSCC was performed using the x-ray spectrographic analysis that is provided by the SEM machine. This work was performed for the purpose of determining the "true state" of any fabrication flaws, conditions, and degradation to contribute to the knowledge base of PWSCC, especially its morphology and location.

During the DE, the location of degradation was recorded in the coordinate system used by the NDE inspections. These data were combined with images of the NDE responses. The purpose of this portion of the project was to quantify the sensitivity and specificity of the NDE to the shape and form of the degradation.

This work is being conducted as a collaborative effort between the NRC and the Electric Power Research Institute (EPRI), which provided the North Anna 2 CRDMs for these studies. Figure 1.3 shows a CRDM penetration-nozzle assembly as received at PNNL after removal from the North Anna 2 reactor vessel head, wrapped, bolted, and strapped to the bottom of a shipping container. The outer wrapper for the assembly is taped to help prevent the spread of radioactive contamination. The portion of the CRDM nozzle assembly that would be above the vessel's top head is shown on the left in the photograph and resting on the lumber portion of the shipping fixture. On the right side of the photograph is a portion of the vessel's top head, flame-cut from its location and surrounding a potentially degraded CRDM nozzle weldment.

In Figure 1.4, a CRDM nozzle assembly is shown being lifted from the container in which it was shipped to PNNL. The assembly is surrounded by additional wrapping to prevent escape of radioactive contamination that may have been dislodged during transport to PNNL facilities. The staff member shown is assisting by guiding the CRDM as it is lifted by an overhead crane (not shown).

This report documents work to date on the NDE of CRDMs removed from service. Section 2 describes the decontamination activities at PNNL and shows a CRDM penetration-nozzle assembly prepared for removal of its radioactive oxide layer. The NDE probes and measurements used for the inspection of CRDM penetration assemblies and mapping of degradation are described in Section 3. The pre-inspection testing done using calibration pieces is described in Section 4. The results of the NDE examinations are described in Section 5. Section 6 details the process and results for the DE of CRDM 31. A discussion of all results is provided in Section 7, and conclusions are presented in Section 8.

Figure 1.3. CRDM Penetration-Nozzle Assembly As Received at PNNL

Figure 1.4. CRDM Nozzle Assembly Being Removed from Shipping Container

2.0 Decontamination of Control Rod Drive Mechanism Nozzle Assemblies

Before the CRDM penetration-nozzle assemblies could be inspected by the NDE techniques, the assemblies needed to be decontaminated to minimize radiation exposure for PNNL personnel. Figure 2.1 shows a CRDM penetration-nozzle assembly in a glove box. The flame-cut surface of the top head of the vessel is shown after being painted red to secure the remaining small amounts of contamination. The CRDM penetration tube that extends above the vessel top head can be seen clearly. This portion of the assembly is not wetted by the reactor primary coolant water and is largely free of radioactive contamination. The wetted surfaces of the inside of the top head and the penetration tube are coated with a highly radioactive, hard oxide layer. PNNL decontaminated the CRDM using a carbon dioxide (CO_2) pellet blasting process and repeated application of replica material. These worked well for removing the loose contamination but did not reduce the dose level. Thus, it was concluded that the oxide layer must be removed to reduce the dose. This hard oxide layer was removed by repeated application of a commercially available etchant-gel. The gel dries after application in about 2 hours, and then the etched portion of the dissolved reactive oxide layer can be wiped away with a cloth.

Figure 2.1. CRDM Penetration-Nozzle Assembly in Glove Box

The decontamination gel was effective at removing the contamination on the surface of the CRDMs and at reducing the radiation dose rate near the CRDMs. The contamination levels on Nozzle 59 went from well over 1 million decays per minute (dpm) per 100 square centimeters (dpm/100 cm^2) at the most contaminated areas to less than 100,000 dpm/100 cm^2. Similar results were obtained on Nozzle 31, with the lowest contamination levels remaining at around 200,000 dpm/100 cm^2. The contact dose levels also were reduced significantly. The decontamination results for different locations for Nozzle 59 and Nozzle 31 are given in Tables 2.1 through 2.4.

Table 2.1. Effects of Etchant Gel Decontamination on Removable Contamination Levels for Nozzle 59

Location	Removable Contamination (dpm/100 cm^2)/1000		
	Initial	**Application 1**	**Application 8 (Final)**
Dry surface (pressure vessel)	500	50	5
OD nozzle – dry side	200	40	1.5
ID nozzle – dry side	>1000	>1000	1
Wetted surface (pressure vessel)	200	800	40
OD nozzle – wetted side	300	900	65
ID nozzle – wetted side	600	800	45

Table 2.2. Effects of Etchant Gel Decontamination on Contact Dose Levels for Nozzle 59

Location	Contact Dose Rate (mRem/hr)	
	Application 1	**Application 8 (Final)**
ID nozzle – dry side	270	40
Dry side surface	250	90
ID nozzle – wetted side	3000	1100
Wetted side surface	1200	580

Table 2.3. Effects of Etchant Gel Decontamination on Removable Contamination Levels for Nozzle 31

Location	Contact Dose Rate (mRem/hr)	
	Application 1	**Application 13 (Final)**
Dry surface (pressure vessel)	5	<MDA[(a)]
OD nozzle – dry side	5	<MDA
ID nozzle – dry side	1000	<MDA
Wetted surface (pressure vessel)	300	10
OD nozzle – wetted side	130	200
ID nozzle – wetted side	450	200
(a) Less than minimum detectable activity.		

Table 2.4. Effects of Etchant Gel Decontamination on Contact Dose Levels for Nozzle 31

Location	Contact Dose Rate (mRem/hr)	
	Application 1	**Application 13 (Final)**
ID nozzle – dry side	300	40
Dry side surface	400	70
ID nozzle – wetted side	2100	1400
Wetted side surface	1200	500
Note: After Application 9, the dose rate at 30 cm ranged from 6 to 37 mrem/hr.		

3.0 Nondestructive Examination Probes and Measurements

The six NDE techniques used for studying the CRDM penetration nozzle-assemblies removed from service are listed in Table 3.1. Eddy current testing was used to detect surface-breaking flaws on the inside of the Alloy 600 tube of both nozzles and on the J-groove weld of Nozzle 31. The ET technique examines the near-surface region with a depth of penetration that varies between 1 to 3 mm (0.04 in. to 0.12 in.), depending on the frequency of coil excitation and size of the coil. Ultrasonic testing with spherically focused probes was applied from the inside of Alloy 600 nozzles of both nozzles to inspect the fusion zone of the J-groove weld with the nozzle and beyond, into the weld metal. Time-of-flight diffraction (TOFD), an ultrasonic technique, was applied to the volume of the Alloy 600 nozzle from the inside surface of the tube. Visual testing was performed on replicas of the surface of the J-groove weld and buttering using a high-resolution camera. The J-groove weld of Nozzle 31 was examined using penetrant testing, and all relevant indications found in the J-groove weld of Nozzle 31 were photographed directly using a high-resolution camera.

Table 3.1. NDE Techniques for Study of CRDM Nozzle Assemblies Removed from Service

NDE Technique	Product Form	Volumetric or Surface
Eddy current testing	Alloy 600 nozzle J-groove weld	Near-surface examination (1–3 mm depth of penetration)
Time-of-flight diffraction	Alloy 600 nozzle	Volumetric examination
Spherically focused probe ultrasound	J-groove weld and buttering	Volumetric examination
Visual testing via replicant	J-groove weld crown Alloy 600 of Nozzle of 59	Surface examination
Bare metal visual testing	J-groove weld crown of 31	Surface examination
Penetrant testing	J-groove weld crown of 31	Surface examination

3.1 Scanners

The CRDM nozzles presented two regions of interest for scanning—the interior of the penetration tube and the wetted surface of the J-groove weld crown and buttering. These different regions required different scanners, which are described in this section.

3.1.1 Theta-Z Scanner

The Theta-Z scanning apparatus for examining the inner diameter (ID) of the penetration tubes was constructed by Brockman Precision Machine and Design, Kennewick, Washington. The ID scanner was designed to be used for inner-surface scanning by both ET and UT probes. Figure 3.1 shows the scanner sitting on a laboratory bench and in use on CRDM 31 in a walk-in hood at PNNL. The scanner has a linear (vertical) axis and a rotational axis. The range of linear motion is 40 cm. The rotational motion is

Figure 3.1. CRDM Scanner on Laboratory Bench with 30-cm Scale (left) and in Use on CRDM Nozzle 31 in PNNL Walk-In Hood (right)

continuous, with no hard limits, but is practically constrained to approximately 1.5 revolutions by the cables attached to the motor drivers and the NDE probes.

3.1.2 *x-y* Scanner

The eddy current data acquisition system is based on a computer-controlled linear *x-y* scanner as shown in Figure 3.2 and an eddy current instrument and probe. The scanner was designed to allow examination of the welded surface of a CRDM nozzle assembly. The probe, described later, is attached to the scanner, held on to the specimen with spring loading, and scanned over the piece while magnitude and phase data are recorded from the material over the defined scanning grid. Raster scanning of the surface of the sample consists of line scans in *x* (left to right) while incrementing in *y* (back to front). The scanner was manufactured by Parker Hannifin Corporation, Motion Control Systems, North America. The scanner assembly was mounted in an aluminum tray. A Plexiglas box beneath the scanning bridge holds the sample and provides additional containment to reduce the spread of contamination inside the fume hood. Additionally, a lock-down turntable (shown as light brown) with five-degree marked increments

was fabricated and is seen in Figure 3.2 holding the cutout nozzle section inside the Plexiglas box. The turntable facilitated rotational or circumferential positioning of the nozzle assembly for inspection.

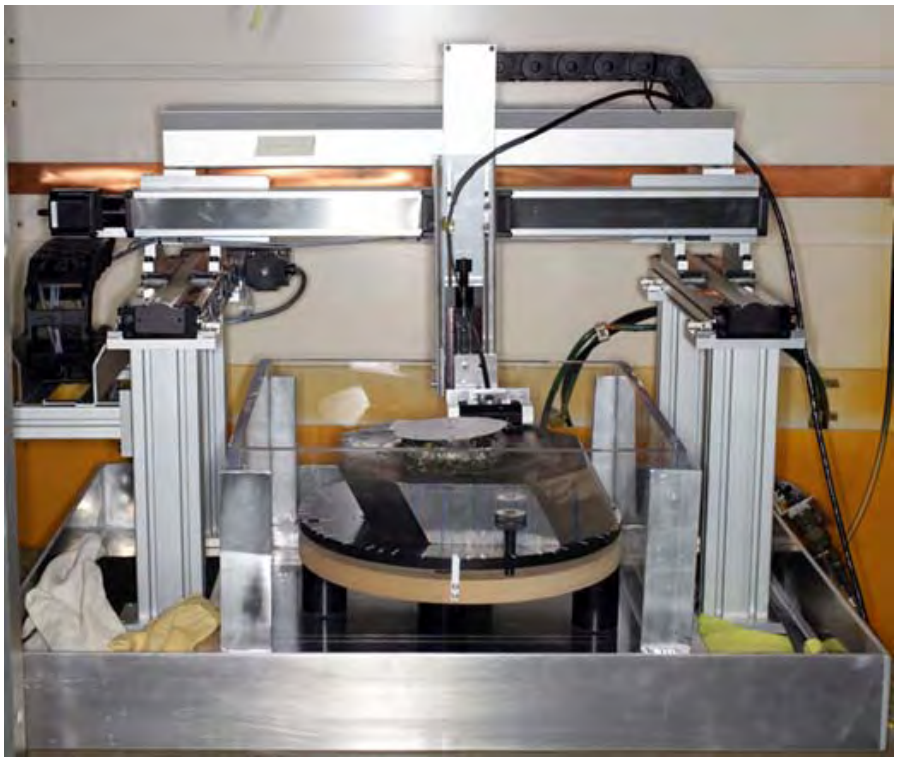

Figure 3.2. Eddy Current Scanner with Attached Probe on a Cut-Down Version of CRDM Specimen 31 from the North Anna 2 Plant

3.2 Eddy Current Probe Assembly and Sensors

The sensitivity of the ET probes as a function of angle is shown in Figure 3.3. The data for this graph were acquired by scanning the sensors across two scribe marks in the calibration piece (one axial and one circumferential). The sensors were rotated 1/16 turn (22 ± 5 degrees) between scans, over a range of ¼ turn (90 ± 5 degrees).

The ET data collection apparatus is shown in Figure 3.4. The apparatus consists of a Zetec MIZ-27 ET instrument, a Gateway GP7-800 computer, and motor control electronics. The computer uses a National Instruments 16-bit digitizer card (PCI-MIO-16XE-10) and counter-timer card (PCI-6602) to digitize data from the ET instrument analog output. The counter-timer uses signals from encoders on the linear axis motors to synchronize data-taking with probe position.

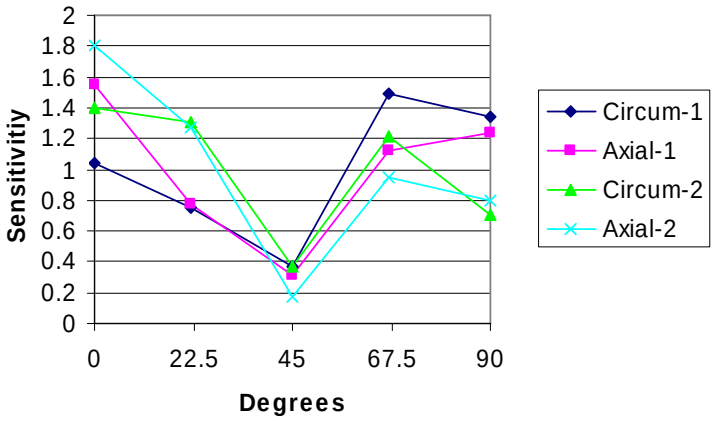

Figure 3.3. Eddy Current Probe Sensitivity as a Function of Angle, Normalized So That the Average for Each Set of Measurements is 1

Figure 3.4. Data Collection Apparatus: Zetec Eddy Current Instrument (left), Computer (lower right), and Control Electronics (bottom center)

3.2.1 Eddy Current Using the Theta-Z Scanner

The ET probe assembly consists of a housing with two sensor seats and is shown in Figure 3.5. The sensors used were differential plus-point probes supplied by Zetec, Inc. The plus-point probe is preferentially sensitive to localized features such as cracks but is relatively insensitive to irregular surface features that may cause "lift-off." These probes are also direction-sensitive. For this reason, two sensors were used, one oriented at 45 degrees to the other. This provided consistent and uniform detection for cracks in any orientation. The probe design uses spring-loaded ball bearings to hold the probe assembly centered in the penetration tube to account for variations in the inside diameter of the nozzles. Figure 3.6 shows how the probe assembly fits into the penetration tube for scanning.

Figure 3.5. Redesigned Probe Assembly, Showing Roller Bearings and Both Sensors

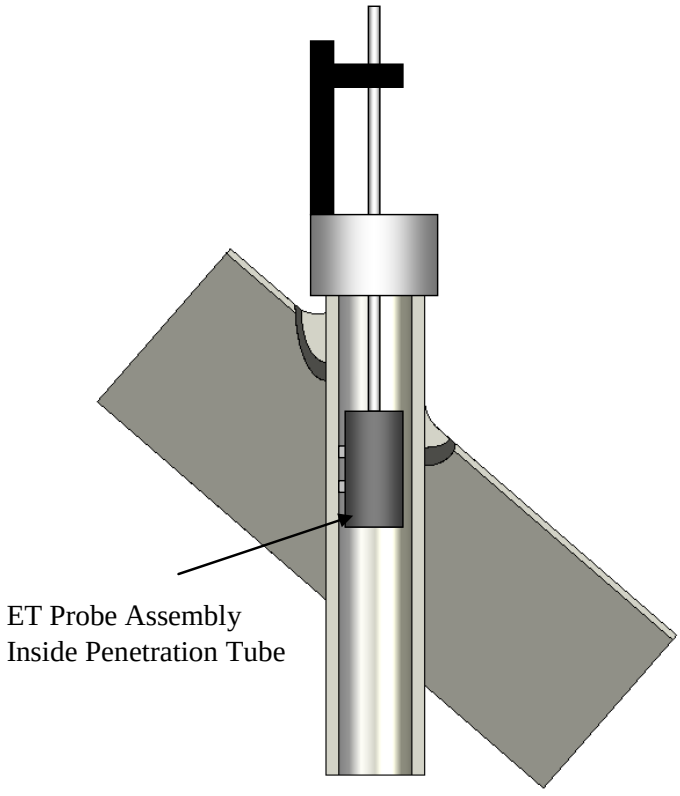

Figure 3.6. How the ET Assembly Fits in the Penetration Tube

3.2.2 Eddy Current Using the *x-y* Scanner

The ET probe assembly consists of a rectangular housing held onto the piece using a spring-loaded slide. The sensor used was a differential plus-point probe supplied by Zetec, Inc. The spring-loaded slide is shown in Figure 3.7. The spring-loaded slide holds the probe on the part while allowing the probe to ride over surface irregularities. The probe and probe holder are shown in Figure 3.8. This holder provides a spring-controlled up-and-down motion for the probe as well as wheels for smooth left and right movement. Additionally, the probe holder is mounted to the vertical slide with a horizontal aluminum piece that pivots on the slide. This pivoting action, the probe's up and down motion, and the wheels provide increased stability and more uniform coupling to the material over rough and welded surfaces.

Figure 3.7. Spring-Loaded Slide Assists in Holding the Probe on the Specimen

Figure 3.8. Plus-Point Probe in a Spring-Loaded Holder (left) and the Probe Holder Assembly Attached to the Scanner's Vertical Slide at a Pivot Point (right)

This portable scanner assembly was developed on a benchtop and moved to the Radiochemical Processing Laboratory (RPL) where the North Anna 2 CRDM nozzle assembly was evaluated.

3.3 Time-of-Flight Diffraction Probe Assembly and Transducers

Two sets of TOFD probes were used for data acquisition on the nozzles. The transducers used were Krautkramer round probes, 6 mm (0.25 in.) in diameter, attached to screw-in wedges. A 5-MHz, 60-degree longitudinal pair, the industry standard for the TOFD technique, and a 7.5-MHz, 60-degree longitudinal pair were used. The probe holder with two transducers is shown in Figure 3.9. When mounted on the search tube, the probe orientation is vertical with a top and bottom transducer. Each probe is individually pushed out via spring loading to provide contact with the inner surface of the nozzle wall. A water line for coupling is shown to the left of the transducer. This holder was later modified to provide an additional coupling water line to the right transducer. Signal consistency and quality was improved with this modification. Water dripped along the inside wall of the nozzle and was collected in a pan under the CRDM. A peristaltic pump in the tubing loop circulated approximately 2 L/min of water from the drip pan to the TOFD probes. Secondary water containment was provided by a large plastic berm that held the entire CRDM assembly, including the CRDM support frame, all water lines, and the pump. Figure 3.10 shows how the probe would fit into the penetration tube for scanning.

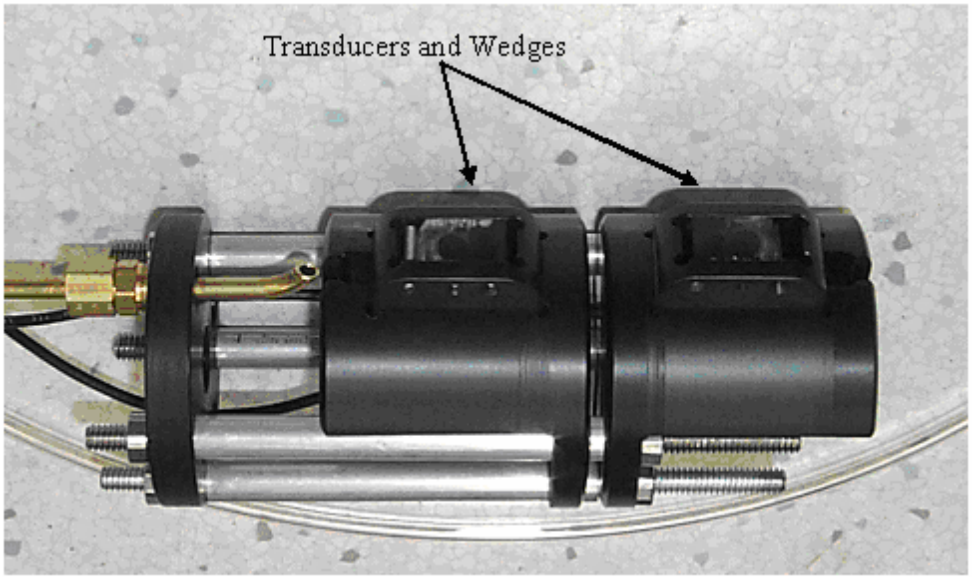

Figure 3.9. Time-of-Flight Diffraction Transducers Mounted in Holder Assembly with Signal and Water Lines

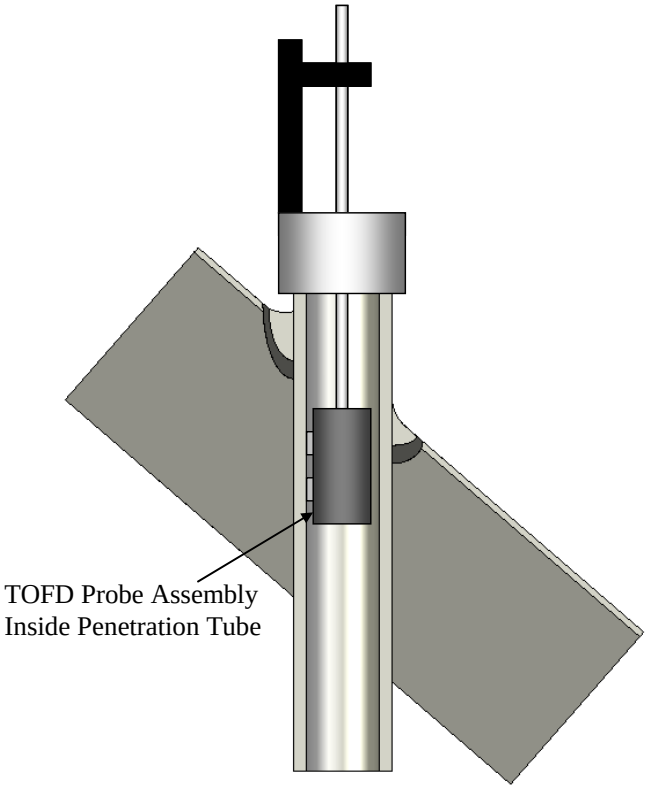

Figure 3.10. How the TOFD Assembly Fits in the Penetration Tube

3.4 Immersion Ultrasonic Probe Assemblies and Transducers

Immersion UT data at a 0-degree incident angle (perpendicular to the penetration tube ID surface) was acquired on Nozzles 59 and 31 at frequencies of 500 kHz, 1 MHz, 2.25 MHz, and 5 MHz. Two of the transducers and a probe in the large-diameter mirror assembly are shown in Figure 3.11. The reflective mirror provided a 0-degree incident angle for the inspection. To inspect a nozzle, a plug was placed in the bottom of the CRDM assembly (ID) for the CRDM in the orientation shown in Figure 3.10. A cap was placed over the nozzle (outer diameter; OD) that extended approximately 50 mm (2 in.) axially and was secured with a hose clamp. This provided double containment of the water in the nozzle. Additionally, a catch basin was kept under the CRDM assembly, and a large berm held the entire assembly. Once the nozzle was sealed, water was added to bring the fill level to approximately 25 mm (1 in.) below the top surface. An inadvertent small tilt in the vertical position of the CRDM assembly helped to prevent an air bubble from becoming trapped on the transducer surface as it was lowered into the water. The bubble formation was a potential problem for the 5-MHz focused probe (100-mm focus) with its concave surface 19 mm (0.75 in.) in diameter. The 2.25-MHz probe had a 6-mm (0.25-in.) diameter and was unfocused (flat). The 1-MHz and 500-kHz transducers were both 12.5 mm (0.5 in.) in diameter and also unfocused. The data were processed using the synthetic aperture focusing technique (SAFT) and envelope-detected prior to data analysis.

Figure 3.11. Two Immersion Ultrasonic Transducers with Mirror Assembly in Center. The mirror provided a 0-degree incident angle for the inspection.

3.4.1 Front Surface Alignment

A variable water path distance to the inner surface of the nozzle was noted in the immersion UT data. This was due to weld shrinkage and the tilt of the CRDM assembly in the metal frame holder. The tilt from a vertical position likely caused the transducer at the end of the search tube to slightly wander from its center position as the scanner moved circumferentially around the CRDM assembly. To correct for this misalignment, each A-scan in the data file was threshold-detected and shifted in time (or depth), if necessary, to place all the ID nozzle surface signals at the same zero start position in time. This alignment step is critical for subsequent data analysis to ensure that indications are mapped to the correct depth.

3.4.2 Signals and Areas of Interest

The areas investigated with immersion UT were from the ID out: the nozzle material, the first fusion zone, the J-groove weld, the second fusion zone, the buttering, the third fusion zone, and the top head carbon steel material. The Alloy 600 nozzle wall is approximately 16 mm (0.63 in.) thick. The J-groove weld varies around the penetration tubes and nominally is approximately 13 to 18 mm (0.5 to 0.7 in.) thick, and the buttering layer is approximately 10 mm (0.4 in.) thick. The lower frequencies penetrated deeper into the material and could potentially detect flaws out in the buttering material and beyond, while the higher frequencies provided better resolution at shallower depths.

3.5 Visual Testing of J-Groove Weld Surface

Enhanced VT, when applied properly, can be a useful tool in detecting and characterizing component surface features. To achieve a proper level of resolution with the system, one needs a high–pixel-count camera system, a high-quality lens, and a proper lighting arrangement. A low-resolution camera or incorrect lighting can greatly reduce the reliability of a visual system. For the visual tests, PNNL used a Canon 1Ds Mk 2 camera with a 180-mm 1:1 macro lens. The camera with the 180-mm lens was able to resolve 41 lines/mm using a 1951 Air Force resolution target.

This magnification is very useful for detecting and identifying cracks. Stress corrosion cracks of the PWSCC style (called interdendritic stress corrosion cracking or IDSCC by some) in nickel alloys typically have widths of 0–120 µm (0–0.05 in.) with median widths of 31 µm (0.0012 in.) (MacDonald 1985; Ekstrom and Wale 1995). The Canon camera system using diffuse lighting has a pixel size of 7 µm (0.0003 in.) and would be able to, under ideal conditions, detect a crack as narrow as 5 µm (0.0002 in.), and definitively identify it as a crack at the higher magnification.

3.5.1 Replicant Testing

Because the CRDMs are highly radioactive and contaminated and have a complex geometry, the VT of the J-groove weld was performed using a replica of the weld region. An epoxy-like polymer (Microset Products Ltd., Warwickshire, UK) is applied on a surface as a liquid; it then hardens, making an extremely high-resolution replica of the surface. The replica is then peeled from the surface and examined. This surface replication can capture details of as small as 0.1 µm (0.000004 in.). Images of cracks on the order of 10–100 µm (0.0004–0.004 in.) wide would be captured by the replica.

When the replicas were being photographed, the camera was mounted on a graduated slide bar and a graduated tripod. The camera and slide-bar arrangement is shown in Figure 3.12. This arrangement allows for precise raster scanning of the sample. The replicas were mounted on a flat board, and the camera slide bar was set parallel to the board at a distance that gave 1:1 macro focusing. The slide bar and tripod height were adjusted to put the camera at the top left-hand corner of the sample and then indexed across, taking a photograph every 33 mm (1.3 in.). When the length of the sample was scanned, the tripod height was lowered by 19 mm (0.8 in.), the camera repositioned at the left-hand edge of the sample, and the next indexed series across the replica was photographed. This procedure allowed for complete coverage of the sample with very high resolution and some overlap on the edges. The images were then examined at 100%–200% magnification on a high-resolution monitor.

Figure 3.12. High-Resolution Camera Mounted on a Slide Bar and Tripod

3.5.2 Penetrant Testing

To find cracks that are too small or camouflaged for replicant testing, penetrant testing was used to examine the J-groove weld surface of Nozzle 31. As PWSCC was suspected to be very tight and challenging to PT, PNNL selected high-sensitivity fluorescent dye. To meet these parameters, Magnaflux Zyglo ZL-27A dye was used along with Spotcheck SKC-S cleaner and SKD-S2 developer. A dwell time of 30 minutes was used to ensure that the dye had sufficient time to be drawn into possible cracks.

4.0 Pre-Inspection Calibration and Testing

Before the CRDMs were examined, PNNL researchers characterized the NDE equipment and experimental methods to be used for the NDE methods. The pre-inspection tests were performed also to provide practice with the procedures in a non-radioactive environment to work out any problems and gain familiarity with the techniques. The test pieces used to calibrate and set inspection sensitivity are described in Section 4.1 for each NDE technique employed. Section 4.2 documents the responses for each NDE technique on the calibration pieces.

4.1 Test Pieces

The equipment and procedures for each NDE technique were tested and characterized prior to use on the removed-from-service CRDMs. The ET and TOFD equipment was tested using an Alloy 600 tube with machined notches and holes. The immersion UT was tested using a non-radioactive CRDM cut from the Midland Nuclear Power Plant pressure vessel head that was cancelled and never irradiated. The VT equipment was tested using cracked steel samples with a variety of crack sizes and surface conditions.

4.1.1 Penetration Tube Test Piece

The calibration standard for the ET and TOFD systems consists of a 100-mm-OD (4-in.) Alloy 600 tube with 12 electrical discharge-machined (EDM) notches cut into the inner- and outer-diameter surfaces. Each EDM notch was 25 mm (1 in.) long and 0.38 mm (0.015 in.) wide. Three 1-mm-diameter (0.04-in.) flat-bottom holes were drilled from the outside surface, terminating at 10.4, 6.9, and 1.3 mm (0.41, 0.27, and 0.05 in.) from the inner surface. The locations of the EDM notches are shown in Figure 4.1; the notches are described further in Table 4.1.

4.1.2 Immersion UT Test Piece

The immersion testing equipment and scanning technique were characterized using the Midland CRDM. The Midland CRDM has no service-induced or machined flaws, but it contains several fabrication flaws in the weld. This allowed PNNL to determine which UT frequencies and SAFT processing parameters were needed to effectively examine different regions of the J-groove weld. The Midland CRDM is shown in Figure 4.2.

4.1.3 Visual Testing Test Piece

The high-resolution camera and scanning equipment were tested using replicated surfaces made from stainless steel sample surfaces. The stainless steel samples were produced to be similar to stainless steel reactor internal surfaces (not clad) and have a variety of artificial cracks implanted in them. The crack opening dimensions range from less than 10 μm (<0.0005 in.) wide to 150 μm (0.006 in.) wide. The surfaces of the samples have been machined smooth, but some contain grinding marks that make VT much more challenging. Two of the stainless steel samples employed in this work are shown in Figure 4.3.

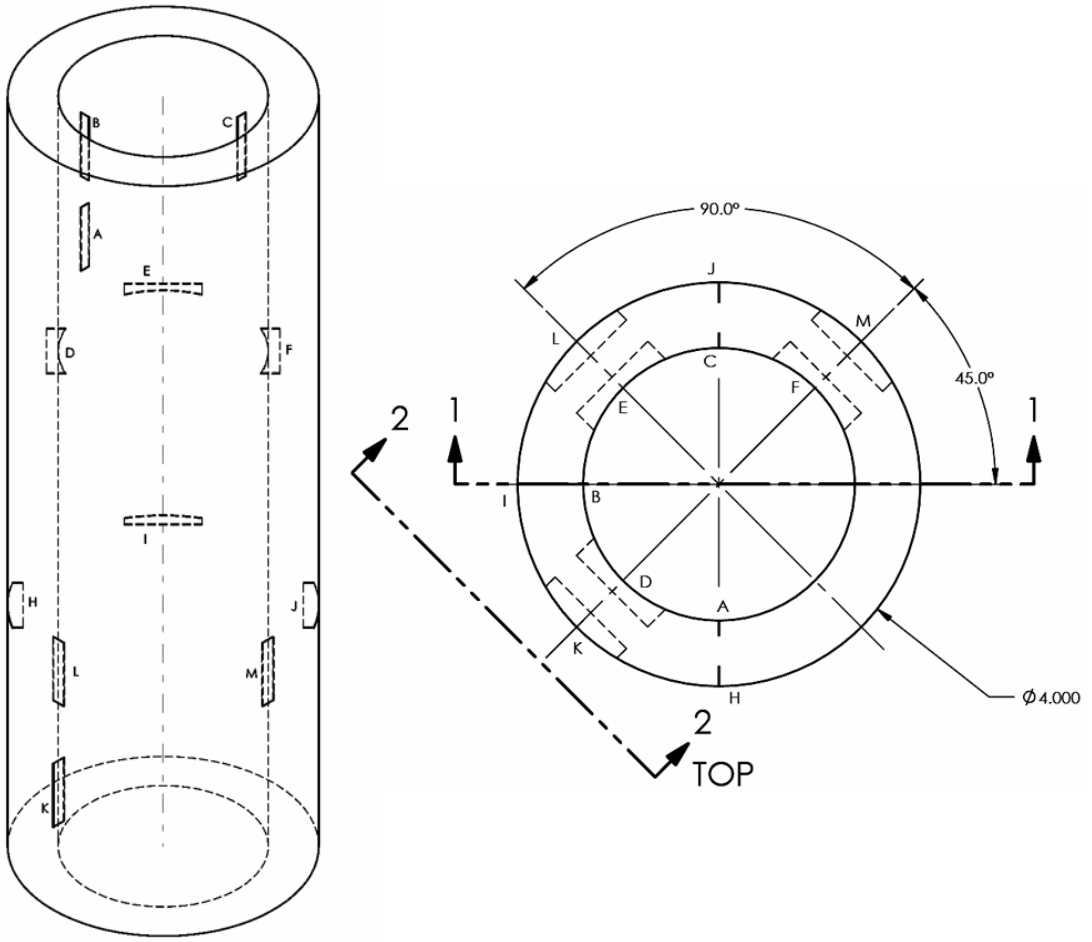

Figure 4.1. Penetration Tube Calibration Standard Isometric and Top View

Table 4.1. Calibration Tube Flaw Descriptions

Notch Designation	Surface	Orientation	Depth
A	ID	Axial	2 mm (0.08 in.)
B	ID	Axial	4 mm (0.16 in.)
C	ID	Axial	8 mm (0.31 in.)
D	ID	Circumferential	2 mm (0.08 in.)
E	ID	Circumferential	4 mm (0.16 in.)
F	ID	Circumferential	8 mm (0.31 in.)
H	OD	Circumferential	2 mm (0.08 in.)
I	OD	Circumferential	4 mm (0.16 in.)
J	OD	Circumferential	8 mm (0.31 in.)
K	OD	Axial	2 mm (0.08 in.)
L	OD	Axial	4 mm (0.16 in.)
M	OD	Axial	8 mm (0.31 in.)

Figure 4.2. Midland Control Rod Drive Mechanism Used for Testing Immersion UT Equipment and Techniques

Figure 4.3. Two Cracked Stainless Steel Samples Used To Test Visual Testing Procedures and Equipment Using Replicas

4.1.4 Notched Plate Piece

At the beginning and end of a series of scans using the *x-y* scanner, a calibration check was made using an EDM notch "I" in an Inconel Alloy 600 plate 5.88 mm (0.625 in.) thick (Figure 4.4). The notch was 0.3 mm wide and 25 mm long with a 100% through-wall depth. Notch response variations were monitored to ensure a uniform system performance throughout the test period.

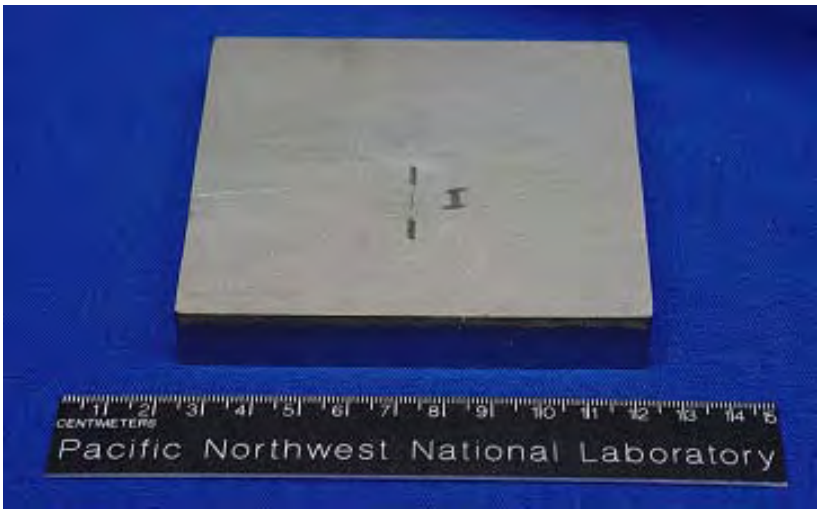

Figure 4.4. Calibration Notch "I" in Inconel 600 Plate Material Used To Assess Equipment Performance or Calibration

4.2 Nondestructive Evaluation Results from the Test Pieces

4.2.1 Eddy Current Responses to Artificial Flaws

The EDM notches for testing the ET procedure were on the inside surface of the Alloy 600 cylinder. The inner-surface EDM notches consist of two sets of three each—an axially oriented set and a circumferentially oriented set. All were 25 mm (1 in.) long and 0.4 mm (0.015 in.) wide. Their depths were 2, 4, and 8 mm (0.08, 0.16, and 0.31 in.). In addition, three flat-bottom holes were drilled from the outside surface, terminating at 10.4, 6.9, and 1.3 mm (0.41, 0.27, and 0.05 in.) from the inner surface.

Eddy current testing responses to all the inner surface notches were very large. None of the outer-surface notches was detectable by ET. Only the flat-bottom hole terminating 1.3 mm (0.41 in.) from the inner surface was detectable. Figure 4.5 shows the response of the 0-degree ET probe to the notches. The axis of the cylinder runs from lower left to upper right; thus, the left-hand set of notches is axial and the right-hand set is circumferential. Two images of the 2-mm-deep (0.08-in.) axial notch, at 90 degrees and at 270 degrees (58 mm and 175 mm), can be seen, although the second image is truncated by the end of the scan. Figure 4.6 shows the ET response to scribe marks as well as to the notches when high gain was used.

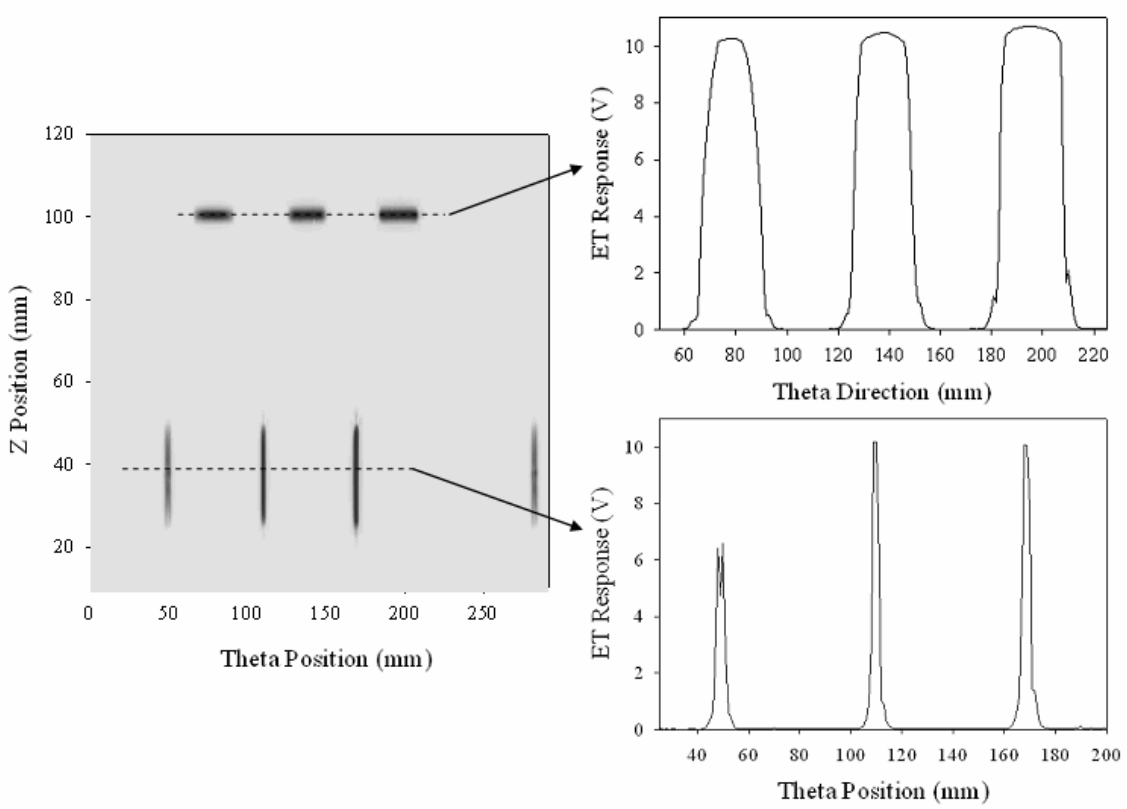

Figure 4.5. Eddy Current Response to 2-, 4-, and 8-mm (0.08-, 0.16-, and 0.31-in.) EDM Notches in Calibration Tube at 350 kHz, 15 dB Gain, and 0 Degrees Probe Rotation

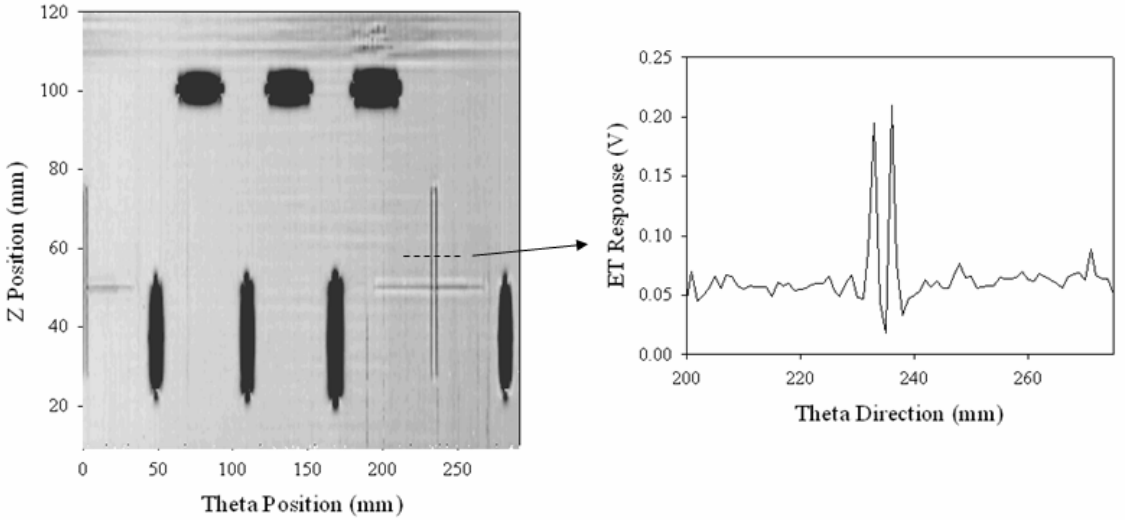

Figure 4.6. Eddy Current Response in the Calibration Tube to Scribe Marks at 350 kHz, 15 dB Gain, and 0 Degrees Probe Rotation

Figure 4.7 shows the response of the 45-degree plus-point sensor to the 0- and 90-degree notches. The amplitudes are much lower, and the peaks are often at the ends of the notches. The only difference between the 0-degree and 45-degree sensors is how the probes are oriented in their holders. Figure 4.8 shows the response of the 45-degree probe at high gain, 150 kHz. The response to a far-side flat-bottom hole, terminated at 1.3 mm (0.050 in.) below the surface, is visible at 200 mm (7.9 in.) horizontal (axial), 0 and 233 mm vertical (0 and 9.2 in.) (circumferential). The response to the scribe lines at lower left is visible mainly at the tip of each line, as is expected for a 45-degree orientation of the plus-point probe.

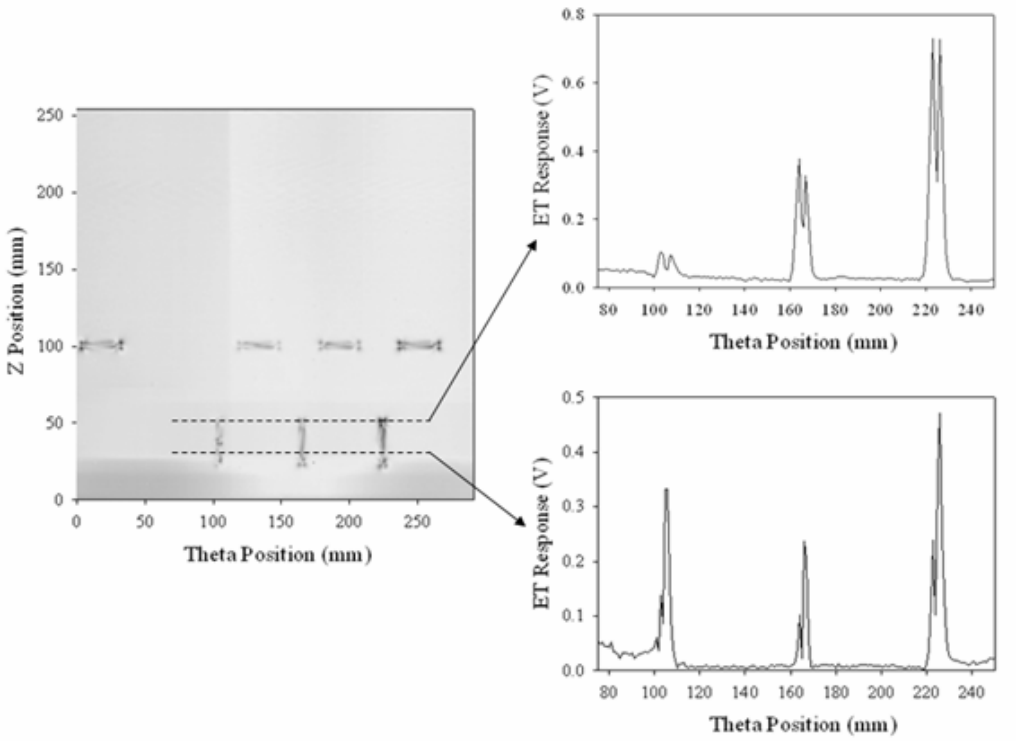

Figure 4.7. Eddy Current Response to 2-, 4-, and 8-mm (0.08-, 0.16-, and 0.31-in.) EDM Notches in Calibration Tube at 350 kHz, 15 dB Gain and 45° Probe Rotation

Typical voltage magnitudes and phases for various artificial flaws, for the 0-degree probe at 15 dB gain, are as shown in Table 4.2, from the calibration reference scan performed after inspection of Nozzle 31. Because the person who needed to move the scanner from the test piece to the CRDM was physically required to be in a radiation field during the pre-scan calibration, a complete one-hour calibration scan was not performed immediately before the inspection. A shorter scan over a notch with a known response was taken to ensure that the equipment was working properly.

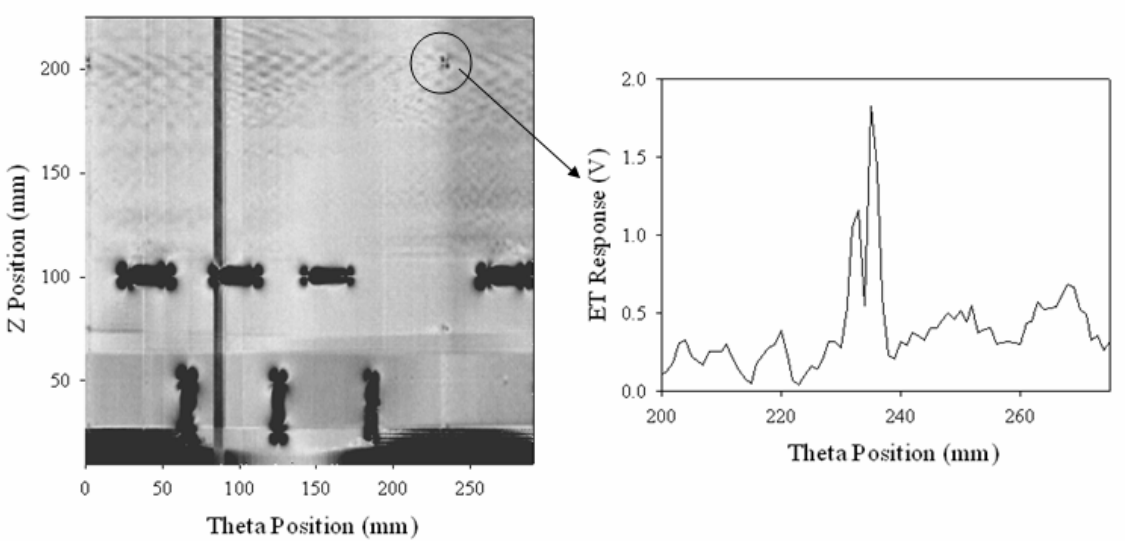

Figure 4.8. Calibration Check of the Calibration Tube Using 150 kHz and 35 dB Gain

Table 4.2. Typical Eddy Current Artificial Flaw Responses at 15 dB Gain (Nozzle 31 Post-Inspection)

	Axial		Circumferential	
Depth (mm)	**Magnitude (volts)**	**Phase (degrees)**	**Magnitude (volts)**	**Phase (degrees)**
2	9	170	10	345
4	10	165	10	340
8	10	170	11	340
Scribe mark	0.2	185	0.1	185

A complete scan of the calibration piece was not performed for the calibration scans before or after the inspection of Nozzle 59. The available data from two notches (0-degree probe) show 3 V at 240 degrees for an axial notch 2 mm (0.08 in.) deep and 3 V at 62 degrees, for a circumferential notch 2 mm (0.08 in.) deep.

The results for the eddy current scans of the EDM notch in the Inconel flat-plate sample were similar to the result in the Inconel tube. The peak voltage across the notch at 350 kHz and 15 dB gain was 10.3 V with the probe oriented favorably, and the peak voltage is much lower (2 V at the ends and 0.6 V in the middle) if the probe is oriented at 45 degrees to the notch. The ET results for the EDM notches with the probes at 0 degrees and 45 degrees are shown in Figures 4.9 and 4.10.

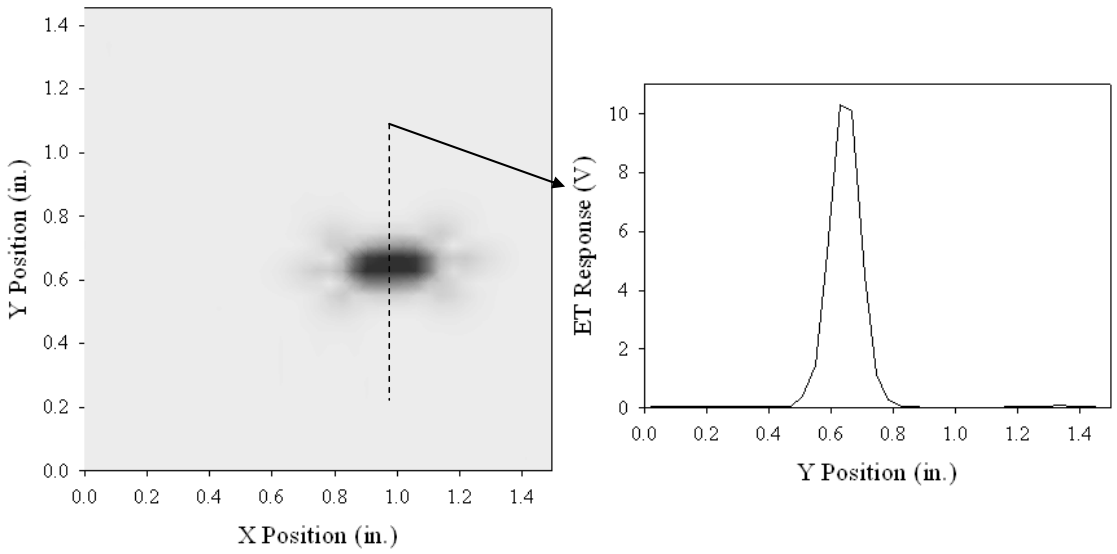

Figure 4.9. Eddy Current Calibration Check of 0-Degree Probe on Calibration Plate, 350 kHz and 15 dB Gain

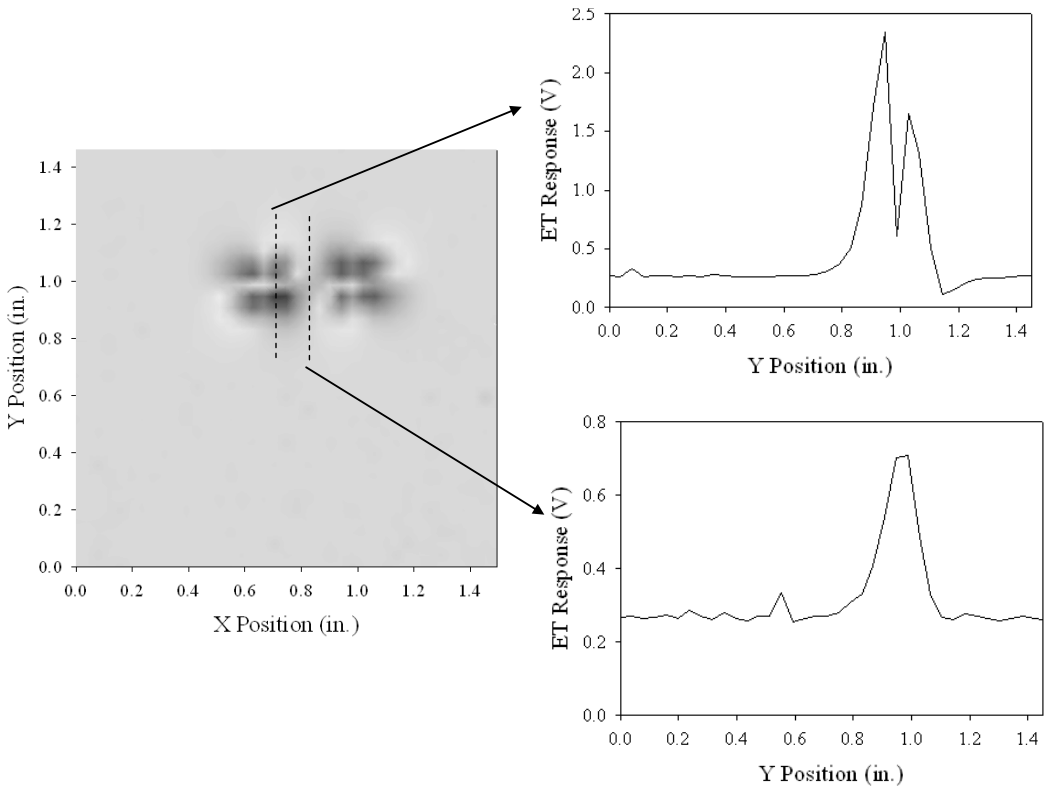

Figure 4.10. Eddy Current Calibration Check of 45-Degree Probe on Calibration Plate, 350 kHz and 15 dB Gain

4.2.2 Time-of-Flight Diffraction Responses to Calibration Notches

The calibration cylinder was examined using TOFD. Data were acquired at 7.5 MHz in a laboratory setting, and the signal responses from the notches with depths of 2, 4, and 8 mm (0.08, 0.16, and 0.31 in.) were recorded. Figure 4.11 shows rectified data from an axial OD notch 4 mm (0.16 in.) deep. The four views in Figure 4.11 are from top left and going clockwise as follows: A-scan data, a B-scan side view, a B-scan end view, and a C-scan or plan view. The A-scan view shows three main reflections. They are, from left to right, the lateral wave signal, the notch signal, and the back surface signal. A red marker line is placed on the peak response from the notch signal, allowing a measurement of the amplitude. In this data set, the response is –6.4 dB. This response is relative to the lateral wave response, which was chosen as a reference signal for each data file. Both the side and end views also show the lateral wave, notch, and back surface responses. The lateral wave is at the top of the side view image and at the left in the end view. A TOF shape, typical for a notch, is seen in the side view of the data. The TOF shape in the end view is very narrow for an axial notch but is discernable in the data set. Finally, the C-scan view locates the notch relative to the entire scan (horizontal) and increment (vertical) axes at the intersection of the two red lines.

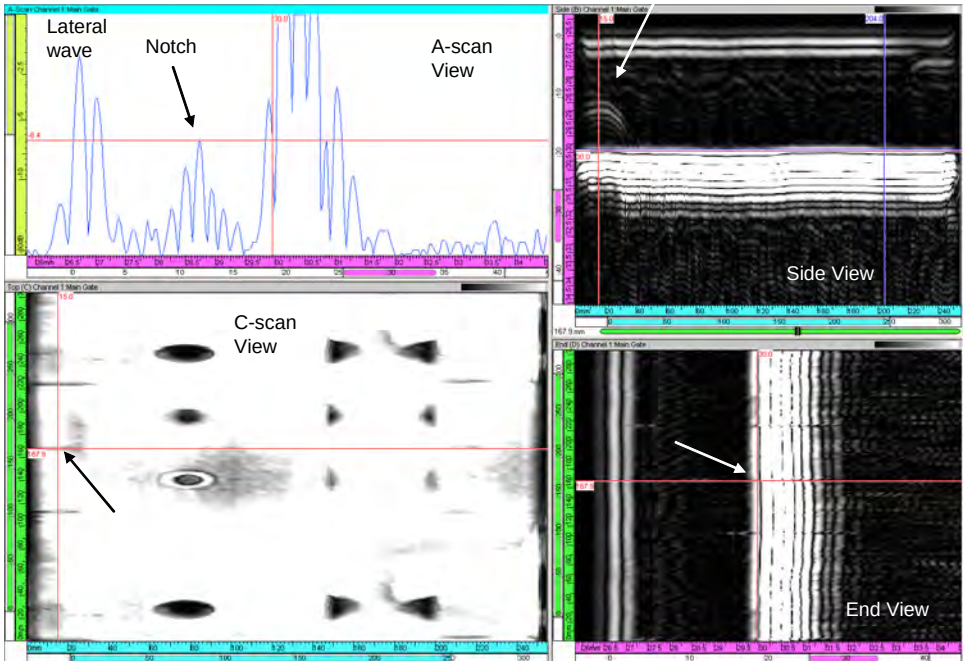

Figure 4.11. Time-of-Flight Diffraction Data from Axial Outside-Diameter Calibration Notch 4 mm (0.16 in.) Deep, at 167.9 mm (31.1 in.) Horizontal, 15 mm (0.59 in.) Vertical, and −6.4-dB Response. The arrows locate the notch signal in the various views.

The TOFD responses from several notches are listed in Table 4.3. These response levels were used as a baseline for comparison of signals from Nozzles 59 and 31.

Table 4.3. Time-of-Flight Diffraction Responses from Notches in Alloy 600 Calibration Cylinder

Flaw Orientation	Flaw Location	Depth	Response (dB)
Circumferential	Outer Diameter	2 mm (0.08 in.)	1.7
		4 mm (0.16 in.)	4.2
Axial	Outer Diameter	2 mm (0.08 in.)	-4.5
		4 mm (0.16 in.)	-6.4
		8 mm (0.31 in.)	-6.8
Axial	Inner Diameter	2 mm (0.08 in.)	Not Detected
		4 mm (0.16 in.)	-0.4
		8 mm (0.31 in.)	-3.8

4.2.3 Immersion Ultrasonic Testing Responses from Fabrication Flaws

Although the Midland CRDM specimen contains no cracks, the weld contains several fabrication flaws in the fusion zone between the penetration tube and the weld metal. These fabrication flaws were isolated and point-like and are likely very small lack-of-fusion defects or slag inclusions. The immersion UT was able to penetrate into the weld and was sensitive to features such as the small differences in reflectivity along the weld beads. Figure 4.12 shows a 2.25-MHz UT scan of the Midland CRDM focused first on the fusion zone and then deeper into the weld. The wetted tube is to the left and shows up in the left-hand image as pink. The interference fit is to the right and also shows up as pink. The blue stripe in the middle of the figure is the J-groove weld. The fabrication flaws show up as green or red spots in the blue stripe (right-hand image). In the section focused deeper into the weld, the weld passes are visible, demonstrating good sensitivity for flaws in the weld.

The immersion UT is expected to have a very high sensitivity for circumferentially oriented cracks through the weld metal. Axial cracks may be difficult to detect, as they would present a very small cross section to the UT beams.

4.2.4 Visual Testing Results from Cracks in Calibration Standards

The VT results on replicas of the cracked stainless steel samples showed that on a surface containing deep grinding marks, only cracks with a crack opening dimension (COD) larger than 100 μm were readily detected. On very smooth surfaces, cracks as small as 10 μm (0.0004 in.) wide were detected easily. On surfaces with some machining marks, cracks from 10–25 μm (0.0004–0.001 in.) wide were detectable with difficulty. The crack orientation relative to the machining marks and other surface textures also strongly affects the crack visibility. A crack ranging from 10–25 μm (0.0004–0.001 in.) wide that follows the machining marks on a machined surface is shown in Figure 4.13. A crack 28 μm (0.001 in.) wide that is perpendicular to the machining marks is shown in Figure 4.14.

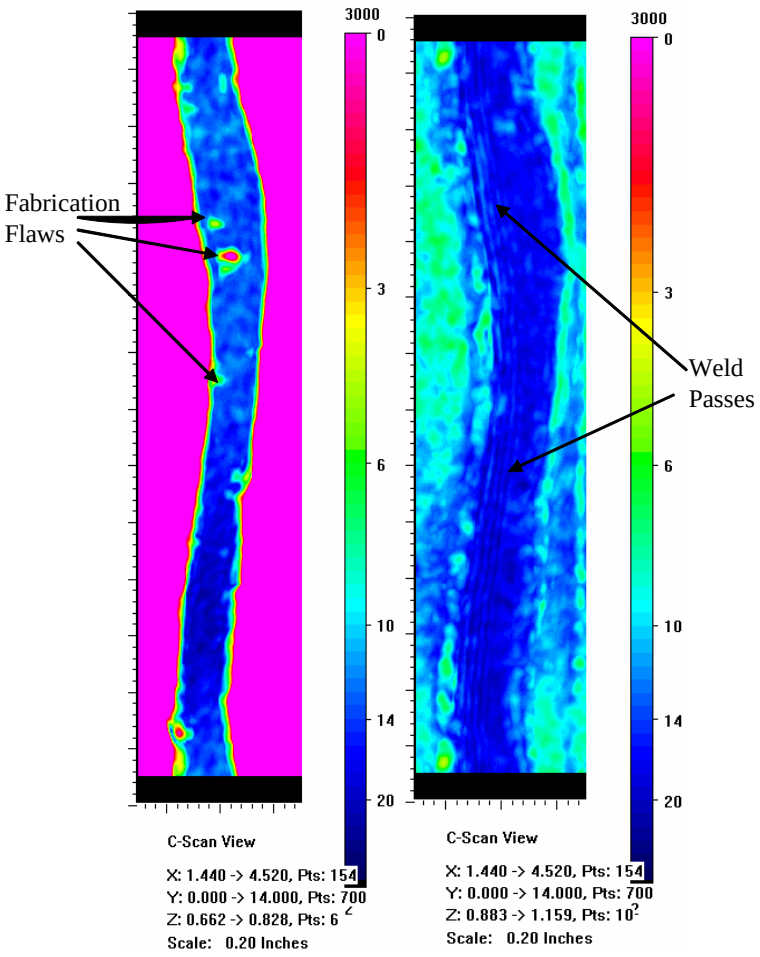

Figure 4.12. Ultrasonic Testing Responses for 2.25-MHz in Midland Control Rod Drive Mechanism. The first image shows the fusion zone of the weld where fabrication flaws were detected. The second image shows the J-groove weld area where the individual weld passes were detected.

The metal J-groove weld on Nozzles 59 and 31 have not been ground down and show the topography common to as-built welds but have relatively smooth surfaces. Based on the work on the replicas of the stainless steel samples, one would expect high sensitivity for crack detection on cracks that cut across the weld passes or that occur in the middle of a weld bead. The smooth weld surface allows for very good crack visibility. One would expect very low sensitivity for detecting cracks that follow weld beads, as the cracks easily could be hidden by the topography of the weld. This suggests that VT will be highly sensitive to axially oriented cracks and relatively insensitive to circumferentially oriented cracks that initiate at the boundaries of weld beads.

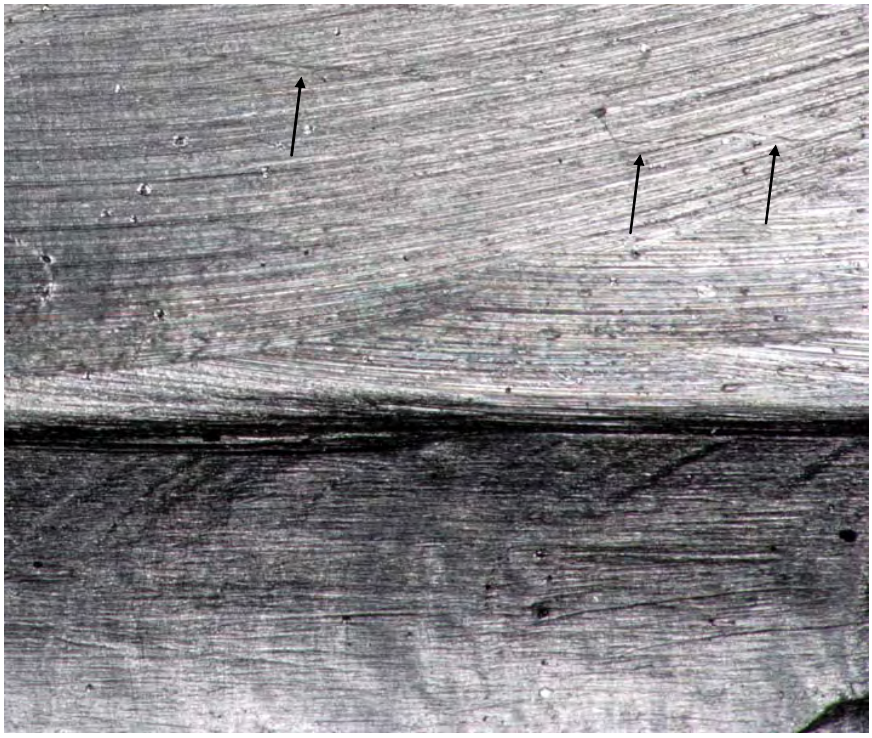

Figure 4.13. Narrow Crack Ranging 10–25 µm (0.0004–0.001 in.) Wide on a Machined Surface. The crack is easy to see when it cuts across machining marks and is difficult to see when it follows the marks.

Figure 4.14. A Crack 28 µm (0.001 in.) Wide Cutting Perpendicularly Across Machining Marks

5.0 Nondestructive Examination Results

PNNL staff examined the CRDM nozzles from July through December 2005. Nozzle 59 was first examined with ET, as it required no coupling fluid. The nozzle was then examined using TOFD. After the TOFD examination was completed, the bottom of the penetration tube was plugged and filled with water for the immersion UT testing. Finally, the J-groove weld was covered in Microset polymer, and the replica was set aside for later VT. This procedure was repeated with Nozzle 31. The results of these NDEs are presented in this section. The NDE inspection results for Nozzle 59 are presented in Section 5.1; those for Nozzle 31 are presented in Section 5.2. The NDE results for both nozzles are summarized in Section 5.3.

5.1 Control Rod Drive Mechanism Nozzle 59

5.1.1 Eddy Current Testing

The scanning protocol was as follows:

- Data were taken on a grid having 1-mm (0.4-in.) spacing.
    - This was exact in the axial direction because the drive mechanics use metric threads.
    - This was approximate in the circumferential direction, assuming an inner diameter of 74.2 mm (2.9 in.) (in which case 360 degrees corresponds to 233 mm).
- Data were recorded only while the probe was moving down. Because the CRDM nozzle was inverted in the fixture, the data were taken from bottom to top (inner end to outer end) of the part.
- Between vertical scans, the probe was indexed clockwise. Initially, the plan had been to rotate counterclockwise, but it was found that the probe assembly would sometimes become unscrewed from the center shaft.
- The scan covered 450 degrees (291 mm, 11.5 in.), providing overlap on 25% of the part. This provided a check on the consistency of the data and facilitated spatial registration with the ultrasonic data.

The data presentations in this section show the cylinder axis from left to right and the circumferential direction from top to bottom, so the data are presented as if unwrapped and viewed from the outside of the nozzle.

Data from Nozzle 59 showed some high-amplitude indications, as shown in Figure 5.1 (150-kHz data). The horizontal line is shown to mark 360 degrees (233 mm, 9.2 in.), where the data begin to repeat. Figure 5.2 shows data at 350 kHz from the same scan.

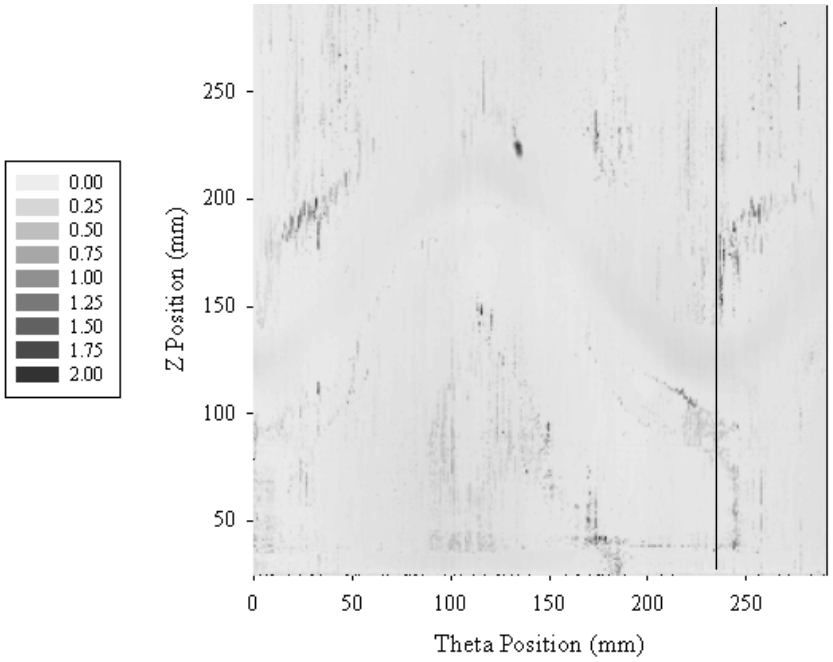

Figure 5.1. Eddy Current Data (150 kHz) on Nozzle 59. Indications are shown in grey to white scale. Horizontal line shows 360 degrees (233 mm, 9.2 in.). Indications in grey-black are greater than 1 V.

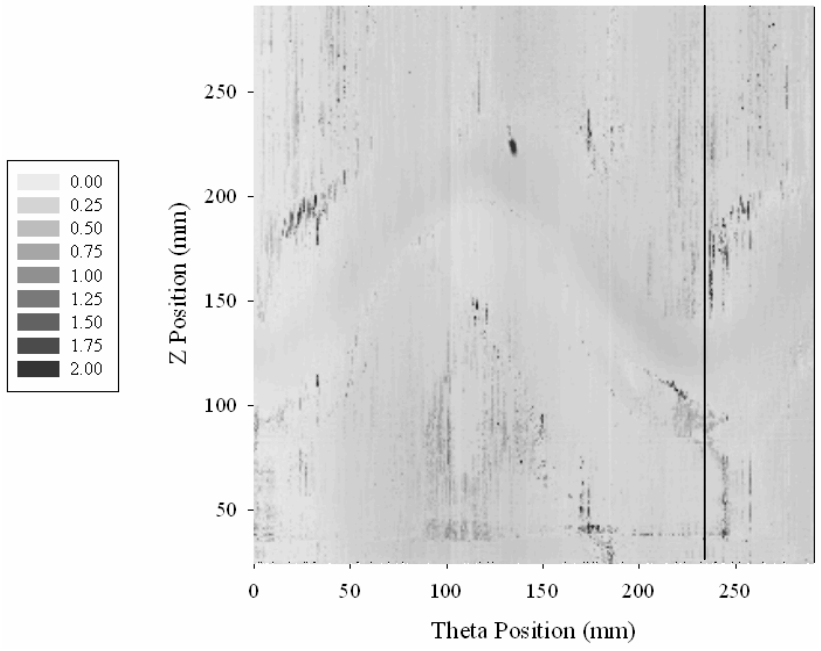

Figure 5.2. Eddy Current Data (350 kHz) on Nozzle 59. Indications are shown in grey to white scale. Vertical line shows 360 degrees (233 mm, 9.2 in.). Indications in grey-black are greater than 1 V.

5.1.2 Time-of-Flight Diffraction Results

The TOFD data were reviewed for relevant indications. An interesting indication was defined as one with a TOF shape or one with amplitude large enough to stand out. The amplitude cutoff was not firmly fixed but was approximately 10 to 12 dB less than the lateral wave response. This range is nearly double the response level sensitivity measured from the axial OD notches on the calibration cylinder.

Figures 5.3 through 5.5 shows weld repair intrusions in Nozzle 59. The C-scan view in the lower left portion of Figure 5.3 shows the weld image in the data. The start of the scan is in the lower left corner of the C-scan, with the axial scan direction proceeding left to right and the circumferential increment proceeding from bottom to top. A weld repair intrusion indication is marked by arrows in both the C-scan and B-scan side views. The side view, top right, shows the TOF shape expected from a flaw. The C-scan view locates the repair intrusions near the start of the scan at 24 mm (0.95 in.) counterclockwise (CCW) from the reference position (start of the scan). An axial position is also given. Figure 5.4 shows a second area with weld repair intrusion indications. This region is 122 mm (4.8 in.) CCW from the start. The third area with weld repair intrusion indications shown in Figure 5.5 is at 231 mm (9.1 in.) CCW from the start. This is a repeat of the first area because the data overlap circumferentially starting at 224 mm (8.8 in.). Response levels from these signals are approximately 5 to 7 dB below the lateral wave signal. From the C-scan (plan) views, it appears that the weld repair intrusion condition is occurring near the axial top and bottom extremes of the weld.

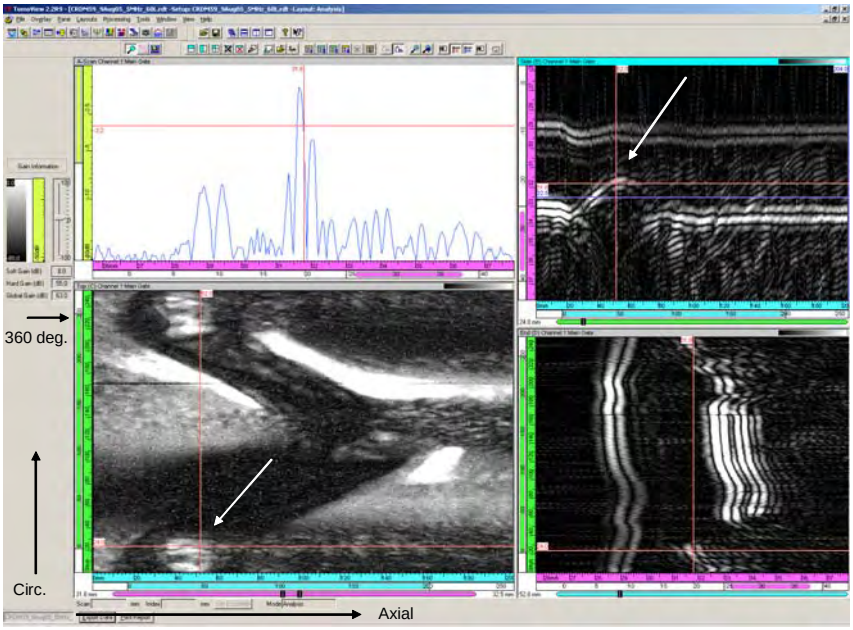

Figure 5.3. Nozzle 59 Weld Repair Intrusion Indication Detected with Time-of-Flight Diffraction at 24 mm (0.95 in.) CCW, 52 mm (2 in.) Axial, with a −5.6-dB Response. The axial and circumferential axes are also noted. One revolution (360 degrees) was represented by 224 mm (8.8 in.) circumferentially.

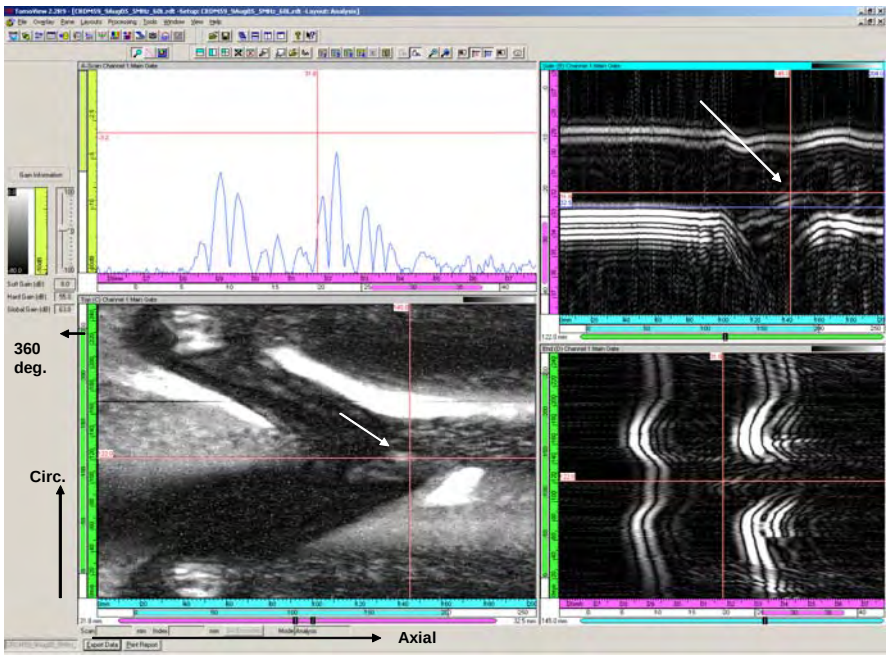

Figure 5.4. Nozzle 59 Weld Repair Intrusion Indication Detected with Time-of-Flight Diffraction at 122 mm (4.8 in.) CCW, 145 mm (5.7 in.) Axial, with a −7-dB Response

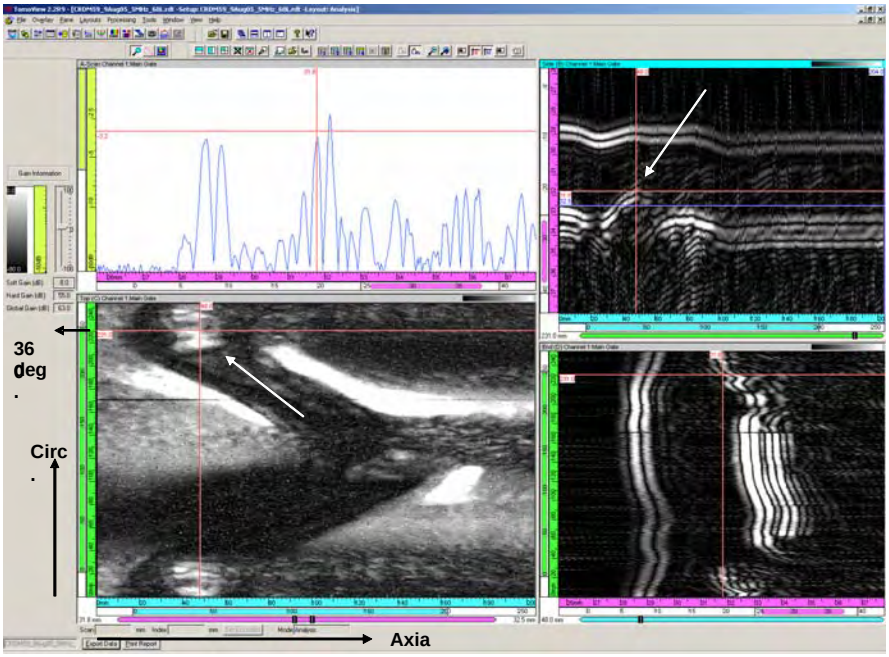

Figure 5.5. Nozzle 59 Weld Repair Intrusion Indication Detected with Time-of-Flight Diffraction at 231 mm (9.1 in.) CCW, 48 mm (1.9 in.) Axial, with a −5.7- to −6.8-dB Response

Interesting indications or regions with many indications based on response were noted from the 5- and 7.5-MHz data. No TOF shapes were seen in Nozzle 59 data outside of the weld repair penetration indications. Additionally, the indications appeared to be axial and did not break the inner surface, noted by a lack of lateral wave interruption. Two typical indications are shown in Figures 5.6 and 5.7. The indication in Figure 5.6 is closer to the back surface signal, while the indication in Figure 5.7 is closer to the front surface lateral wave signal. Figure 5.7 also shows a region with numerous indications with approximately double the response amplitude of the indication in Figure 5.6.

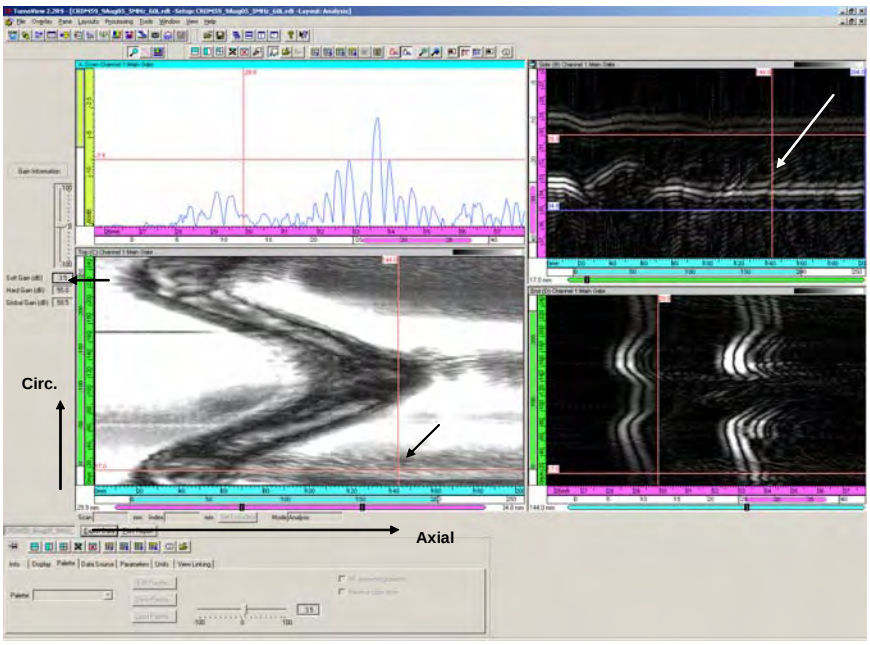

Figure 5.6. TOFD Nozzle 59, 5-MHz Typical Indication. The indication is at 17 mm (0.67 in.) CCW, 144 mm (5.7 in.) axial, with a response of −7.5 dB.

5.1.3 Immersion Ultrasonic Testing Results

C-scan images of Nozzle 59 with the four frequencies are shown in Figures 5.8 through 5.12. The 5-MHz data focuses on the penetration tube and the fusion zone between the penetration tube and the weld metal. The 2.25-MHz data focuses clearly on the fusion zone and slightly into the weld metal. The 1-MHz data focuses deeper into the weld metal, and the 500-kHz data penetrates very well through the weld. Figure 5.8 shows an indication that possibly starts in the nozzle material. Figures 5.9 through 5.12 show lack-of-fusion types of indications in the J-groove weld material at the four different frequencies. The 5-, 2.25-, and 1-MHz data presented in Figures 5.9 through 5.11, respectively, are best and show similarity in locating two areas with lack of fusion. With the decreasing frequency, however, the resolution drops as expected. The 500-kHz data in Figure 5.12 shows a different area that is possibly lack of fusion at approximately 89 mm (3.5 in.) circumferentially.

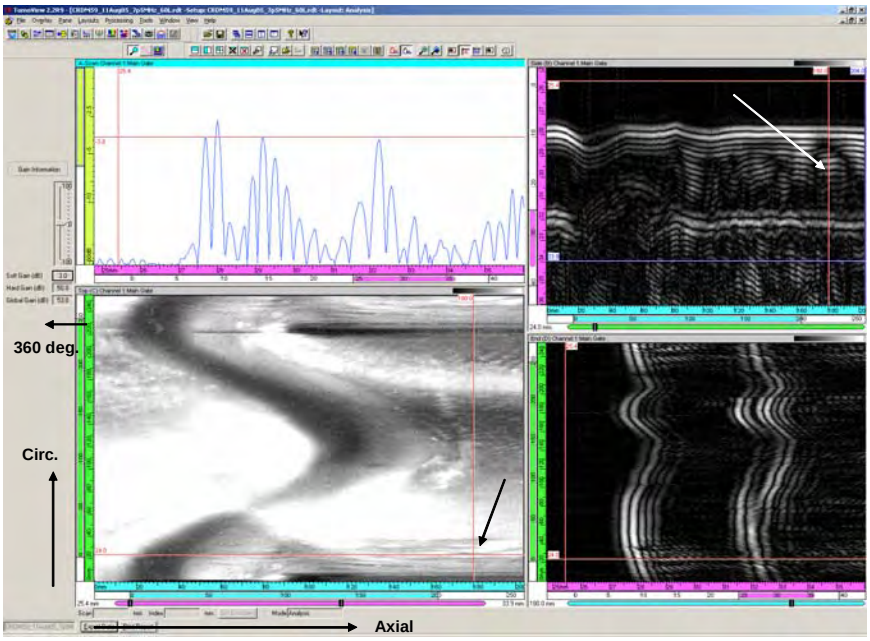

Figure 5.7. TOFD Nozzle 59, 7.5 MHz, Interesting Indication at 24 mm (0.95 in.) CCW and 180 mm (7.1 in.) Axial Position with a Response of −3.8 dB in a Region with Many Indications

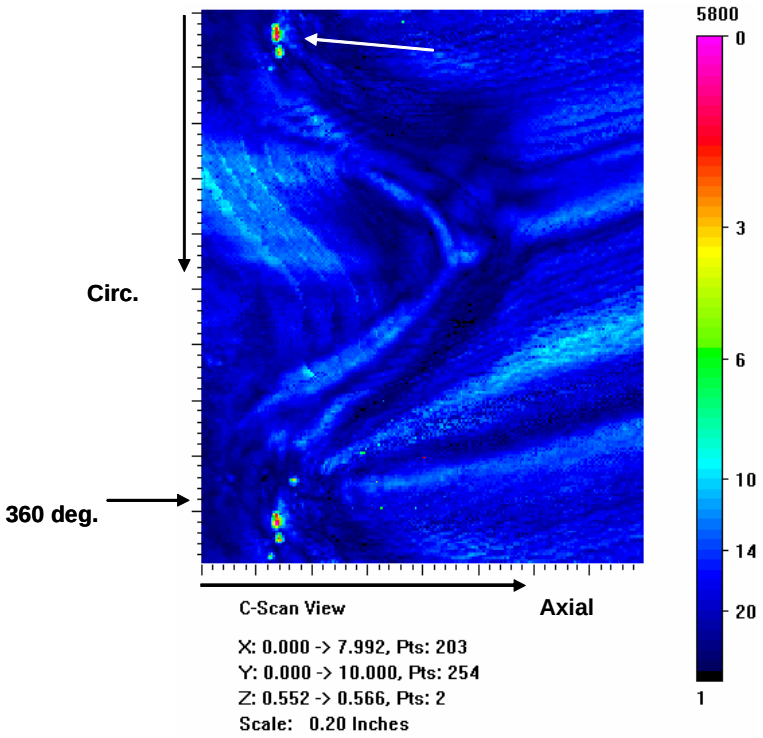

Figure 5.8. Nozzle 59, 5-MHz Immersion Data Showing Potential Indications Starting in the Nozzle Material

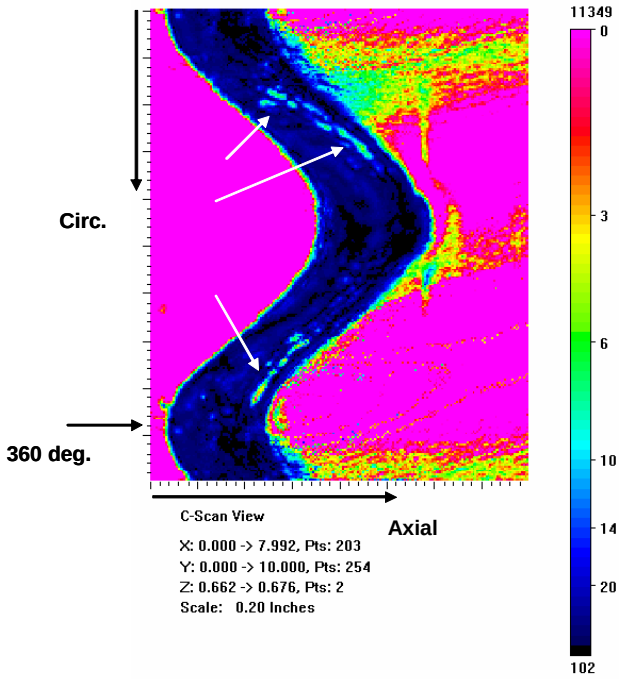

Figure 5.9. Nozzle 59, 5-MHz Immersion Data Showing Indications Which Respond Like Lack-of-Fusion Starting in the J-Groove Weld Material

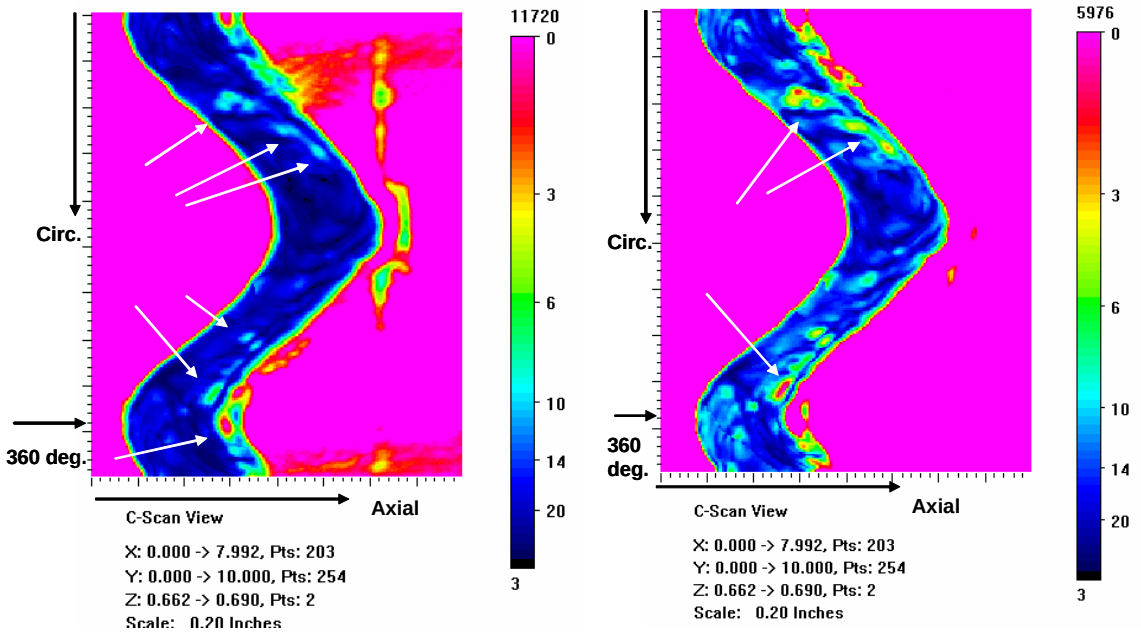

Figure 5.10. Nozzle 59, 2.25-MHz Immersion Data Showing Indications Which Respond Like Lack-of-Fusion Starting in the J-Groove Weld Material at Two Different Displayed Amplitude Settings

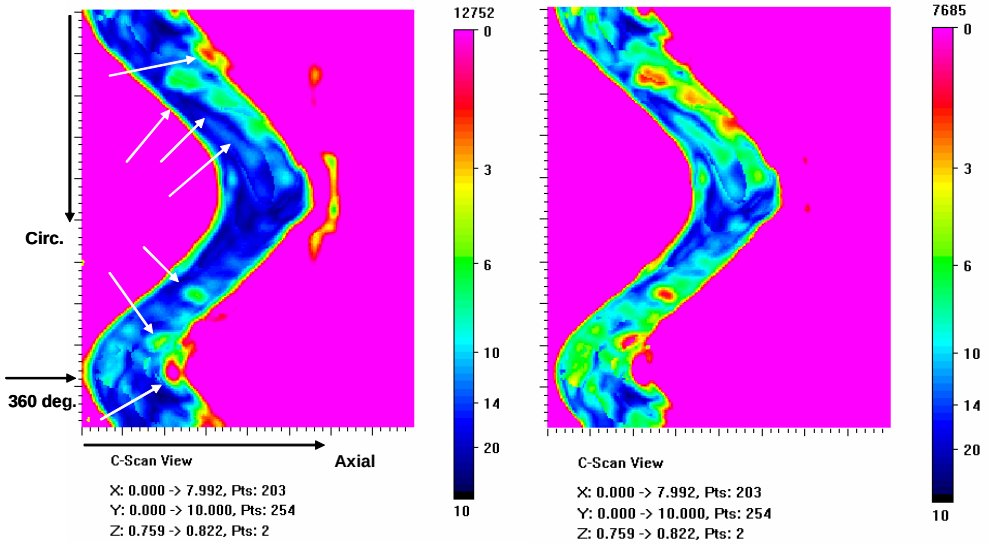

Figure 5.11. Nozzle 59, 1-MHz Immersion Data Showing Indications Which Respond Like Lack-of-Fusion Starting in the J-Groove Weld Material at Two Different Displayed Amplitude Settings

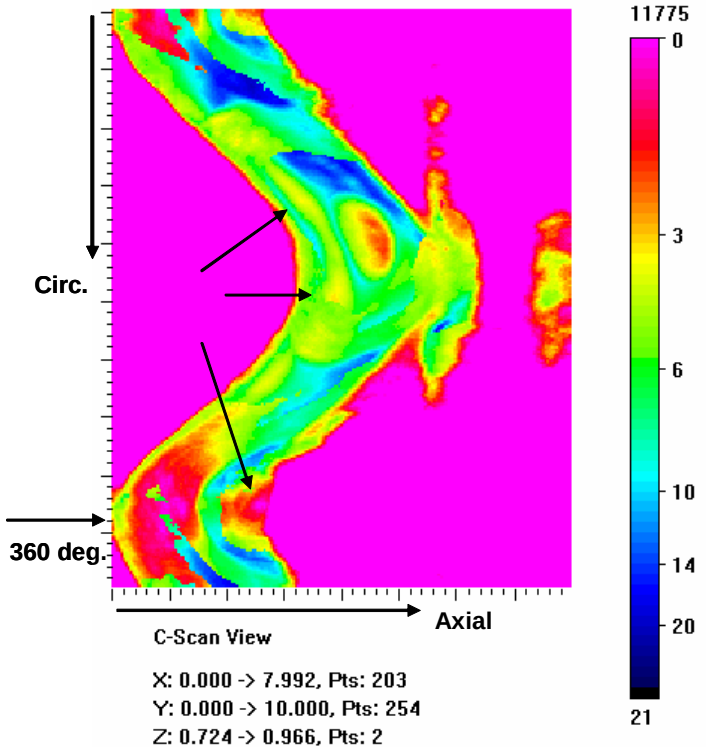

Figure 5.12. Nozzle 59, 500-kHz Immersion Data Showing Possible Lack-of-Fusion Indications Starting in the J-Groove Weld Material

5.1.4 Visual Testing Results

5.1.4.1 Penetration Tube Interior

Based on the strong ET responses for the penetration tube of Nozzle 59, a replica of the interior was recovered and examined. This Microset replica was made as part of the initial decontamination of the nozzles during a previous series of examinations on the nozzles. The Microset replica of the interior was in the form of a continuous tube approximately 254 mm (10 in.) long. The tube was cut lengthwise, stretched out, and pinned to a foam core board. The replica was then photographed in sections using the slide bar and tripod arrangement described in Section 3.5.

A 0-degree mark had been scribed onto the interior surface of the penetration tube in previous tests, and this mark was found and used to orient the results from the visual tests. The 0-degree mark was very shallow and wide, which is likely why it did not show up in the eddy current tests. The 0-degree mark is shown in Figure 5.13.

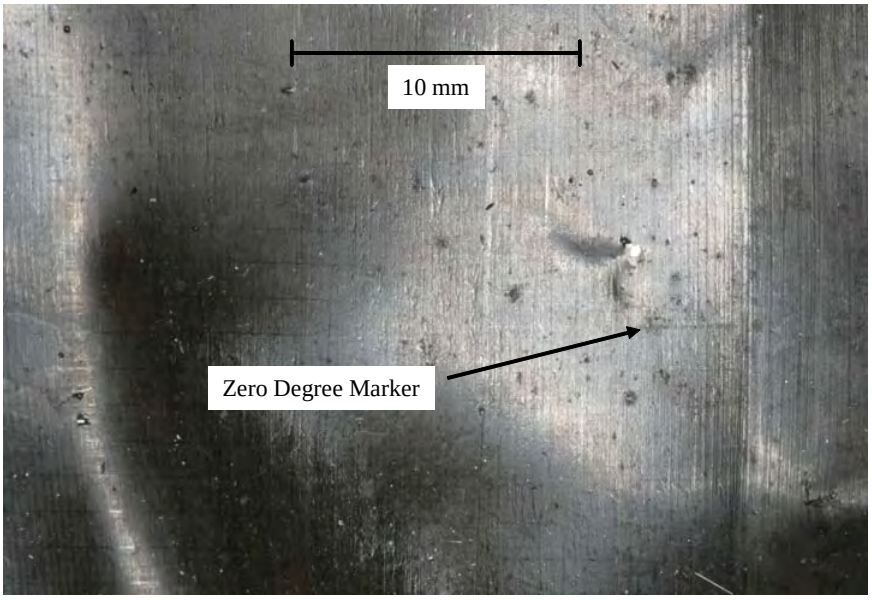

Figure 5.13. Zero-Degree Marker and Wetted End of Penetration Tube Imaged Using Replicant

The photographs were examined individually at 100% magnification using a variety of sharpness, brightness, and contrast settings. The interior of the tube showed regular circumferential machining marks and many axial scratches. Some of the deepest axial scratches were coincident with the larger voltage responses seen using ET. Figure 5.14 shows deep axial scratches cutting through the circumferential machining marks.

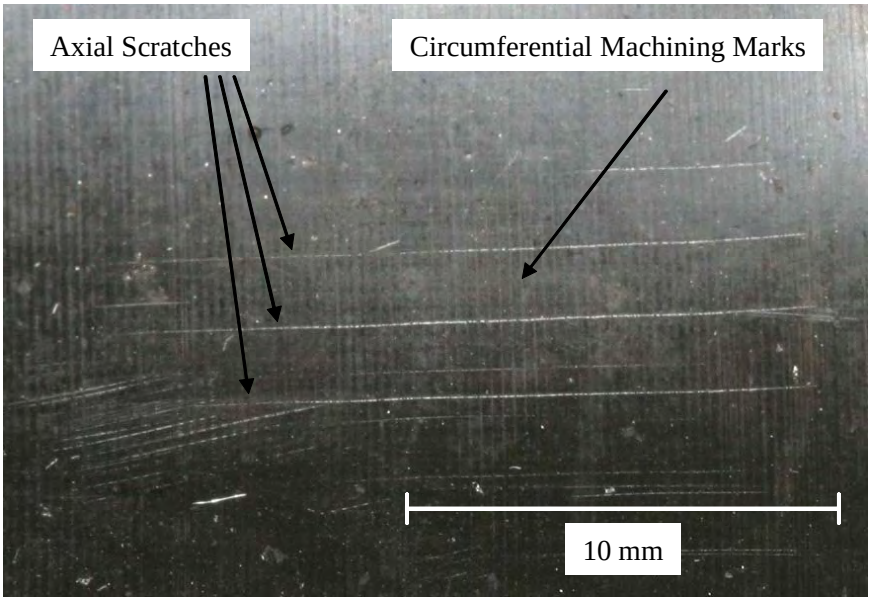

Figure 5.14. Machining Marks and Axial Scratch-Like Indications on the Interior of the Penetration Tube in Nozzle 59

Evidence for pitting or inclusions was seen in the interior of the penetration tube. It is impossible to know from the images if the pits observed are the result of inservice corrosion or are fabrication flaws. It should be noted again that this replica was taken before the etchant gel was used on the interior surface of the tube, so the pits were not caused by the acid gel. It is likely that these indications could be partially responsible for the ET responses seen in Nozzle 59. The pitting is dispersed throughout the inner surface of the tube and exists in some clusters such as the one shown in Figure 5.15. Another interesting indication was detected at close to 180 degrees, 200 mm (7.9 in.) axially into the tube. This indication appeared to be a 1.5–mm-long (0.06-in.) rough section in the tube. This section corresponds almost exactly in location to the "bright spot" ET indication seen at close to 180 degrees and below the weld line. Because the Microset polymer compound applied to the interior of the penetration tube was not of uniform thickness, thin regions stand out slightly from thicker regions when the replica is stretched out. This results in a "mottled" texture and appearance that does not reflect the topography of the interior surface of the penetration tube.

One very crack-like indication was detected in the replica of the penetration tube. Unlike the axial scratches commonly seen in the tube, this indication is curved and at an angle to the tube. It is also in a region with several large pit-like indications. This crack-like indication, at 140 mm (5.5 in.) axially into the penetration tube, is shown in Figure 5.16. Another interesting area was a rough patch in the penetration tube with possible micro-cracking. The tube appears to have undergone some sort of degradation in this region. The general area is shown in Figure 5.17; an enlargement of possible micro-cracks is shown in Figure 5.18.

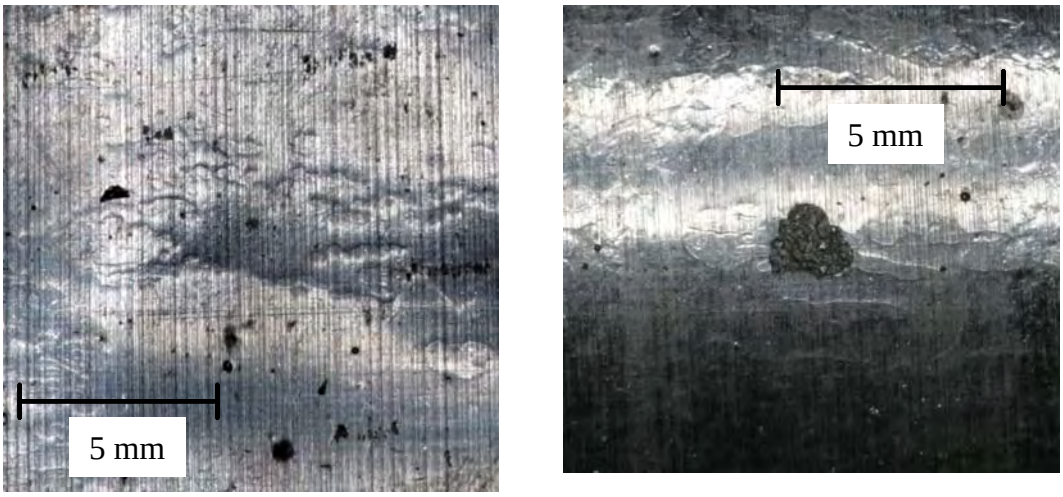

Figure 5.15. Pit-Like Indications and a Rough Patch Imaged Using High-Resolution Photographs of the Replicated Surface. The pit-like indications are located throughout the tube, while the rough patch is located at close to 180 degrees and 200 mm (7.9 in.) axially.

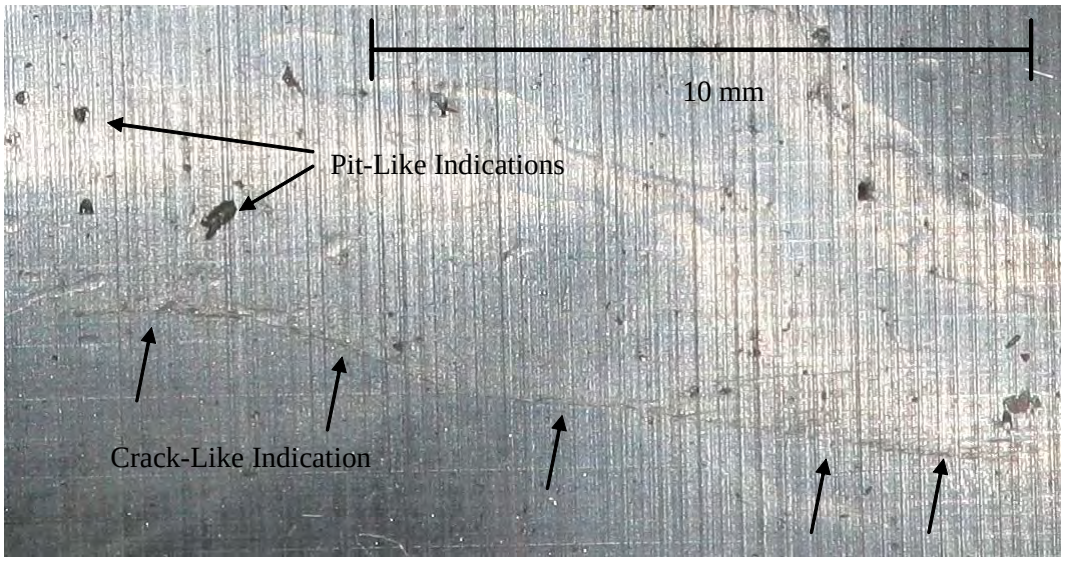

Figure 5.16. Crack-Like Indication Located at 315 Degrees Clockwise Rotation and 140 mm (5.1 in.) Axially in the Penetration Tube

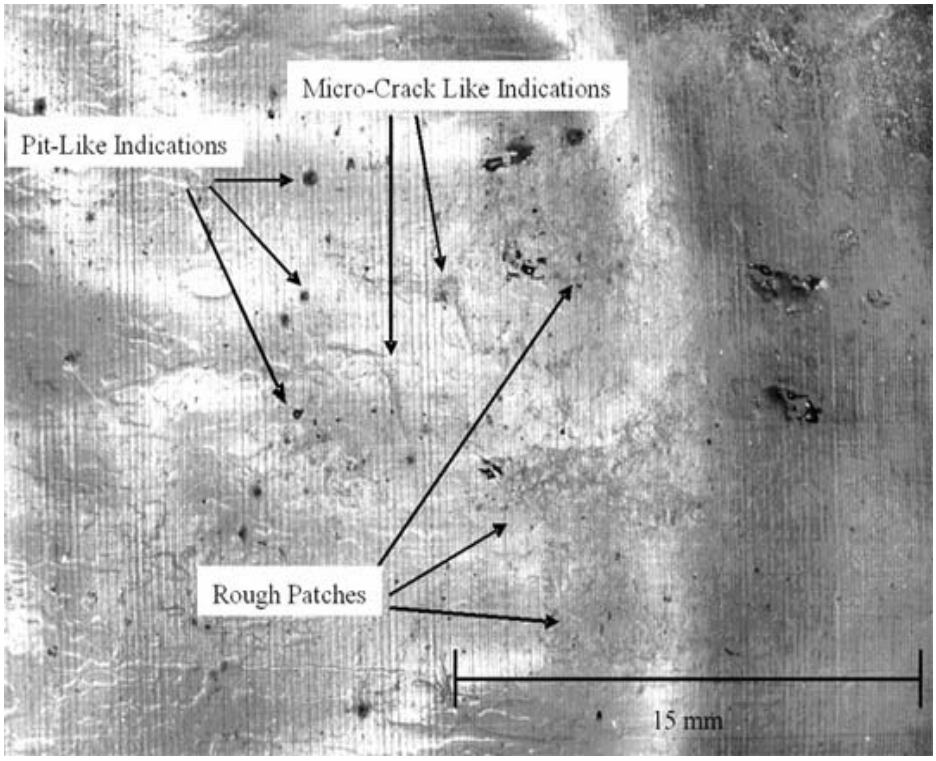

Figure 5.17. Rough Section and Possible Micro-Cracks in the Penetration Tube Interior

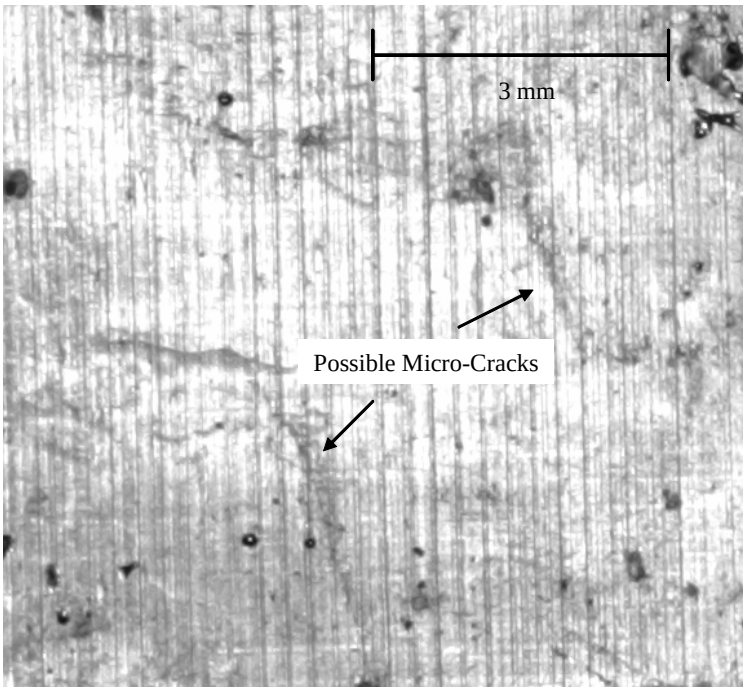

Figure 5.18. Micro-Crack–Like Indications in the Penetration Tube of Nozzle 59

5.1.4.2 J-Groove Weld and Buttering

A replica of the J-groove weld was taken and examined using the high-resolution camera. The surface of the J-groove weld showed no evidence of grinding but did show a lot of texture and features related to the welding process—that is, visible weld passes and ridges between the weld passes. The texture of the weld would make it difficult to find cracks that follow a string of weld beads but also would make it very easy to detect a crack that cuts across several weld beads.

No large cracks were detected in the J-groove weld material. Several small crack-like indications were detected. The small cracks are typically on the order of 1–5 mm (0.04–0.20 in.) in length and are aligned circumferentially along individual weld beads. It is difficult to determine if these indications are actual cracks or tortuous lines on the weld beads. The small crack-like indications are found primarily from 112 to 135 degrees. Two examples are shown in Figure 5.19.

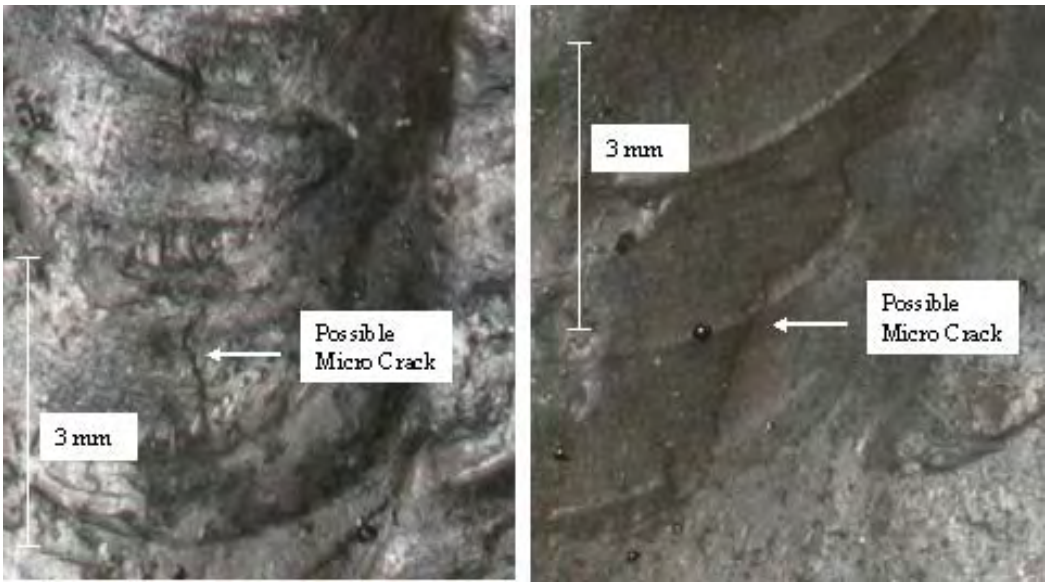

Figure 5.19. Small Crack-Like Indications near 120 Degrees in the J-Groove Weld

The largest detected crack-like indication in the J-groove weld of Nozzle 59 was 10 mm (0.4 in.) long and located at 225 degrees. This indication cut across three weld beads and showed a jagged path (Figure 5.20).

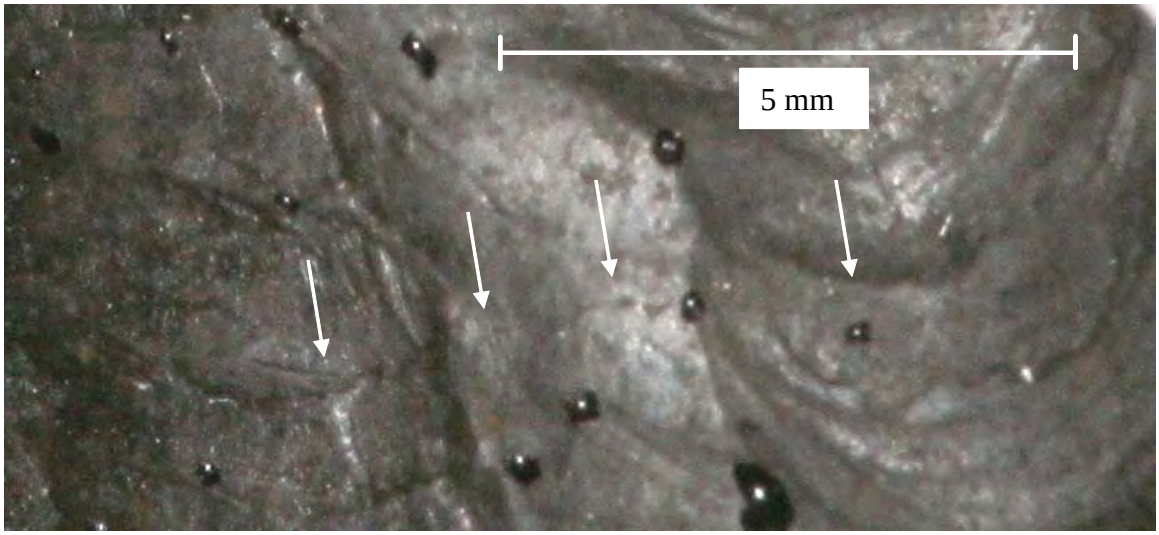

Figure 5.20. Crack-Like Indication in the J-Groove Weld of Nozzle 59 at 225 Degrees

5.2 Control Rod Drive Mechanism 31

5.2.1 Penetration Tube Eddy Current Results

Nozzle 31 had only low-level indications (Figure 5.21). The rectangular indication at the left corresponds to a visible 0-degree mark, repeated at 360 degrees (233 mm). The set of diagonal indications, extending from 50 to 150 mm (2 to 5.9 in.) circumferential and 220 to 270 mm (8.7 to 10.6 in.) axial, corresponds to a visibly scratched region. The scan with the probe oriented at 45 degrees displayed a low-level linear indication (boxed in Figure 5.22), but it was not visible in either of the scans with the probe oriented to 0 degrees.

5.2.2 Eddy Current Examination of J-Groove Weld

The J-groove weld area of Nozzle 31 was examined using a plus-point differential eddy current probe. The scan was conducted by performing a series of rectangular scans using the *x*-*y* scanner. The rectangular scans were made every 30° to cover the weld surface with a large degree of overlap in the scans. The scans were taken as close to the penetration tube as possible and, in general, covered the buttering and 12–15 mm (0.5–0.6 in.) of the weld taper. The scans were made with the probe in the normal position and with the probe rotated to 45 degrees to ensure good coverage of the weld with high sensitivity. The rectangular scans were assembled into an ellipse to show the locations of areas of interest. The assembled ellipses for the 0- and 45-degree rotations are given in Figures 5.23 and 5.24.

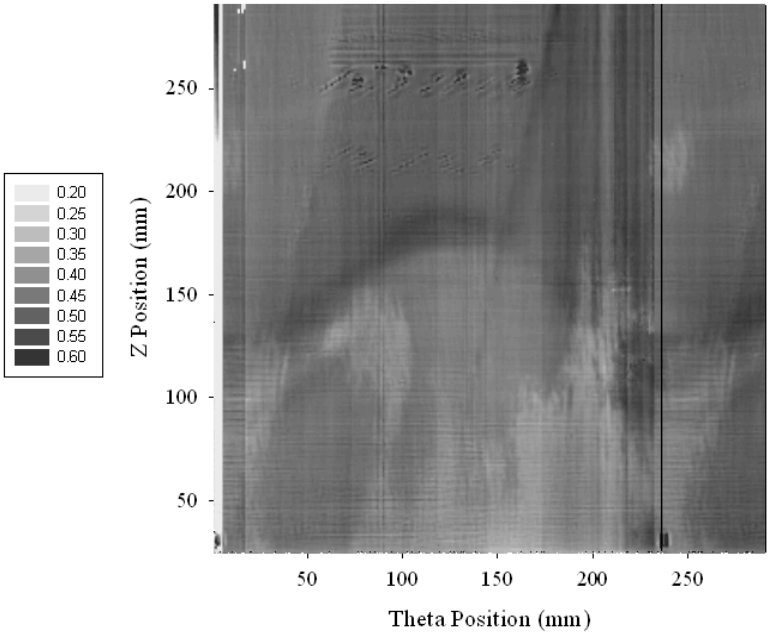

Figure 5.21. Nozzle 31, Scan Taken with Probe Oriented to 0 Degrees, 350 kHz with the Image Set to Display Scratches

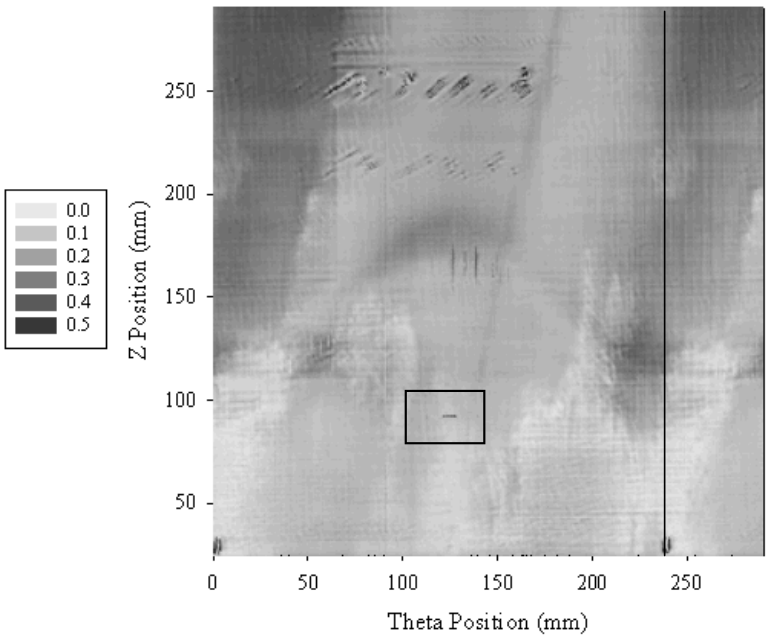

Figure 5.22. Nozzle 31, 45-Degree Rotated Probe Scan, 350 kHz, Showing Linear Indication (centered in box, about 125 mm [4.9 in.]) circumferential and 100 mm [3.9 in.] axial)

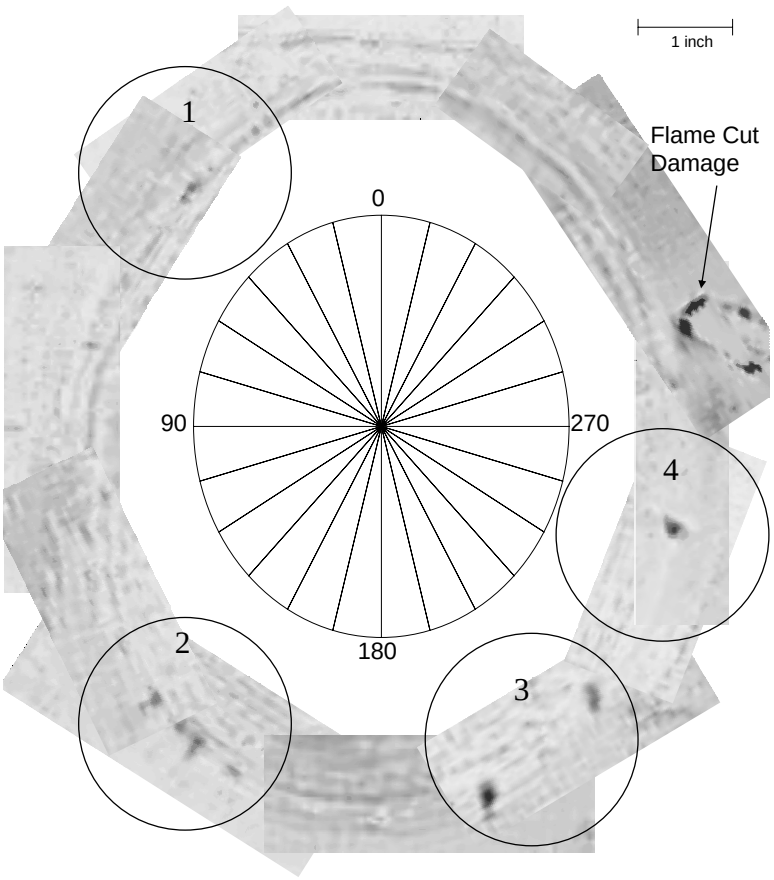

Figure 5.23. Eddy Current Results for 0-Degree Scan of the J-Groove Weld of Nozzle 31. Four areas of interest were found at close to 60, 150, 215, and 270 degrees.

Four areas of interest were found in this data. The areas of interest are at 60, 150, 215, and 270 degrees. These areas were examined again in more detail to quantify the indications. The scans were made using 0.5-mm steps and were repeated until no signs of lift-off or other possible scanning errors were present in the scan. This scanning regime yielded a total of 16 indications considered crack-like. These ET responses, their locations, lengths, and ET response strengths are given in Table 5.1. The ET responses given in the table are the maximum response found during scanning and re-scanning the areas of interest at a variety of probe rotation angles. This ET response strength, 1.8 V with a gain of 15 dB, was determined by using the ET response strength of ET indication 14, which was confirmed as a crack via PT testing (see Section 5.2.6.).

The area near 60 degrees has seven indications between 2 to 5 mm (0.08 to 0.2 in.) in length and with ET responses from 1.8 V to 3.3 V over a 50-mm (2-in.) range at the weld/buttering interface. The flaws appear to be point-like or circumferential, and the responses from the flaws are strongly affected by the probe direction. This cluster of seven indications is unique in the J-groove weld, and no such indications are present at the mirror-image position at 300 degrees, which should have a similar stress field while in service. These indications are numbered 1 through 7 from Table 5.1. Figure 5.25 shows the 0-degree and 45-degree rotation scans of the region near 60 degrees.

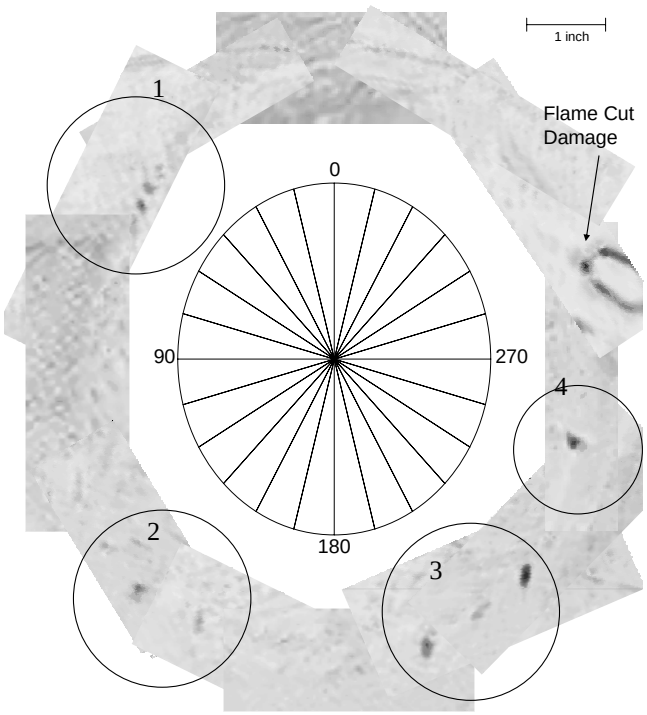

Figure 5.24. Eddy Current Results for 45-Degree Scan of the J-Groove Weld of Nozzle 31. Four areas of interest were found at close to 60, 150, 215, and 270 degrees.

Table 5.1. Comprehensive Eddy Current Testing Responses on the J-Groove Weld of Nozzle 31

Indication	Angle	Length	Max Voltage	% EDM Notch
1	45°	2 mm	2.1	20
2	50°	5 mm	1.9	18
3	55°	4 mm	3.3	32
4	65°	2 mm	1.8	18
5	70°	4 mm	2.2	21
6	75°	3 mm	2.5	24
7	80°	3 mm	2.3	22
8	130°	4 mm	2.3	22
9	145°	10 mm	3.2	31
10	155°	8 mm	3.3	32
11	160°	14 mm	4.1	40
12	170°	5 mm	2.6	25
13	200°	8 mm	4.6	45
14	215°	10 mm	1.8	18
15	225°	9 mm	4.6	45
16	255°	7 mm	4.2	41

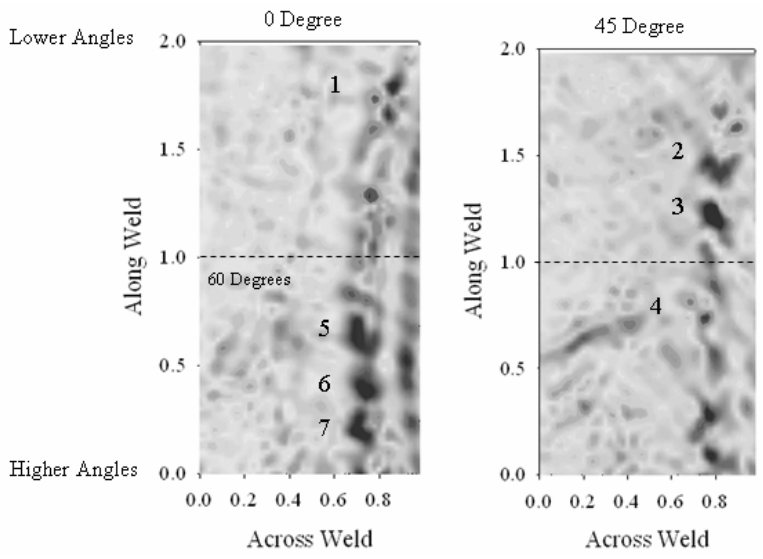

Figure 5.25. 0- and 45-Degree Scans Centered on 60 Degrees on the J-Groove Weld of Nozzle 31

The area near 150 degrees was also re-scanned to quantify the indications in this area. Five indications were found at the weld/buttering interface, ranging from 4 mm to 14 mm and from 2.3 V to 4.1 V. Two of the indications—8 and 12—were point-like, and three—9, 10, and 11—were linear. Only indication 9 gave a significant ET response to both probe rotations. It is worth noting that indications 9, 10, and 11 are axial and are angled slightly toward 180 degrees. The ET results for this region are given in Figure 5.26.

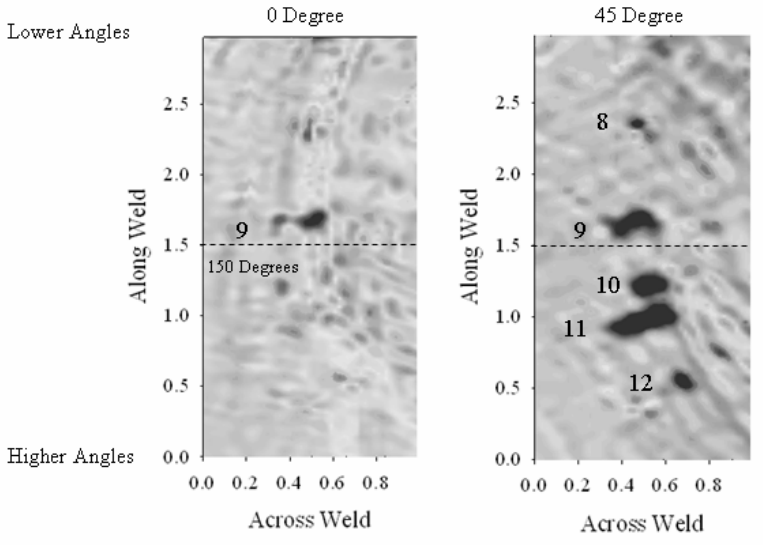

Figure 5.26. 0- and 45-Degree Scans Centered on 150 Degrees on the J-Groove Weld of Nozzle 31

The next region of interest was centered around 210 degrees at the weld/buttering interface. Three indications were found—13 through 15from Table 5.1. Indications 13 and 15 are 8–9 mm (0.3–0.35 in.) long and have responses of 4.6 V. Indications 13 and 15 show up clearly in both probe orientations. Both indications are axial in orientation but are also slightly angled toward 180 degrees, much like the indications centered around 150 degrees. Indication 14 is circumferential, has an ET response of 1.8 V, and has a discernable response only when the probe is oriented at 45 degrees. The ET results for this region are given in Figure 5.27.

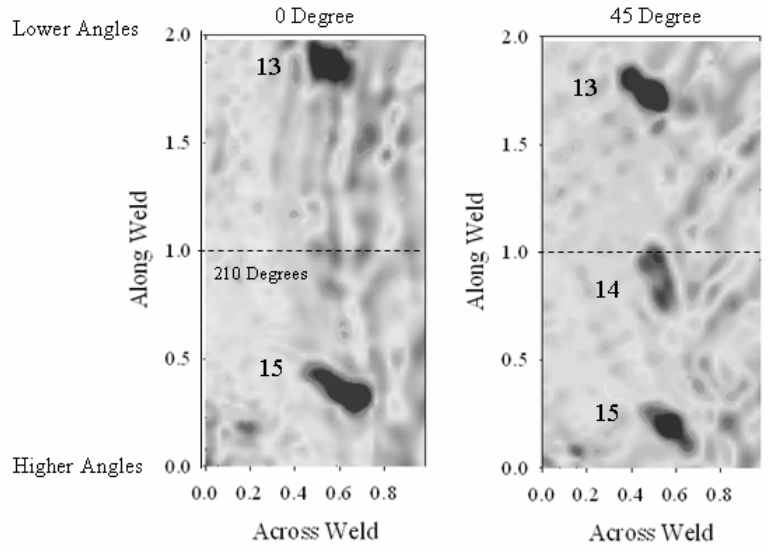

Figure 5.27. 0- and 45-Degree Scans Centered on 210 Degrees on the J-Groove Weld of Nozzle 31

The last ET indication was found at 255 degrees at the weld/buttering interface. This indication is 8 mm (0.3 in.) long and has an ET response of 4.2 V. The indication is much more pronounced when the probe is at 0 degrees but is still present at 45 degrees. The ET results for this region are given in Figure 5.28.

5.2.3 Time-of-Flight–Detected Indications for Nozzle 31

In general, the higher-frequency 7.5-MHz probe set generated many more responses than the 5-MHz set. Figure 5.29 shows a weak TOF-shaped indication located at 91 mm (3.6 in.) from the start. A stronger indication without the TOF shape acquired also at 5 MHz is shown in Figure 5.30. Figure 5.31 shows a TOF shape and two other indications acquired at 7.5 MHz. The TOF-shaped indication in Figure 5.25 is lower in amplitude at −7.2 dB than the other two indications in Figures 5.32 and 5.33, with responses of −5.3 and −3.0 dB, respectively. These response levels are comparable to the responses from the axial calibration notches shown earlier in Table 4.3.

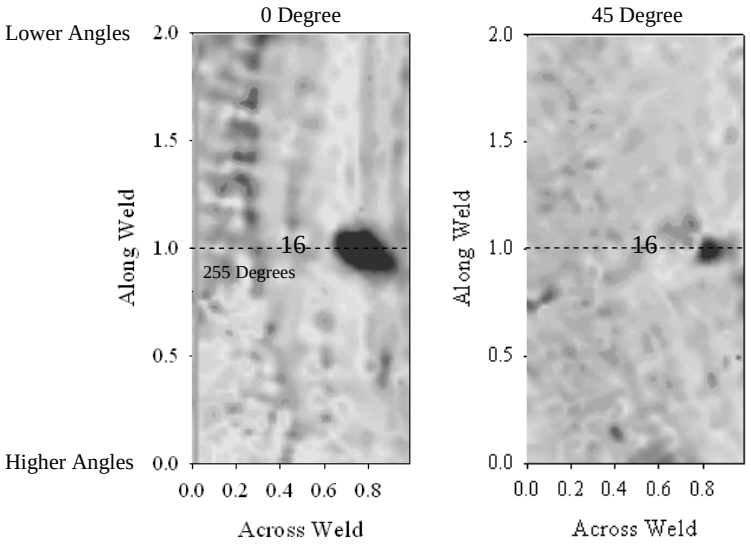

Figure 5.28. 0- and 45-Degree Scans Centered on 255 Degrees on the J-Groove Weld of Nozzle 31

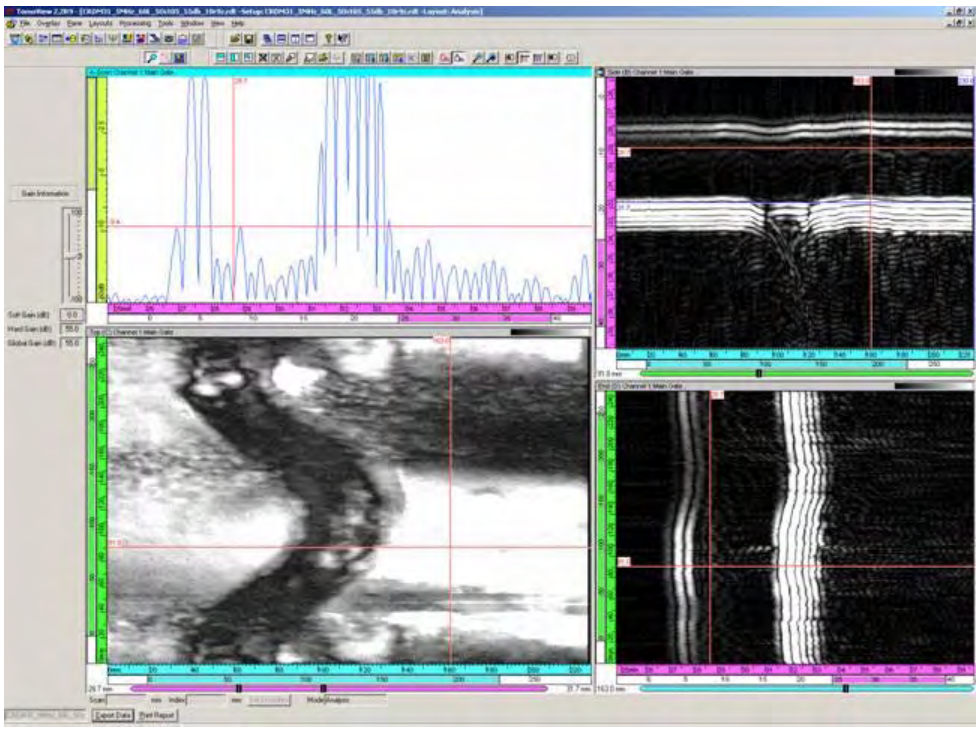

Figure 5.29. Time-of-Flight Shape in 5-MHz Time-of-Flight Diffraction Data from Nozzle 31 at 91 mm (3.6 in.) CCW, 163 mm Axial with −9.4-dB Response

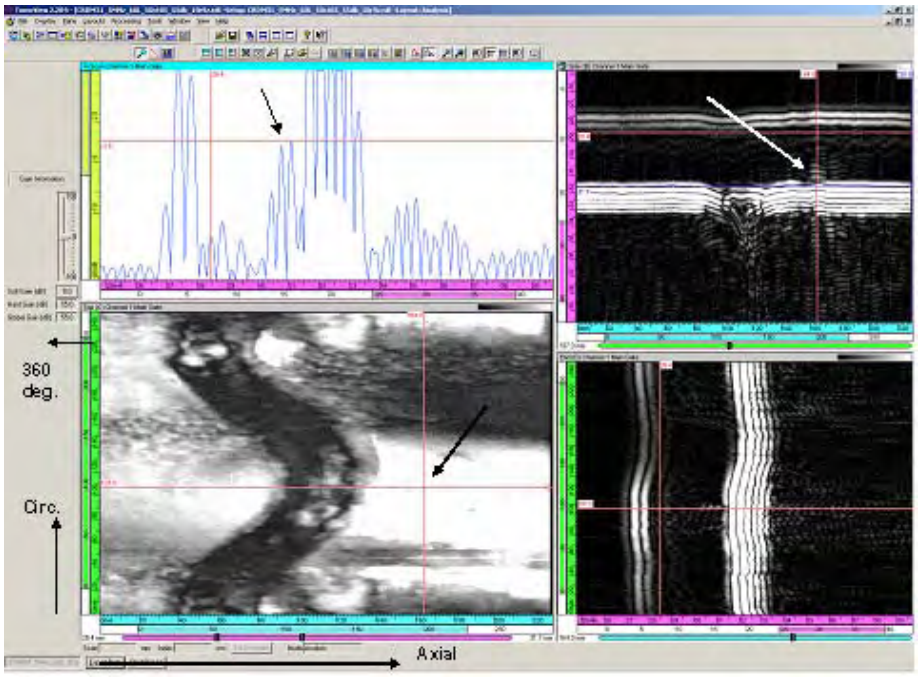

Figure 5.30. Interesting 5-MHz Time-of-Flight Diffraction Indication from Nozzle 31 at 107 mm (4.2 in.) CCW, 164 mm (6.5 in.) Axial with a −3.6-dB Response

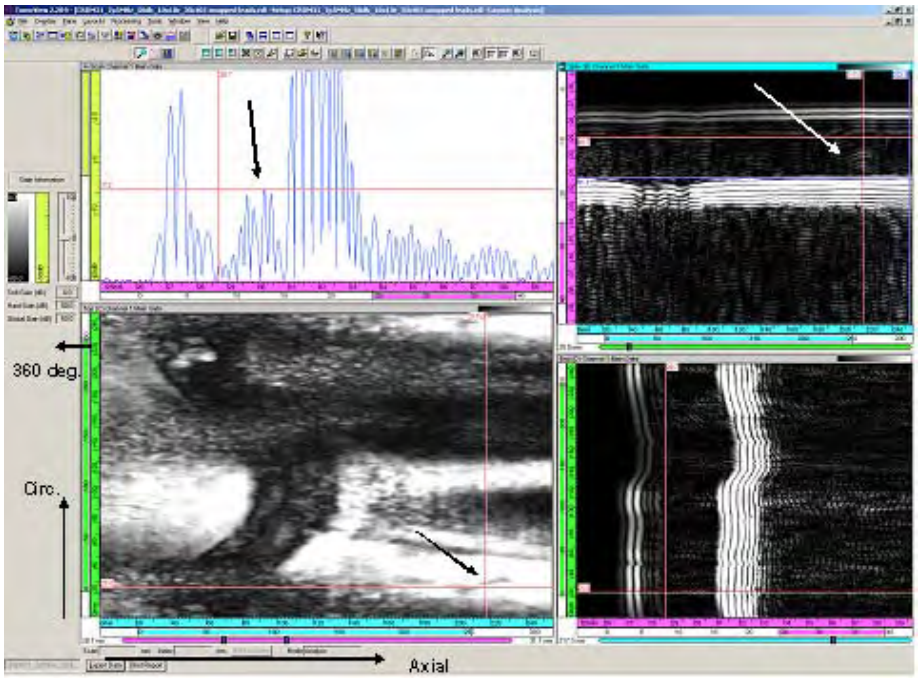

Figure 5.31. Time-of-Flight Shape in 7.5-MHz Time-of-Flight Diffraction Data from Nozzle 31 at 25 mm (1 in.) CCW, 217 mm (8.5 in.) Axial with −7.2-dB Response

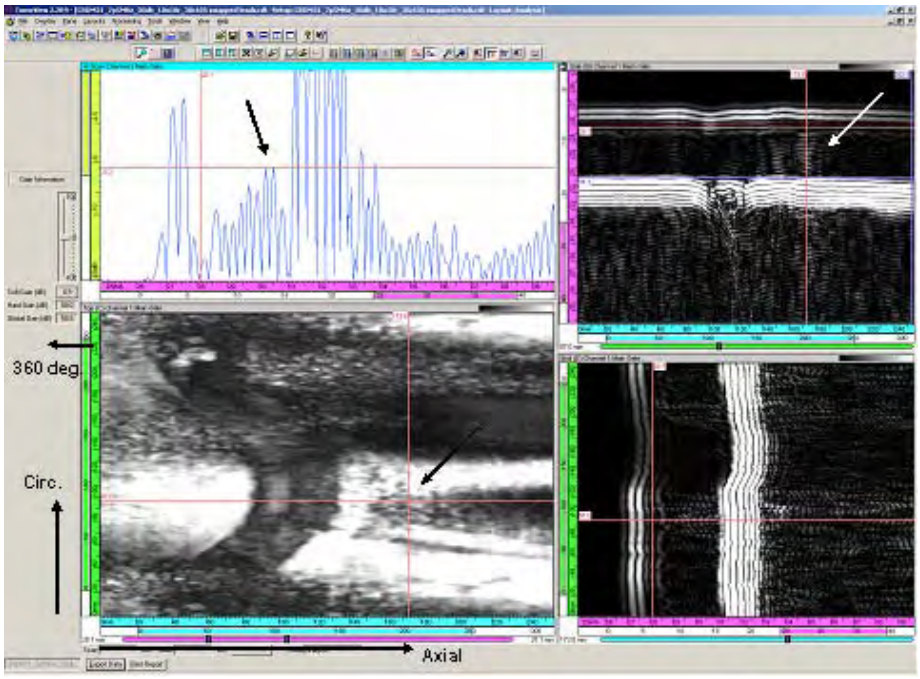

Figure 5.32. Interesting 7.5-MHz Time-of-Flight Diffraction Indication from Nozzle 31 at 97 mm (3.8 in.) CCW, 173 mm (6.8 in.) Axial with a −5.3-dB Response

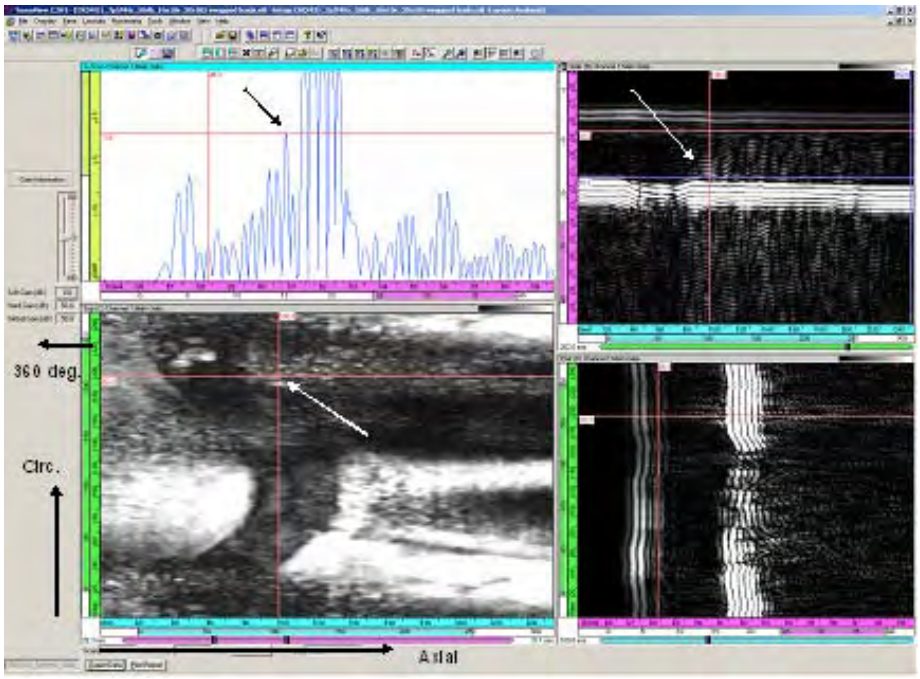

Figure 5.33. Interesting 7.5-MHz Time-of-Flight Diffraction Indication from Nozzle 31 at 202 mm (8 in.) CCW, 100 mm (3.9 in.) Axial with −3.0-dB Response

5.2.4 Immersion Ultrasonic Testing Results

Numerous indications at all depths were found by UT immersion inspection in Nozzle 31 that map out the weld, as do the indications from Nozzle 59. Most of the indications started in the J-groove weld metal.

C-scan images of indications from the J-groove weld material at the four inspection frequencies are shown in Figures 5.34 through 5.38. The 5-MHz data in Figure 5.34 show a large-amplitude indication near 360 degrees. This same indication is seen also in the 2.25-, 1.0-, and 0.5-MHz data (Figures 5.35 through 5.38). While in almost all cases the SAFT process was able to improve the signal-to-noise ratio without causing any significant change to the shape or nature of the indications, the 2.25-MHz data showed some interesting elongated indications prior to applying the SAFT process that became rounded when SAFT was applied. Figure 5.36 shows the unprocessed data. The elongated indications are at 90 degrees and from 270 to 300 degrees and appear to start in the weld metal, not the penetration tube. It should be noted that the Z data shown in Figure 5.25 is not compatible with the others, as the data in Figure 5.36 was not processed in the same way and there is no correction for the curvature of the data. The lower-amplitude lack of fusion indications at 178 mm (7 in., 286 degrees) in the circumferential direction are seen at all frequencies except 500 kHz.

5.2.5 Visual Testing Results

Microset polymer was applied to the J-groove weld surface of Nozzle 31. The replica covered the entire weld, including the buttering and 10 mm (0.4 in.) up the penetration tube. The examination of the replicas of the J-groove weld of Nozzle 31 showed two crack-like indications and two possible micro-crack-like indications. Figure 5.39 shows what appears to be a very wide crack cutting across several weld passes. Penetrant dye testing and ET testing did not confirm this as a crack, however; and it is possibly an irregularity in the weld. Bare-metal photography of this area was inconclusive.

A possible crack was found also at close to 135 degrees. This indication cuts across two weld passes but is very faint, and an indication this weak is common for only very tight cracks. This indication is shown in Figure 5.40. This indication was not confirmed by either PT or ET and is possibly a scratch or an irregularity in the weld. Bare-metal photography of the area was inconclusive.

Another region showing crack-like indications was detected at 275 degrees. This indication shows several small cracks, two of which appear to link. The region and the cracks are small, only 10 mm (0.4 in.) across, and could be craze cracking in the weld. This region is shown in Figure 5.41. A red piece of debris picked up by the Microset polymer is seen in Figure 5.41 as well. These indications are not confirmed by either PT or ET and are possibly a scratch or an irregularity in the weld. Bare-metal photography of the area was inconclusive.

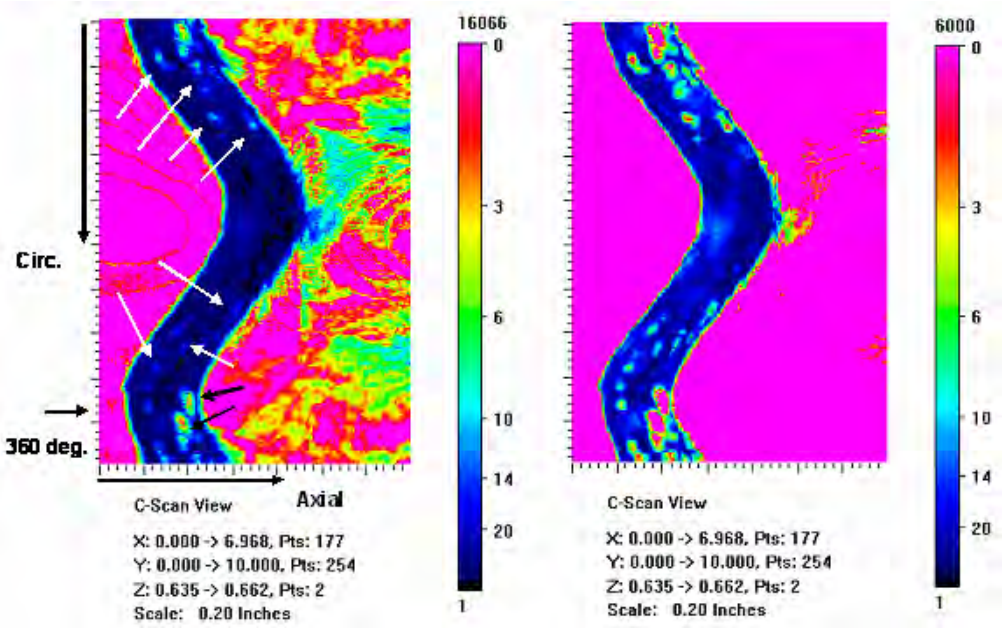

Figure 5.34. Nozzle 31, 5-MHz Immersion Data Showing Indications in the J-Groove Weld Material at Two Different Displayed Amplitude Settings

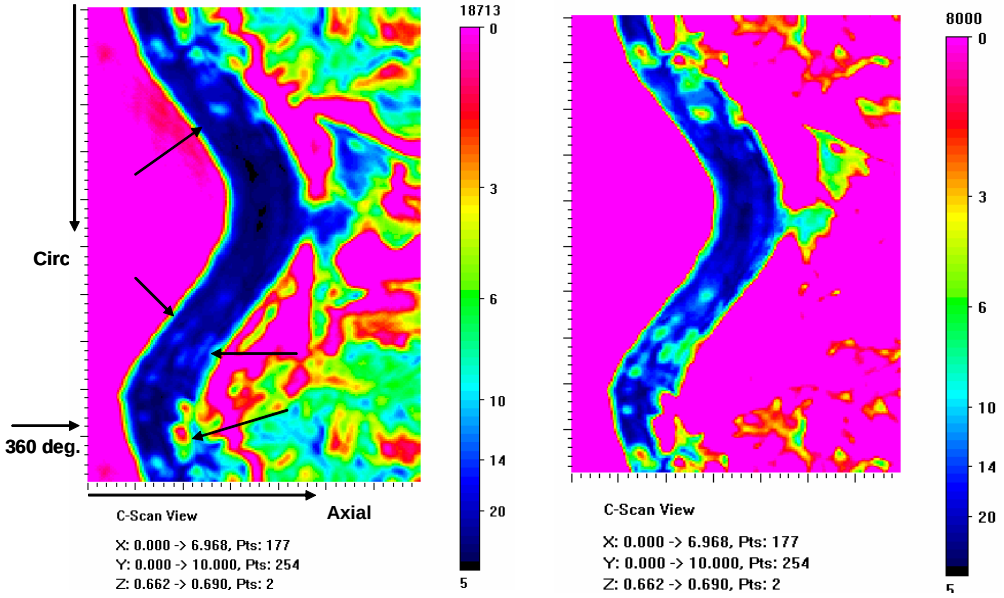

Figure 5.35. Nozzle 31, 2.25-MHz Immersion Data Showing Indications in the J-Groove Weld Material at Two Different Displayed Amplitude Settings

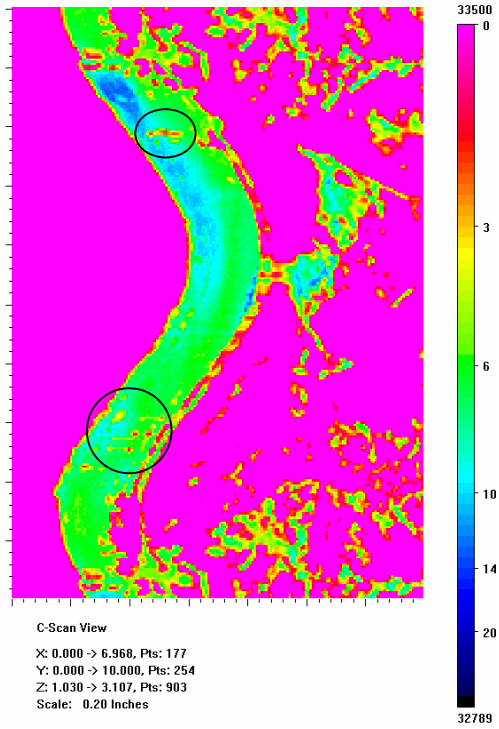

Figure 5.36. Unprocessed 2.25-MHz Data Showing Elongated Indications at 90 Degrees and from 270 to 300 Degrees (circled). These elongated indications are rounded by the SAFT processing.

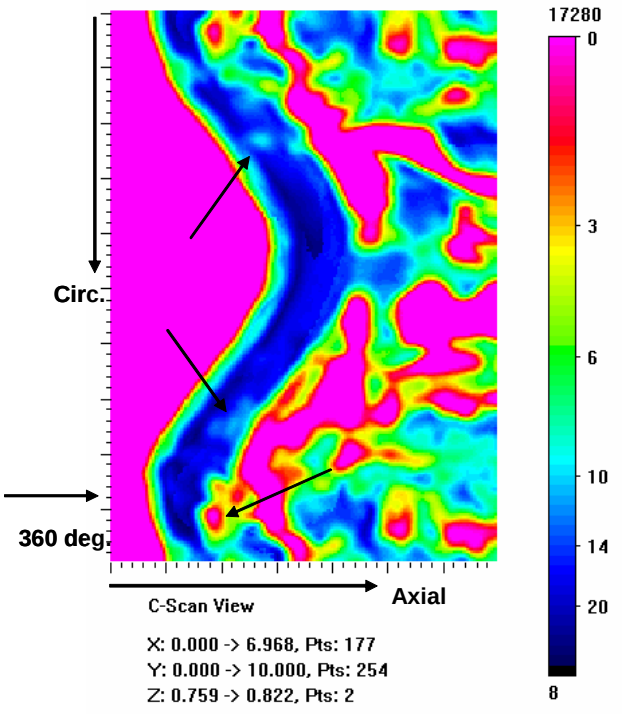

Figure 5.37. Nozzle 31, 1-MHz Immersion Data Showing Indications in the J-Groove Weld Material

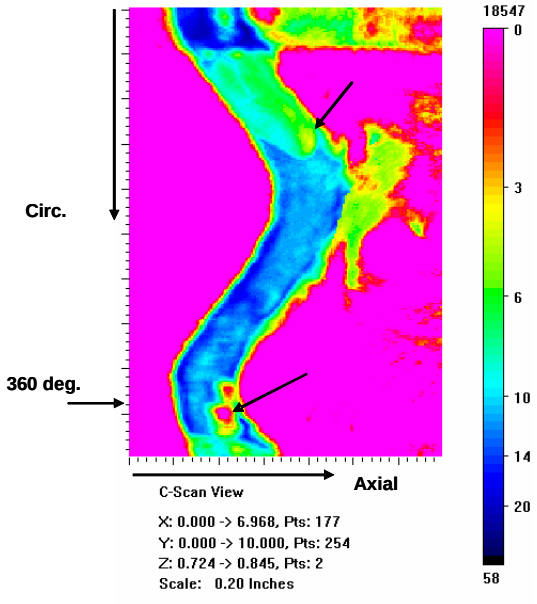

Figure 5.38. Nozzle 31, 500-kHz Immersion Data Showing Indications in the J-Groove Weld Material

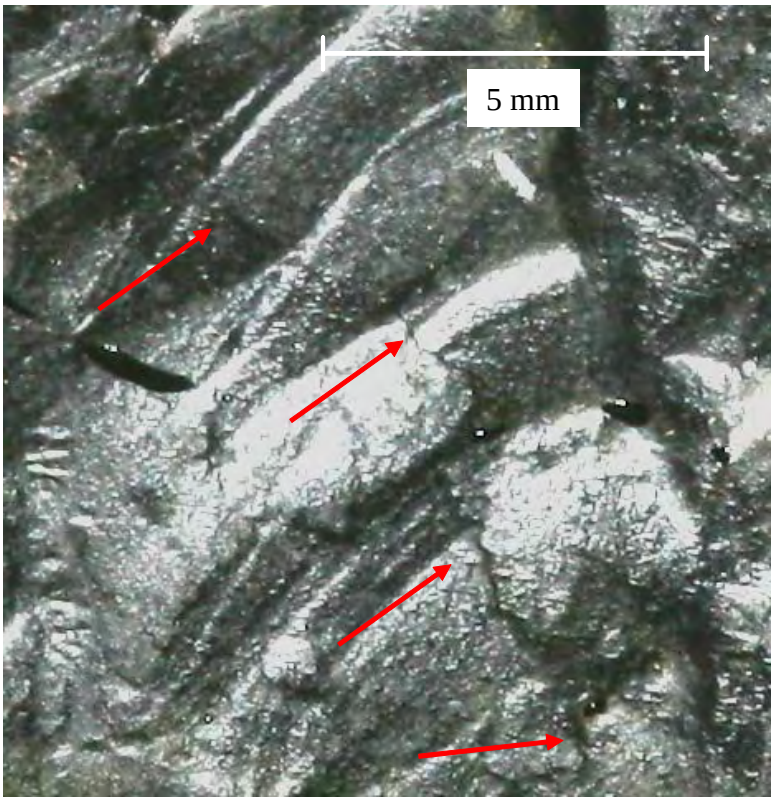

Figure 5.39. Crack-Like Indication 10 mm (0.0004 in.) Long at 145 Degrees CCW

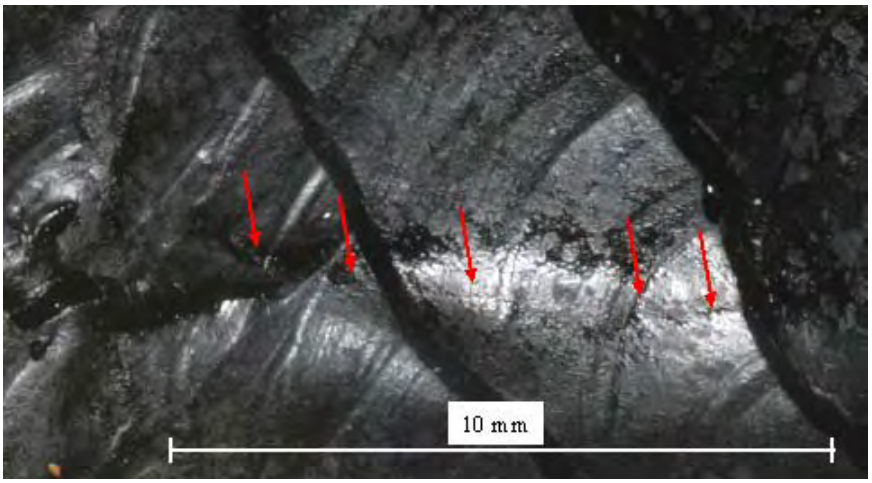

Figure 5.40. Crack-Like Indication at 135 Degrees CCW, 5 to 10 mm (0.0002 to 0.0004in.) Long

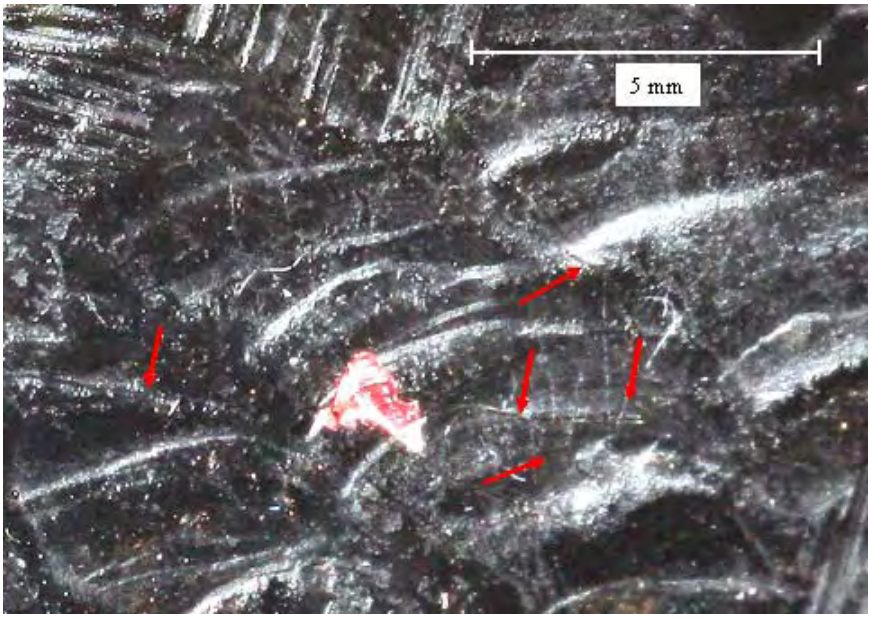

Figure 5.41. Cracked Area at 275 Degrees CCW. This branched crack-like indication traverses through the area. The cracked region is 1 cm^2.

Finally, a longer crack-like indication was detected at close to 270 degrees. This indication was longer, at least 15 mm (0.6 in.) long and possibly 20 mm (0.8 in.) in length. The indication has a low contrast against the black replica, and there are two possible "ends" for the crack. This crack-like indication is shown in Figure 5.42. This crack-like indication was not confirmed with either PT or ET. Bare-metal photography of the area showed it to be a deep scratch and not a crack.

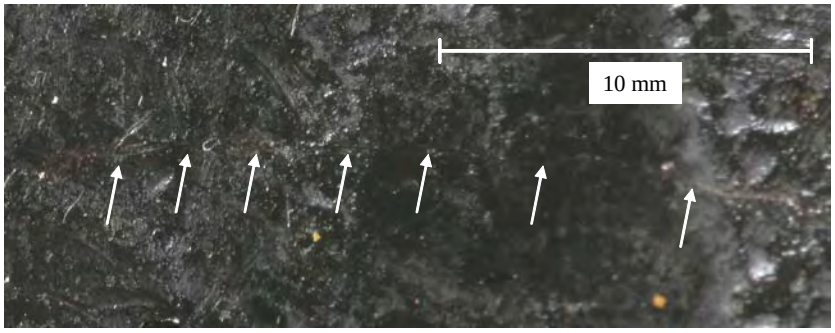

Figure 5.42. Crack-Like Indication at 315 Degrees CCW. The indication leaves the J-groove weld and propagates into the buttering. The indication is 15–20 mm (0.6–0.8 in.) long.

5.2.6 Penetrant Testing Results

Penetrant testing was applied to the surface of the J-groove weld of Nozzle 31. This was done to verify cracks found earlier using Microset polymer and bare-metal photography and to find any cracks missed by these techniques.

The PT testing showed that the major indications found by the examination of the J-groove weld using a replicate were scratches, not cracks. Two short crack-like indications were found using PT, one at 200 degrees and one at 225 degrees. A pore-like indication was found at 190 degrees, and a small linear indication was found at 215 degrees as well. These indications are shown in Figure 5.43. After the penetrant developer was cleaned off, these areas were re-photographed with the 16.7-megapixel Canon camera using the macro lens. The pore at 190 degrees and the linear indication at 215 degrees could not be detected, but the cracks at 210 and 235 degrees were confirmed using the photographs. Figure 5.43 shows these crack-like indications and the pore-like indication.

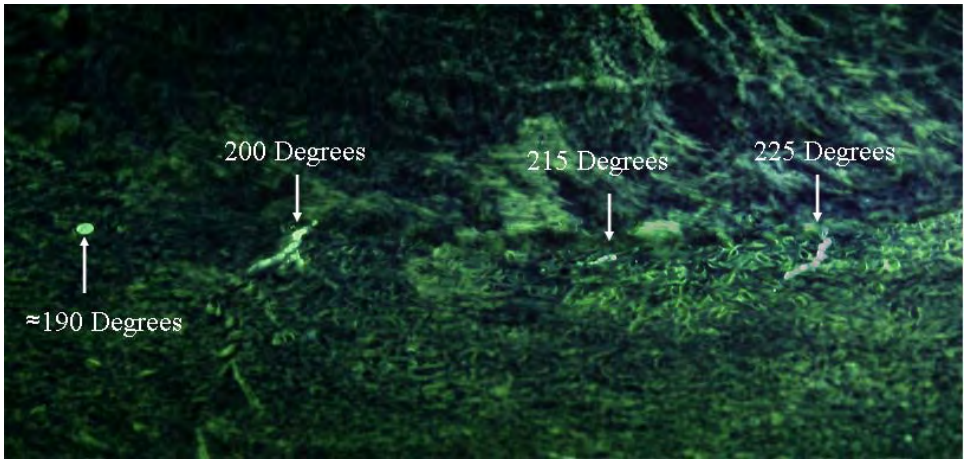

Figure 5.43. Penetrant Results at the Weld/Butter Interface Around 210 Degrees

5.2.7 Direct Photography

The cracked areas identified via VT of surface replicas, ET, and PT were photographed in detail in an attempt to confirm the presence of cracking. No images of cracks were detectable near 60 or 150 degrees or at 255 degrees. Crack-like indications were confirmed by direct photography at 200 and 225 degrees. Both crack-like indications are at the weld/buttering interface and extend primarily into the buttering. These crack-like indications are shown in Figures 5.44 and 5.45. It is difficult to measure the length of the indications, as the beginning and end of the flaws are too tight and the surface is not ideal. The best approximation is that the crack-like indication at 200 degrees is 7 mm long, which is shorter than the 10 mm determined via ET, and the crack-like indication at 225 degrees is 9 mm long, which is the same length as determined by ET.

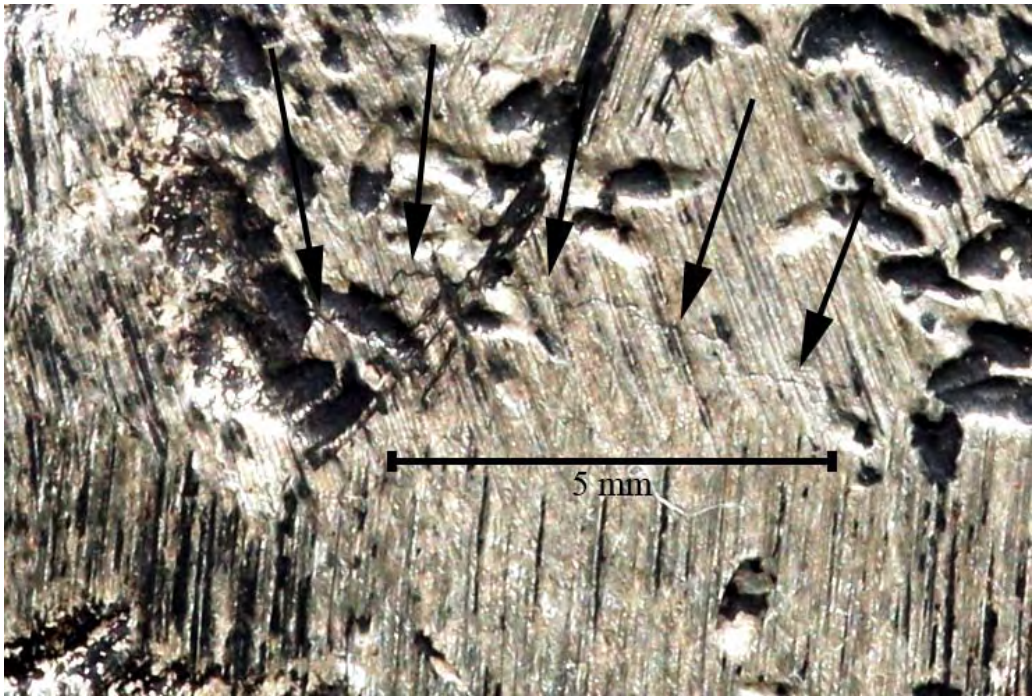

Figure 5.44. Crack-Like Indication Imaged Via Visual Testing at the Weld/Buttering Interface at 200 Degrees

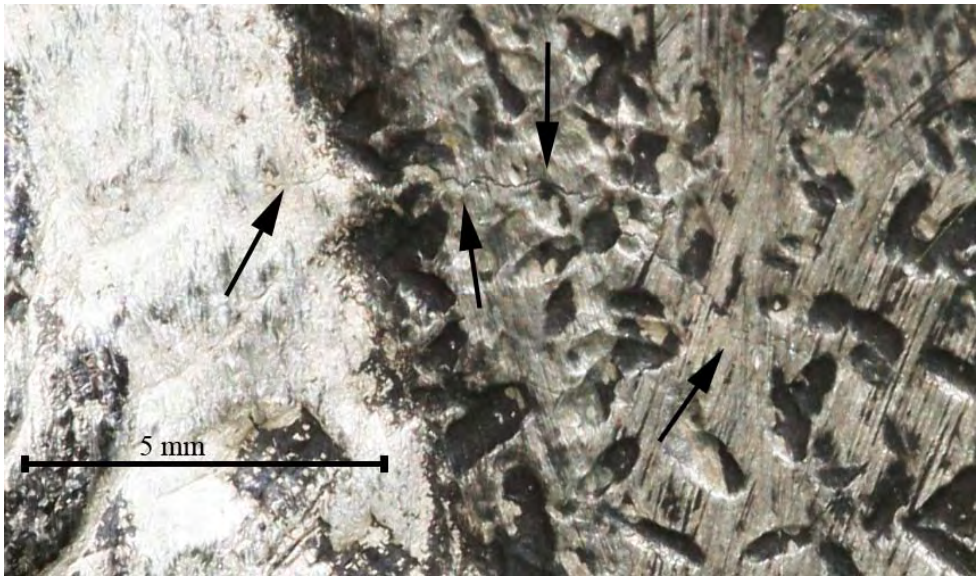

Figure 5.45. Crack-Like Indication Imaged Via Visual Testing at the Weld/Buttering Interface at 225 Degrees

5.3 Nondestructive Examination Results Summary

The NDE techniques found many indications in the two nozzles, and the task of analyzing the data for a possible leakage path is complex. In very few cases did more than one technique agree on any one location as being potentially cracked. It is also important to focus efforts on finding cracks in areas that would lead to leakage. There are two potential leakage paths through the nozzle. The path with the least material between the primary coolant and the outside of the reactor is through the wetted side of the penetration tube to the interference fit. The tube also presents a large surface area for cracking. The second path is through the J-groove and buttering weld metal to the interference fit. This area, which is thicker and has less area than the tube, is a weld and has heat-affected areas and areas where the weld metal has mixed with the carbon steel. The weld also will have residual stresses and service-induced stresses. This section focuses on the areas likely to lead to leakage and presents the data fusion used as part of the data analysis.

5.3.1 Nozzle 59 Penetration Tube

The penetration tube of Nozzle 59 was examined using ET, TOFD, and visual testing via replicas created with Microset polymer. The Nozzle 59 penetration tube contained many ET, TOFD, and VT indications that suggest cracking. One would expect that a crack that penetrates into the tube from the inner surface should show up in each NDE method, while innocuous features are less likely to appear on all three techniques. An embedded volumetric flaw such as an inclusion or a void in the penetration tube would be detectable by TOFD but not by ET or VT. Deep scratches in the surface of the tube would be detected by ET, identifiable as scratches and not cracks by VT, and not detectable by TOFD. TOFD would detect this by loss of the lateral wave if it is a deep scratch.

The combined results of all three techniques are shown in Figure 5.46. The TOFD data have been reversed from what was shown in Section 5.1.2 to allow for the overlaying of the ET data, which were taken clockwise. The TOFD data vertical positions were adjusted to match the ET vertical positions.

The area highlighted in Figure 5.46 Region 1 (and 1a, a repeat of 1) has the weak-voltage ET responses but has only one TOFD indication, and the VT results showed deep scratches but no crack-like indications. This area would be interesting to examine with the tube cut open to determine what caused these ET and VT results.

Region 2 and 2a (repeat of 2) shows up on the VT as an area with a rougher texture and was heavily pitted. Also, some possible microcracks were detected. There were weak ET responses and one TOF-shaped response on the outer edge.

The ET indication at 140 mm (5.5 in.) rotation and 225 mm (8.9 in.) axial (indication 3) was determined via VT to be a round, rough patch on the interior of the penetration tube. The cause of this rough patch is not known. It is unlikely to be interesting in terms of destructive testing but could be looked at using VT if the penetration tube is cut lengthwise.

The results show where the TOFD and the ET results find a common area of interest (Region 4 of Figure 5.46). This area is at 210 mm (8.25 in.) rotation and 225 to 260 mm (8.9 to 10.2 in.) axially into the tube. The VT results for this region show only scratches, however.

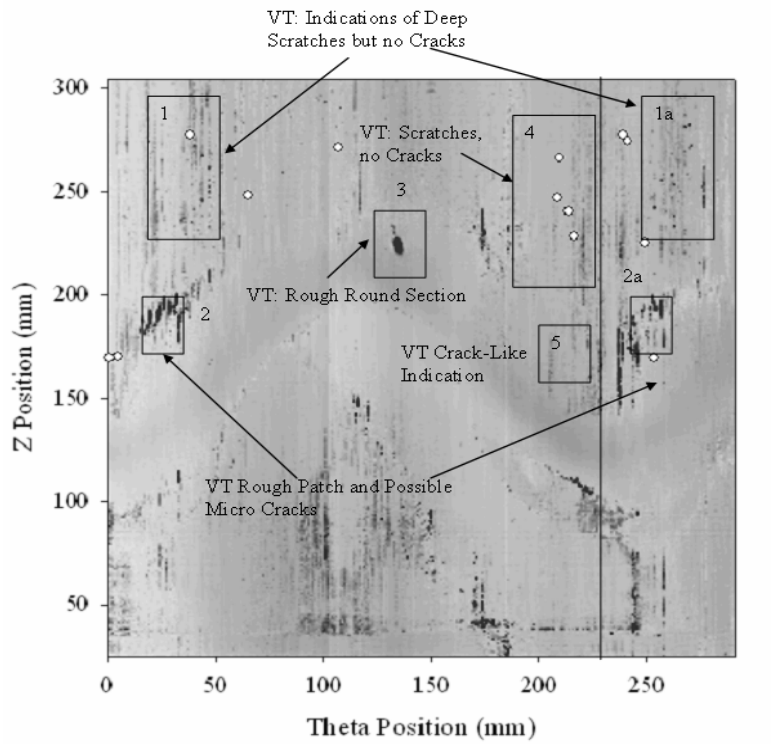

Figure 5.46. Combined Eddy Current Data with Overlaid Time-of-Flight Diffraction Indications and Visual Testing Characterization of the Results for the Penetration Tube of Nozzle 59

Region 5 contained a crack-like indication using VT, but this was not corroborated by the ET or the TOFD and is likely a scratch.

The penetration tube yielded several areas that would be interesting to study using DE but no confirmed cracking. The penetration tube was considered to be a lower priority than the J-groove weld of Nozzle 31, however.

5.3.2 Nozzle 59 J-Groove Weld and Buttering

The J-groove weld and buttering were inspected volumetrically using ultrasound and the surface was examined using visual testing via replicant. No large crack-like indications were found in the J-groove weld using direct VT and VT using replicant, and the immersion UT indications appear to be embedded welding defects. The Microset replica and VT did reveal several small crack-like indications, but no indication was longer than 1 cm. The locations of these defects are given in Figure 5.47.

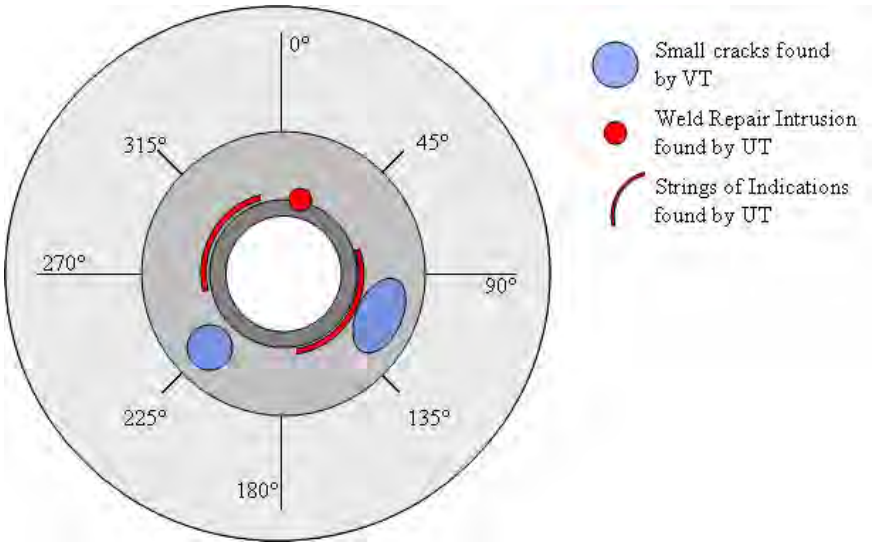

Figure 5.47. Nondestructive Examination Indications Found in Nozzle 59

Although a series of UT signals is coincident with the locations of the small crack-like indications at 90–135 degrees, the UT data in this area look a great deal like a string of fabrication flaws. This area is the most interesting for possible future DE work, but in the absence of confirmed cracking and confirmation that this was a leaker based on boric acid deposits, this weld was designated a lower priority than the weld on Nozzle 31.

5.3.3 Nozzle 31 Penetration Tube

The TOFD and ET examination results for the Nozzle 31 penetration tube showed a good correlation, in that both techniques found the penetration tube to be free of significant surface-breaking defects. The

penetration tube in Nozzle 31 contained no strong ET indications; only weak (<1 V) scratch-like indications were detectable. The only TOFD indications found were determined to be embedded in the tube and not surface-breaking, as no break in the lateral wave was seen.

Because TOFD and ET agreed that the penetration tube was the least likely component thus far to be cracked, the penetration tube of Nozzle 31 was considered the lowest priority for DE. This is interesting, as Nozzle 31 was considered to be leaking based on the presence of boric acid on the pressure vessel head. If Nozzle 31 had leaked, it must have done so through the J-groove weld.

5.3.4 Nozzle 31 J-Groove Weld and Buttering

The J-groove weld of Nozzle 31 was found to have crack-like indications by bare metal VT, ET, and PT. The indications were not detectable using the volumetric UT inspection, but UT inspection did reveal what appeared to be areas with fabrication flaws. The locations of these indications are given in Figure 5.48.

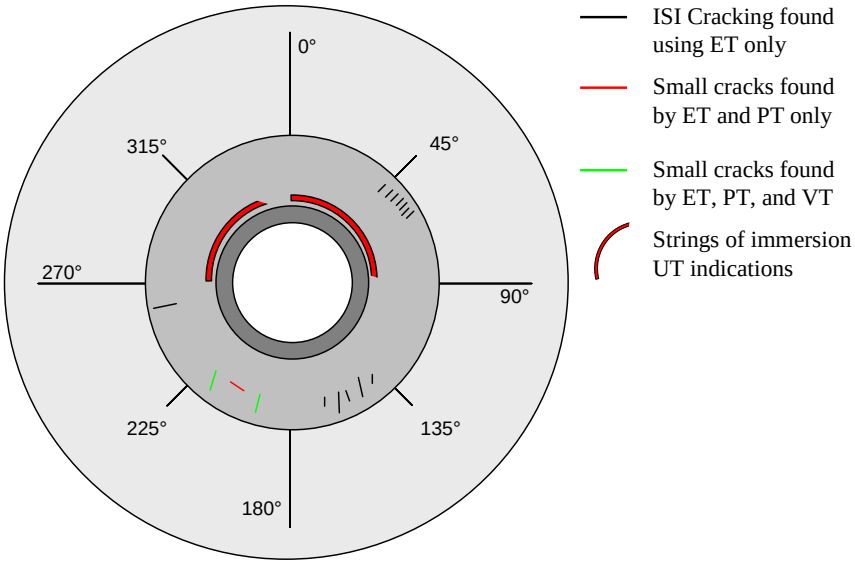

Figure 5.48. Nondestructive Examination Indications Found in Nozzle 31

Sixteen crack-like indications were found by ET testing in four distinct areas. Seven small crack-like indications were found clustered around 60 degrees, five were found clustered around 150 degrees, three were found clustered around 210 degrees (Figure 5.48), and one was found at 255 degrees. The ET indications at 200 and 225 degrees were confirmed as cracks using PT and bare-metal VT.

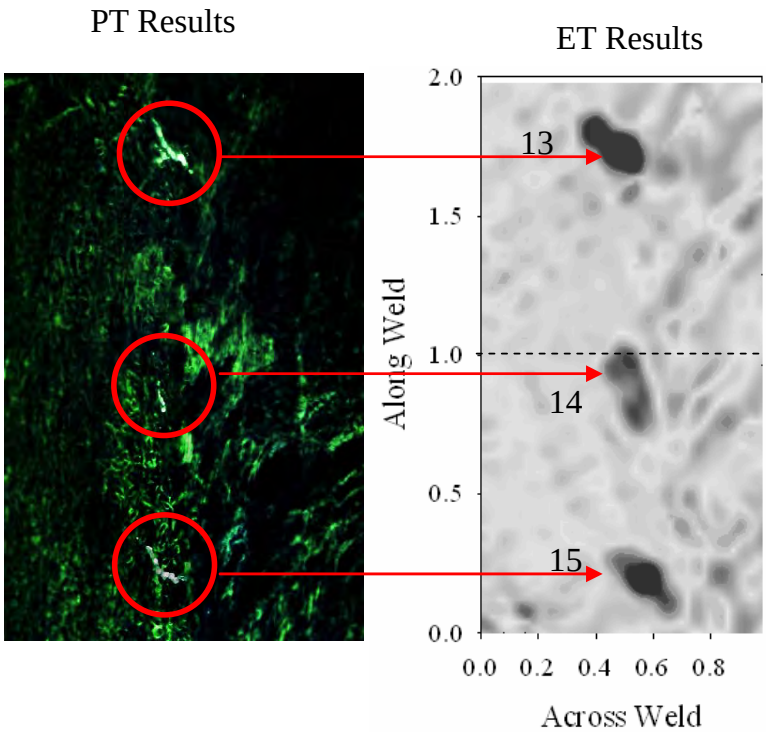

Figure 5.49. Correlated Penetrant Dye and Eddy Current Testing Results for the Weld/Butter Wetted Surface Interface in Nozzle 31 Centered at 210 Degrees

A crack-like indication was found using both PT and ET at 215 degrees. This indication is unusual for two reasons—the indication is circumferential, not axial like the other crack-like indications, and the ET response is relatively weak at 1.8 V at 15 dB. Because of this indication, all ET responses larger than 1.8 V were considered crack-like for this analysis.

The interesting regions for destructive testing using the visual and immersion inspections include the regions found using VT, from 80 to 120 degrees and from 220 to 260 degrees and the regions from -10 to 60 degrees and from 260 to320 degrees as determined using immersion UT. It is worth noting that the region from 260 to 320 degrees has significant overlap with both techniques. Because of the confirmed crack-like indications in the weld, the J-groove weld of Nozzle 31 was considered the highest priority for DE.

One result worth noting was the high false-call rate that PNNL staff obtained using VT via replicant. None of the indications found using VT or the replicas was confirmed using PT or ET, and one was shown to be a scratch by high-magnification photography.

6.0 Destructive Testing and Results

Although a large amount of NDE has been performed on CRDMs in the field, very few CRDMs have been destructively tested. Until the study reported here, no through-weld PWSCC in a CRDM had been analyzed destructively, and understanding the crack morphology is important in understanding the NDE responses of this form of cracking. Some techniques, such as ultrasound or deep-penetrating ET, to find wastage caused by leaking water have not been proven effective.

The destructive examination work is doubly important as the NDE data acquired in the field, at the PNNL round robin tests, and by the NDE examinations performed by PNNL staff in the laboratory have not conclusively shown where the leak occurred. Although many indications have been found, the only strong agreement between different techniques occurs at the interface between the J-groove weld and buttering at 200 and 225 degrees. In these locations, ET, PT, and VT all agree that PWSCC-like indications are present.

6.1 Cutting Plan

After the NDE results for the two nozzles were examined, it was decided to focus on Nozzle 31. Nozzle 31 was considered to be leaking, and the J-groove weld had several crack-like indications via examinations of replicas of the surface. The first round of cutting was designed to remove the excess carbon steel and Inconel tubing. This cutting serves two purposes—it significantly reduces the weight of the sample around the J-groove weld, allowing for easier sample movement, and it creates a more favorable geometry for inspection. The cut plan for the weight reduction and tube removal are shown in Figures 6.1 and 6.2.

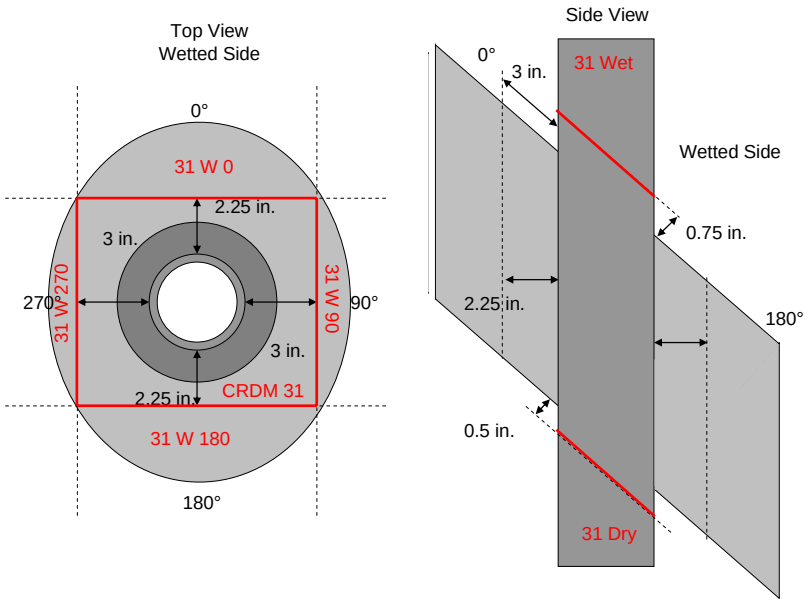

Figure 6.1. Initial Weight-Reduction Cuts Made on Nozzle 31

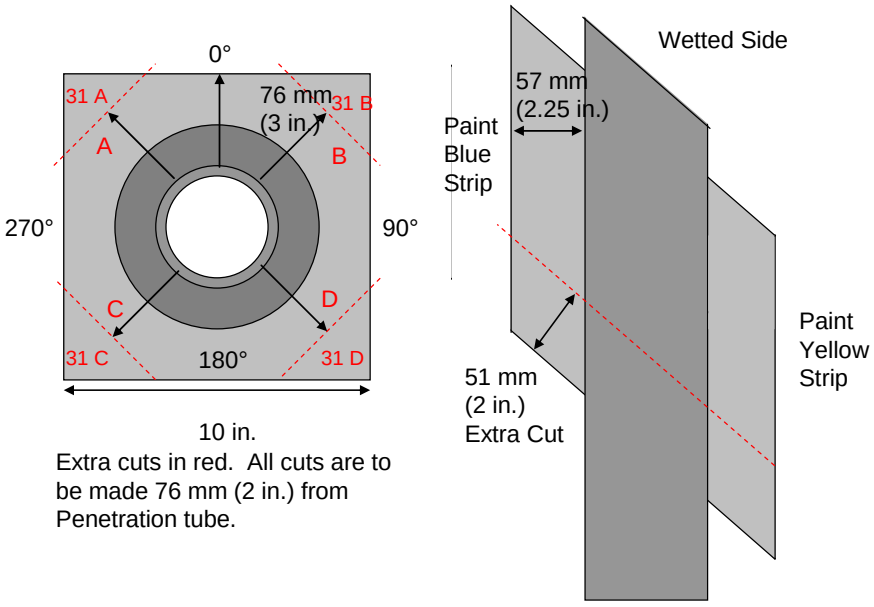

Figure 6.2. Additional Reduction Cuts Made on Nozzle 31

Based on the positive results from ET, VT, and PT, the region from 180 to 270 degrees was considered the most likely to contain a through-wall crack and was designated Section 1. The region from 180 to 120 degrees contained several ET indications and was designated Section 2. The region from 15 to 75 degrees contained a string of small ET indications and was designated Section 3. The section removal plan is shown in Figure 6.3.

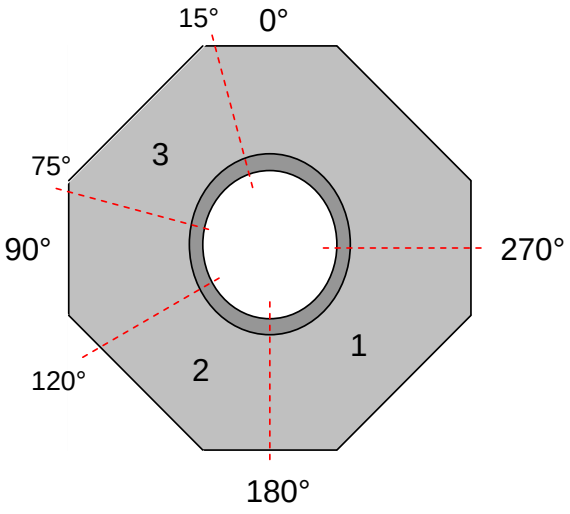

Figure 6.3. Final Cuts Made on Nozzle 31 to Remove Areas of Interest

6.2 Cutting of Nozzle 31

A Marvel Series 8 band saw was used to cut the CRDM. Bimetallic blades were used for the cutting, and the saw and the blades were able to cut thought the flame-hardened steel, the 182 weld and buttering, and the Alloy 600 pipe with precision. The saw was installed into a walk-in fume hood for cutting the nozzle. The saw was lifted in using the same crane used to install and manipulate the nozzle. Figure 6.4 shows some images of the saw installation. A contamination containment tent was built around the saw after the saw was installed into the fume hood. While all efforts were made to prevent the spread of contamination inside the tent, the tent provided a physical barrier to contamination escaping to the uncontrolled areas during cutting and sample movement. The back of the tent was open to the fume hood to allow for constant negative pressure inside the tent. The saw inside the tent is shown in Figure 6.5.

Nozzle 31 was loaded into the tent and cut to remove the extraneous carbon steel that is not of interest. Figure 6.6 shows the uncut Nozzle 31 on the band saw. The cutting was performed inside a tent built partially inside a fume hood. Cutting fluid was used to minimize the probability of the cutting creating airborne contamination. The flame-cut regions were difficult to cut through, as the flame cutting had hardened the surface and made the surface very irregular. Also, for the first cuts, the sample had to be aligned and held in place using wood blocks and clamps because the nozzle had no flat surfaces.

It was determined that the interior of the penetration tube was the most highly contaminated part of the nozzle. Thus, while the penetration tube did present problems by being in the way of the initial cuts, the ends of the penetration tube were left intact.

Figure 6.6 shows Nozzle 31 after the carbon steel had been cut into a square. After the sample was in this shape, it was much lighter and easy to set securely for cutting.

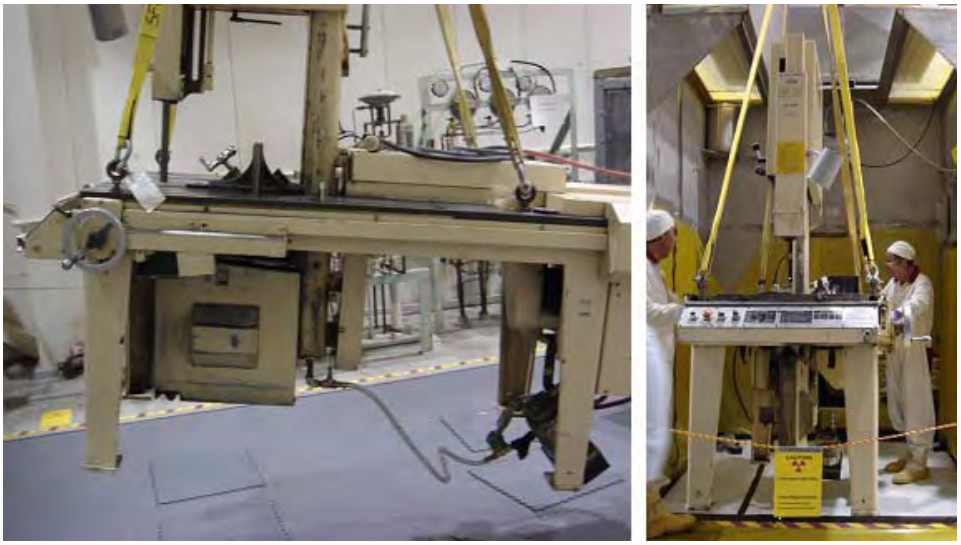

Figure 6.4. Band Saw Installation into the Liquid Fume Hood

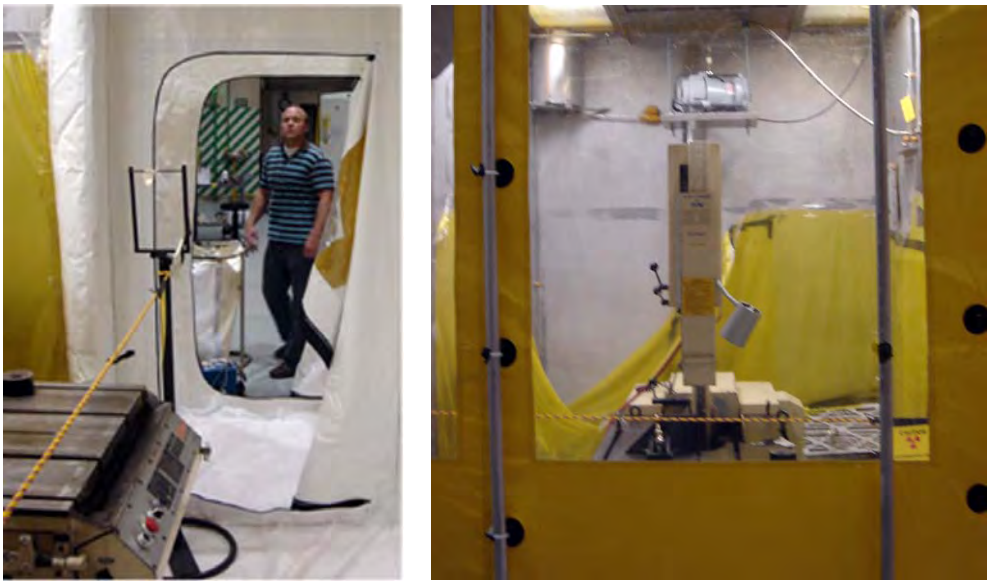

Figure 6.5. Band Saw Inside Contamination Containment Tent

Figure 6.6. Initial Cut on Nozzle 31

The sample was first cut into a square as shown in Figure 6.7, and then the corners were cut off to form an octagon. Once the carbon steel was cut down, the two ends of the penetration tube were cut off.

Figure 6.7. Nozzle 31 After Carbon Steel Was Cut into Square

To further reduce the weight of the sample and to try to confirm that Nozzle 31 had leaked, 51 mm (2 in.) of steel were cut from the dry side of the nozzle. This slice was then cut in half along the 90- to 270-degree plane and split open, and the 51-mm-long piece of penetration tube was removed. Clear evidence for corrosion was visible on the inside of the interference fit, and a white, crusty buildup was visible at close to 180 degrees.

The next step was to cut away the penetration tube and carbon steel below the J-groove weld. This cutting serves two purposes. It reduces the weight of the region of interest, the J-groove weld, and it allows one to examine the leakage path through the interference fit above the J-groove weld. The excess carbon steel and penetration tube were cut off in two steps, first by removing 51 mm (2 in.) of material from the dry side and then by removing an additional 38 mm (1.5 in.). The areas identified as areas of interest in the cut plan were cut an additional 38 mm (1.5 in.) to just above the triple point of the weld. Each segment of carbon steel was cut in half roughly along the 90- to 270-degree line to release the penetration tube from the interference fit and allow access to the annulus.

6.3 Examination of the Interference Fit Region

The annulus showed clear indications of water flow through the interference fit and the associated boric acid deposits left in the annulus. Two main indications of flow through the annulus were found—a small flow indication at 45 degrees and a very large indication with heavy boric acid deposits ranging

from 120 to 190 degrees. A boric acid deposit found from 90 to 120 degrees also is shown in Figure 6.8. Two small flow indications were found close to 200 and 225 degrees. The two main flow indications and the indications near 200 and 225 degrees are shown in Figure 6.9.

Figure 6.8. Two Main Flow Regions at 45 Degrees and 120 to 190 Degrees

While the exact depth of the wastage through the interference fit was not measured, it was certainly less than one millimeter, even at the highest flow regions.

6.4 Final Sectioning

The three regions identified in the cut plan were cut from Nozzle 31 using the large band saw. These regions were cut from the nozzle after removal of the excess carbon steel. After the sections were cut from the nozzle, the position and extent of the weld, buttering, and triple point were obvious. The pieces were cut just above the triple point to release the penetration tube and allow direct inspection of the buttering below the triple point to determine which of the NDE responses was associated with the through-weld crack. Figure 6.10 shows the three sections after removal from the nozzle, and Figure 6.11 shows Section 2 after further cutting to allow inspection of the buttering.

Figure 6.9. Two Smaller Flow Regions at 45 Degrees and 120 to 190 Degrees

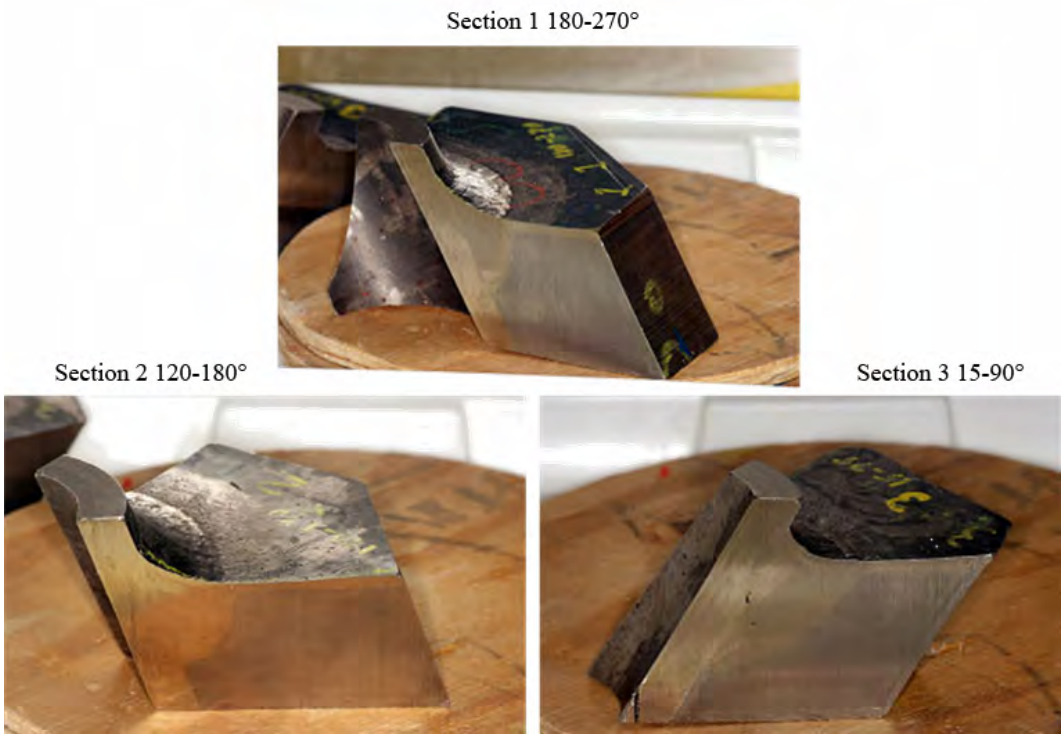

Figure 6.10. Areas of Interest after Sectioning

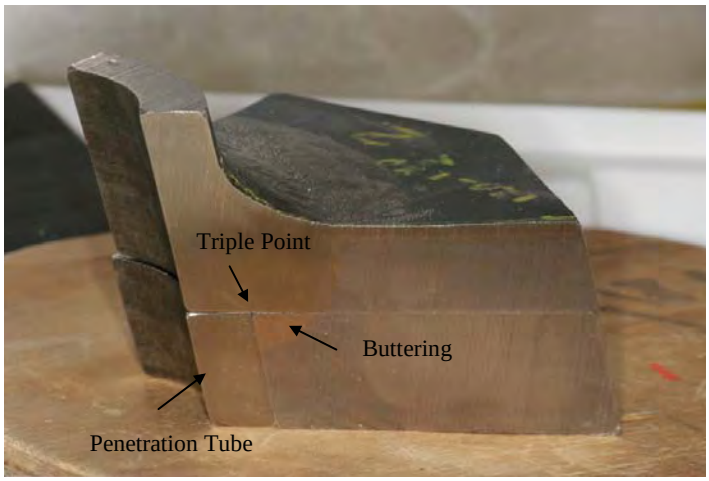

Figure 6.11. Section 2 After Cutting Above Triple Point To Remove Penetration Tube

After the samples were cut above the triple point, the buttering was examined visually and with manual ET. The inspection of the buttering below the triple point would be able to conclusively identify cracks that reached the annulus. The ET scans had to be performed manually because the curved edges and transitions between the buttering and carbon steel produced difficulties in using the *x*-*y* scanner and extraneous signals at the butter-steel interface.

Careful ET examination and high-resolution photography did not find any evidence of through-weld cracking in Sections 1 and 3. A through-weld crack was immediately apparent, however, in the buttering of Section 2 at 135 degrees. This crack was clearly visible with the naked eye and was confirmed with ET and photography. This crack is shown in Figure 6.12. Because this crack was in a region shown to have crack-like indications and none of the other sections showed any indications of through-weld cracking, all attention was focused on Section 2 near this crack.

Figure 6.12. Confirmed Through-Weld Crack Found Above the Triple Point in Section 2 at 135 Degrees

Because five crack-like indications were found by ET centered around 150 degrees, it was not known which crack had propagated through the weld to this point. Additionally, to facilitate destructive testing, the largest piece needed to be less than 16 mm (5/8 in.) thick, so the wetted section was cut into two pieces 8 mm (03 in.) below the wetted surface. Figure 6.13 shows Section 2 after it was cut below the wetted surface.

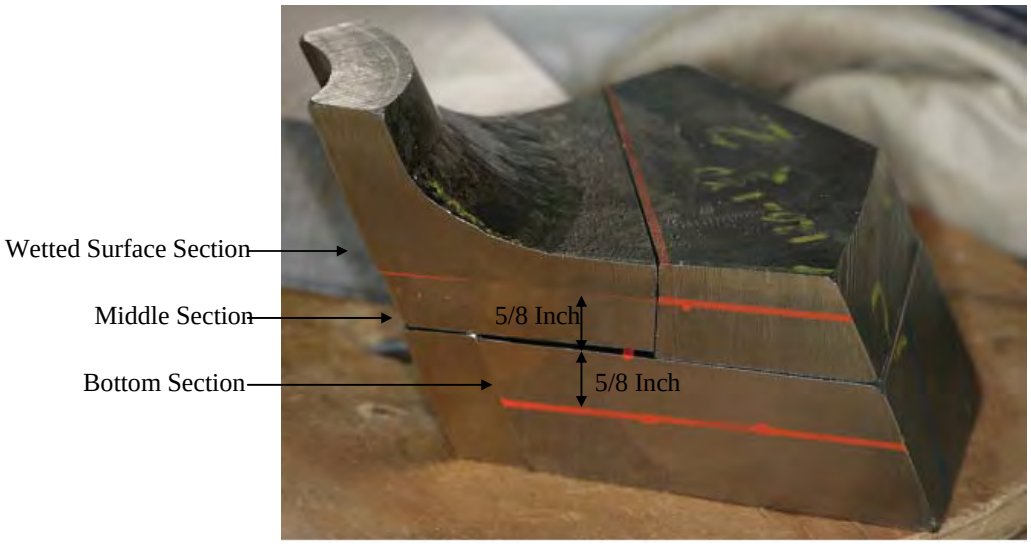

Figure 6.13. Section 2 After Cutting to Find Cracks

After the cutting, it was clear, based on the position and spacing of the cracks, which cracks were associated with which ET indications. Figure 6.14 shows the three cracks on the cut face 8 mm below the wetted surface. One interesting aspect of the cracks and the ET indications is how much longer the cracks are 8 mm into the weld than they were at the wetted surface. ET indication 9 is 8 mm long on the surface, and the visible crack length is 21-mm long at the cut surface. The ET indication #10 is 6-mm long at the surface and is 25 mm long at the cut surface. Indication 11, which is 10 mm long at the wetted surface, is 15 m long at the cut surface. The crack spacing is preserved, with cracks 10 and 11 being 5 mm apart on both surfaces and cracks 9 and 10 being 11 mm apart on the wetted surface and 10 mm apart on the cut surface. By contrast, ET indication 8 is 16 mm apart from ET indication 9. It is worth noting that ET indications 8 and 12 do not represent cracks that penetrated 8 mm into the weld.

As final preparation for the destructive evaluation, the cracked sections were cut out in small pieces for easier fine cutting and polishing. The cracked specimens were cut out in five pieces labeled A through E. The cut nozzle Section 2 is shown in Figure 6.15. The through-weld crack associated with ET indication 10 and the nearby crack associated with ET indication 11 are contained in pieces A, C, and E. The nearby crack associated with ET indication 9 is contained in pieces B and D.

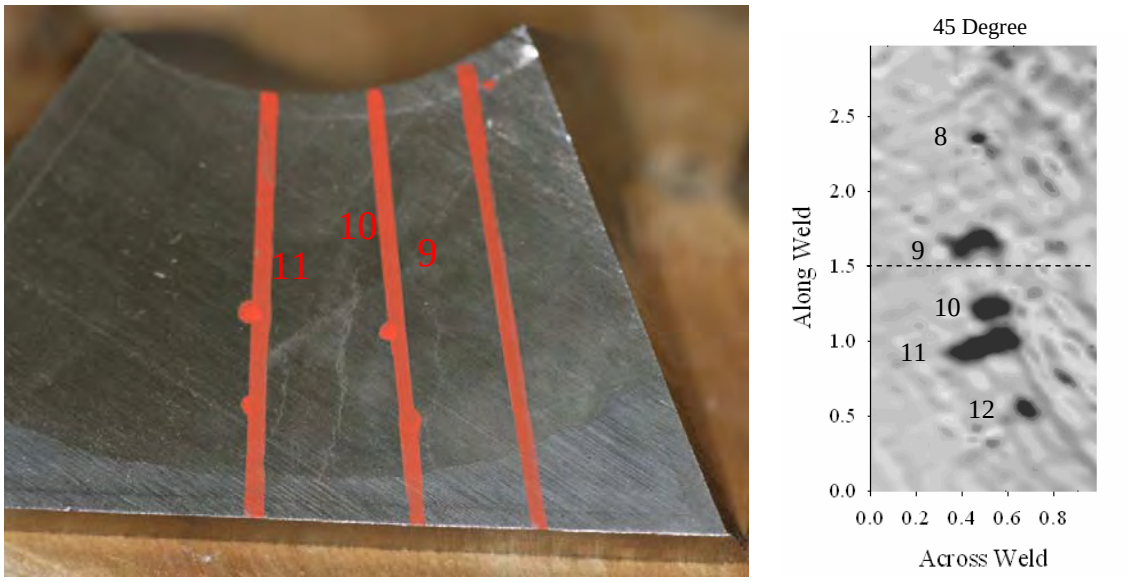

Figure 6.14. Eddy Current Testing Indications at 145, 155, and 160 Degrees Confirmed Using Destructive Examination

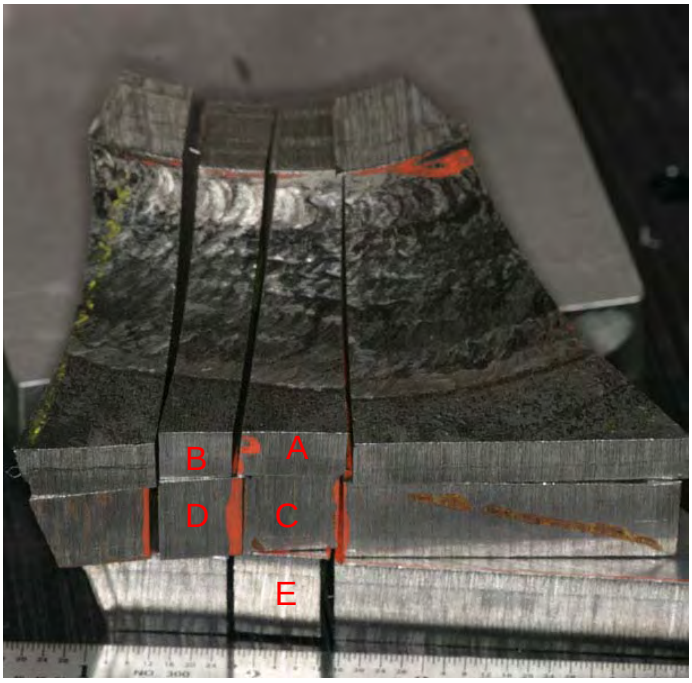

Figure 6.15. Cracked Metal Coupons Removed from Section 2

6.5 Metallographic Examination of Cracking in Nozzle 31 Section 2

The observation of what appeared to be a through-wall crack in Section 2 of Nozzle 31 prompted its further cuting into smaller pieces for destructive examination. Five smaller pieces were received labeled A, B, C, D, and E as shown in Figure 6.15. Pieces A and B are from the inner surface in contact with the PWR primary water, while pieces C and D were directly above these two sections, respectively. The final piece, E, was directly above Section C. The positions for pieces A, C, and E are illustrated in Figure 6.16. Pieces A and C contain the Alloy 600 nozzle, Alloy 182 J-groove weld, Alloy 182 butter passes, and low-alloy steel plate. Piece E was above the J-groove weld and was not joined to the Alloy 600 tube. All initial destructive examinations were performed on A, C, and E because they appeared to contain the main through-wall crack. A long secondary crack was also indicated in A that extended into B and D.

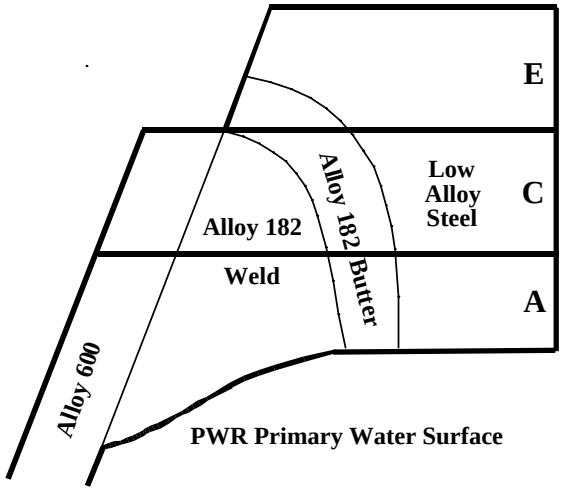

Figure 6.16. Sections A, C, and E Cut from Section 2 of Nozzle31. Relative locations are indicated for the Alloy 600 nozzle, the Alloy 182 J-groove weld, the Alloy 182 butter passes, and the low-alloy steel.

6.5.1 Initial Examinations and Sectioning

The evaluation of the material began with optical examinations of the top and bottom surfaces of each section using a microscope to identify crack locations and determine serial sectioning locations. Low-magnification photographs are presented in Figures 6.17 and 6.18 for each surface. The dimensions for each piece were somewhat different, with A starting at ~8.3 mm thick and increasing through the J-groove weld to ~12 mm thick, while pieces C and E were ~15 mm thick. Careful examinations revealed long cracks on the A, C, and E surfaces, with the longest crack lengths (on A top and C surfaces) reaching ~25 mm. The decision was made to limit the required metallography to ten cross sections per piece and maintain a sufficient slice thickness (~2.4 mm) for subsequent examinations if needed. This resulted in a spacing of ~2.7 mm between the metallographic cross sections (blade thickness cut of ~0.3 mm) that encompassed the entire crack.

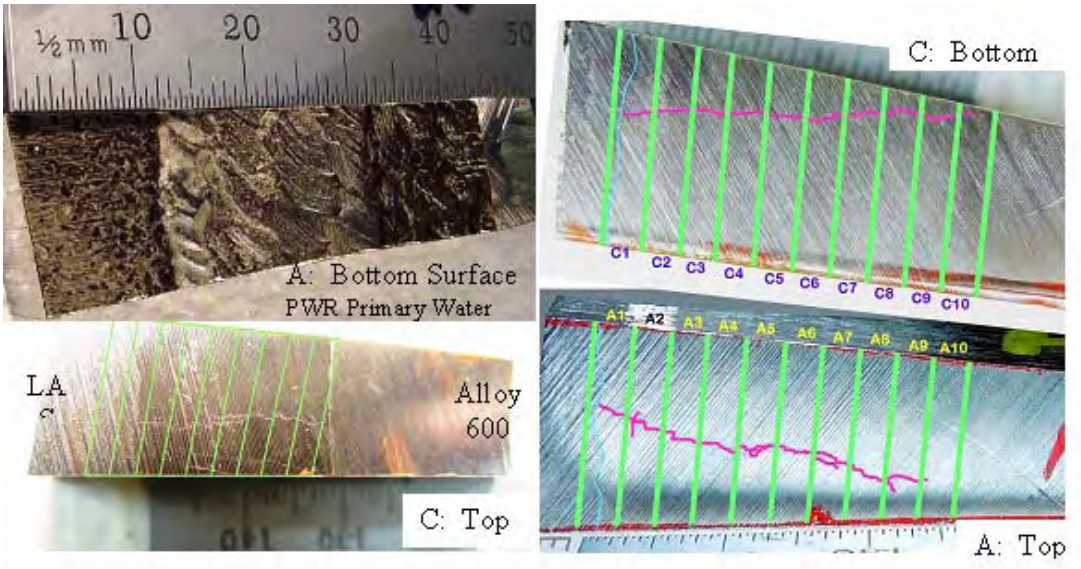

Figure 6.17. Top and Bottom Surfaces for Pieces A and C Are Shown Along with Highlighted Cracks and Proposed Serial Sectioning. The bottom surface for piece A was exposed to primary water during PWR service.

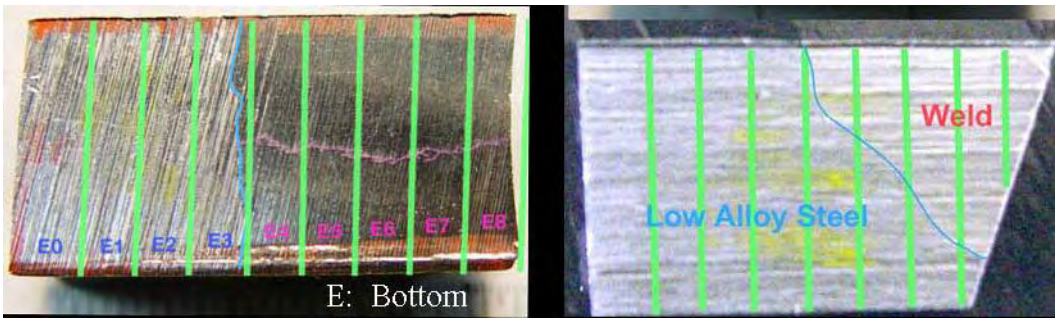

Figure 6.18. Bottom (left) and Side (right) Surfaces for E with Proposed Serial Sectioning. Note that these images are not to scale with those in Figure 6.17.

The sectioning diagram is illustrated in Figure 6.19 on the same schematic for Section 2 of the Nozzle 31 weldment presented in Figure 6.16. The zero cut was made in the low-alloy steel where no cracking was present, and the remaining cuts were produced parallel to this section. Individual metallographic cross-section samples were identified as A1–A10, C1–C10, and E1–E8. Piece E was shorter than pieces A and C because it was above the J-groove weld and the adjoining Alloy 600 tube detached during initial cutting.

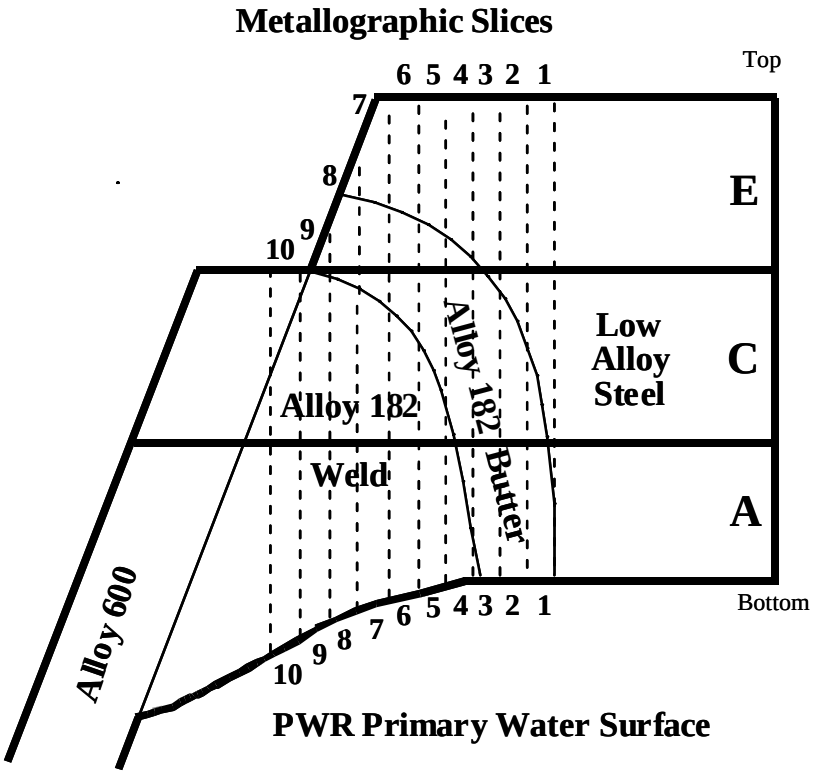

Figure 6.19. Approximate Locations (dashed lines) of Metallographic Sections Through Pieces A, C, and E

Before sectioning the three major pieces A, C, and E, additional surface examinations were performed using scanning electron microscopy (SEM) to better document crack characteristics. The A surface exposed to PWR primary water was rough, and relatively thick oxide corrosion products remained in many locations. The SEM images revealed an obvious crack in the Alloy 182 weld metal, perhaps widest in the region near the transition from the butter passes to the J-groove weld metal. A full crack montage is shown in Figure 6.20(a), with a slightly higher-magnification image illustrating the crack morphology in Figure 6.20(b). It is not possible to accurately determine crack openings from these images, but widest locations were on the order of 30 μm.

The top (inside), saw-cut surface from piece A enabled a much better observation of the full extent of the cracks. The SEM montages for the two primary cracks observed on this surface are shown in Figure 6.21(a) and (b). The main crack extends to the low-alloy steel interface and well into the Alloy 182 J-groove weld, while the secondary crack is near the edge of piece A and appears to have propagated into the adjacent piece B sample that was not examined. The higher-magnification SEM image in Figure 6.21(c) documents the tortuous and branched crack path probably along interdendritic and grain boundaries. This will be examined in much more detail on the individual metallographic cross sections.

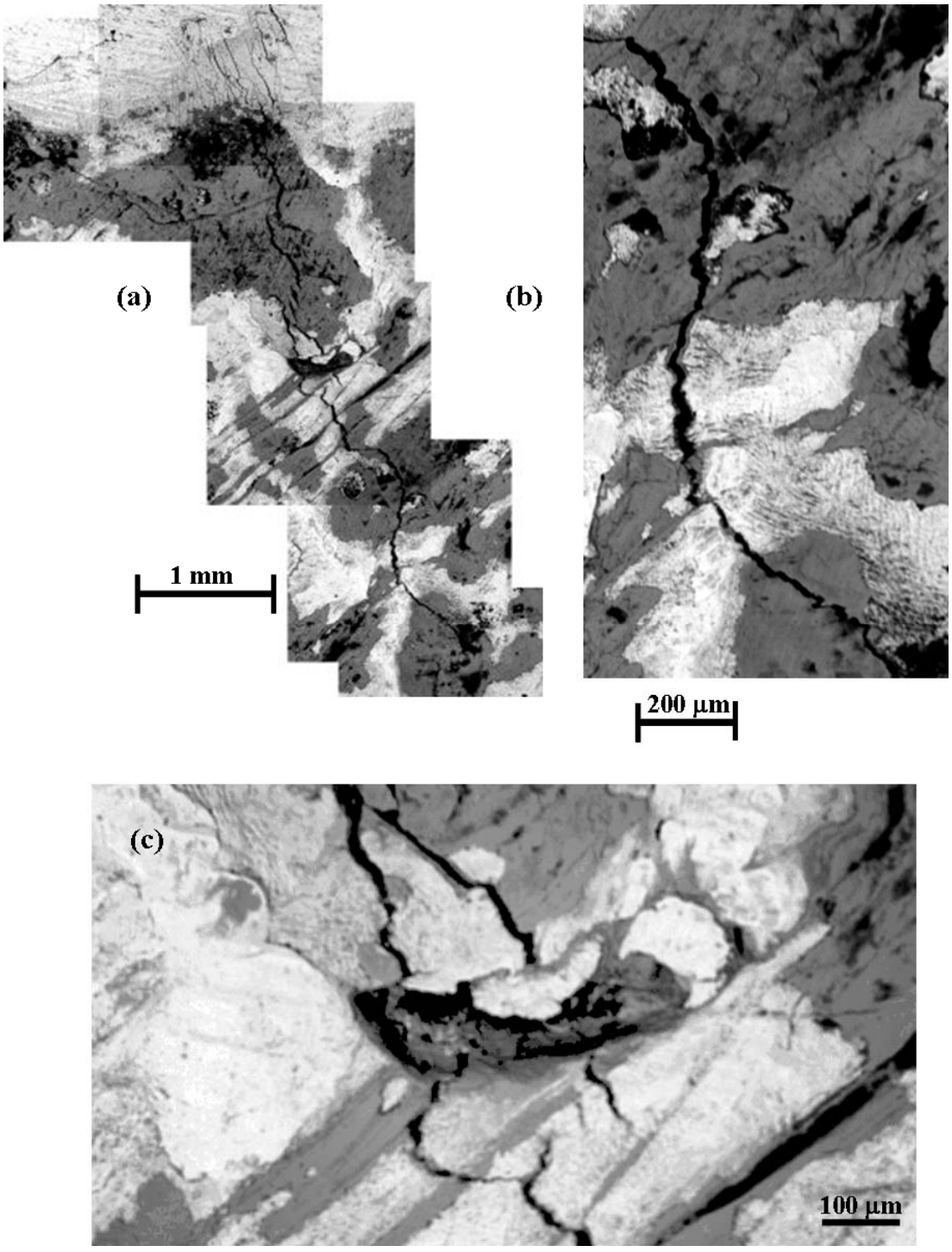

Figure 6.20. Observed Crack on the PWR Water Surface of Piece A at Two Magnifications. The rough as-welded surface and relatively thick corrosion-product oxide in places (white contrast) made SEM imaging of fine secondary cracks difficult. However, the main crack is seen to extend ~6 mm on this surface. A moderate-size defect (pit) near the center of the main crack is shown in (a) and magnified in (c).

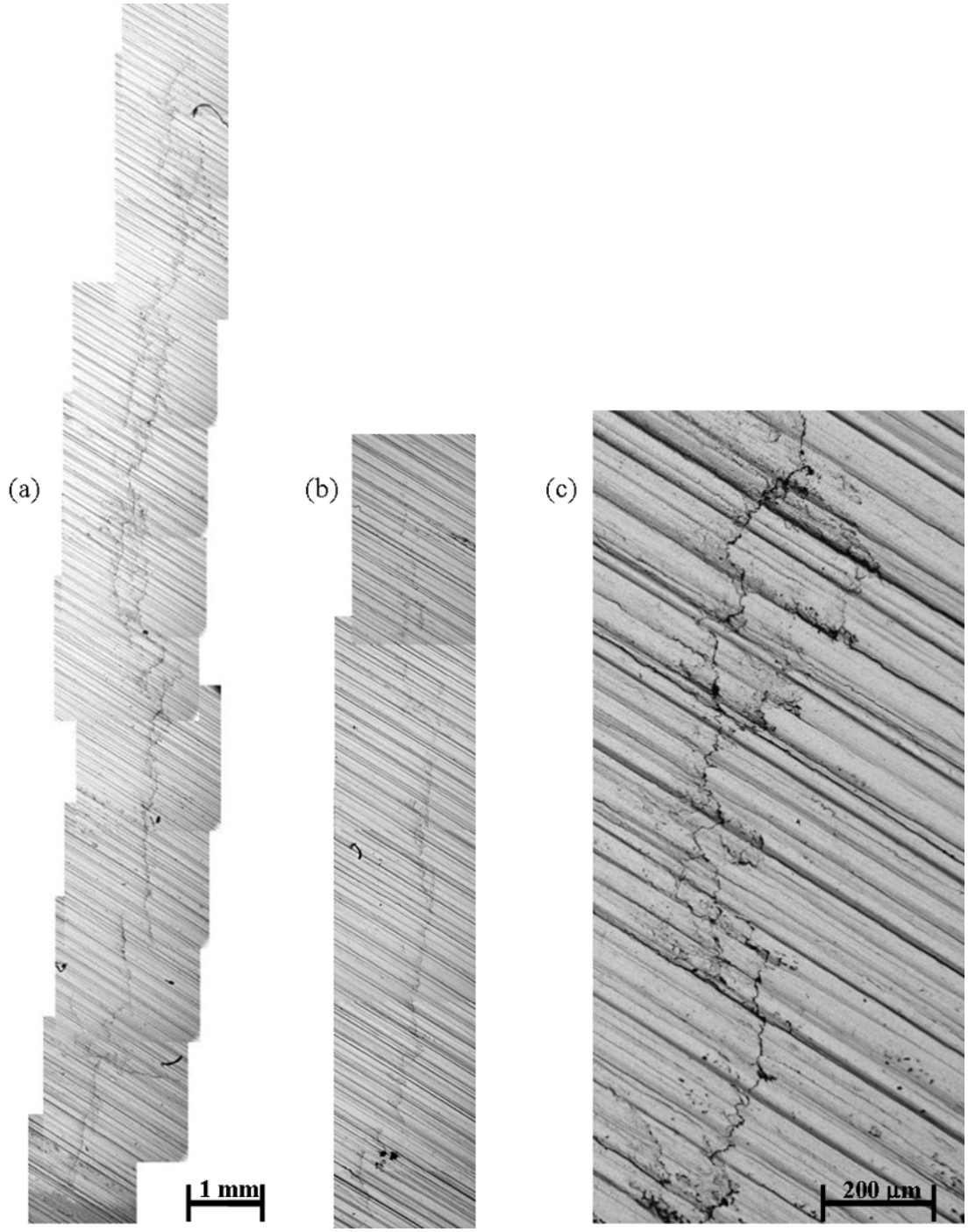

Figure 6.21. Cracks on Piece A Top (inner), Saw-Cut Surface: (a) main crack, (b) secondary crack, and (c) higher magnification of typical crack morphology from (a)

The surfaces of pieces C and E also were characterized with SEM before sectioning. The interference-fit gap was identified on the C top surface (facing E) both optically and by SEM as illustrated in Figure 6.22. In addition to the bottom surface of piece E, the crack exit surface into the gap was

examined. The Alloy 182 machined surface that made up the interference-fit gap with the Alloy 600 tube was found to have two relatively long cracks, as presented in Figure 6.23. Combining the two cracks, a total crack length approaching ~7 mm was found on this exit surface, with crack opening reaching ~10 µm in places. The cracks were filled with an unknown material, probably boric acid powder and corrosion-product oxide.

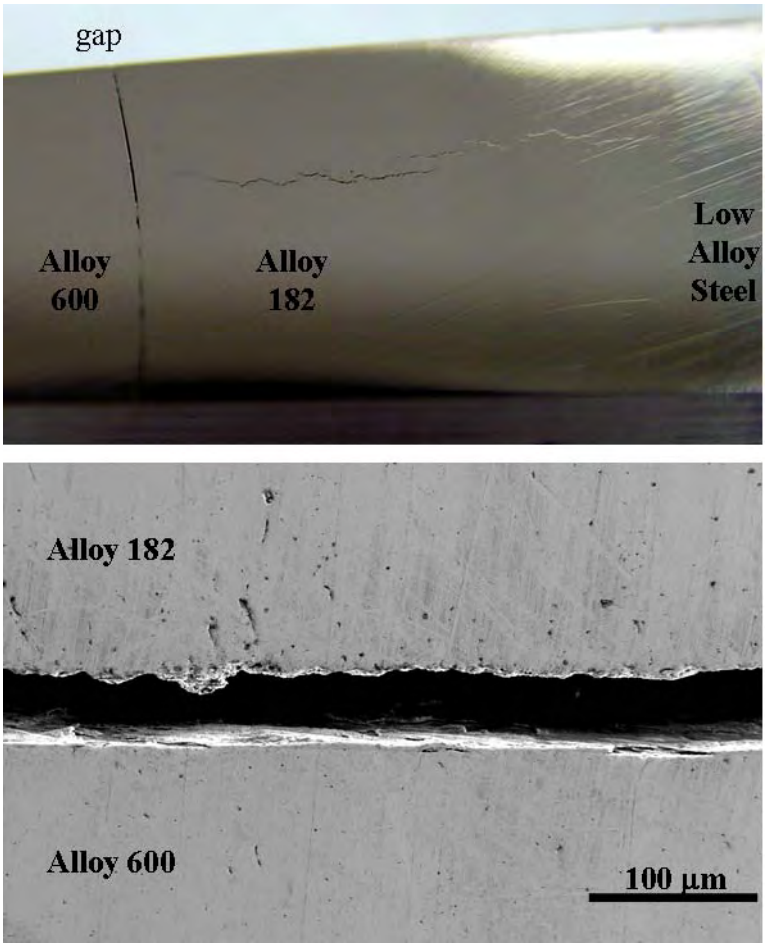

Figure 6.22. Interference-Fit Gap Between the Alloy 182 Butter Passes and the Alloy 600 Tube on Top Surface of Piece C (facing bottom surface of piece E)

The pieces A, C, and E were sectioned sequentially, enabling results from initial metallographic examinations on A to help guide sectioning on C and results for C to guide final sectioning of E. Great care was used during low-speed cutting with a diamond saw to maintain cut locations and orientations so that metallographic cross sections from A (A1 to A10) lined up with C (C1 to C10) and that C1 to C8 lined up with E1 to E8. This was done successfully so that the general schematic in Figure 6.19 properly represents locations for all metallographic cross sections.

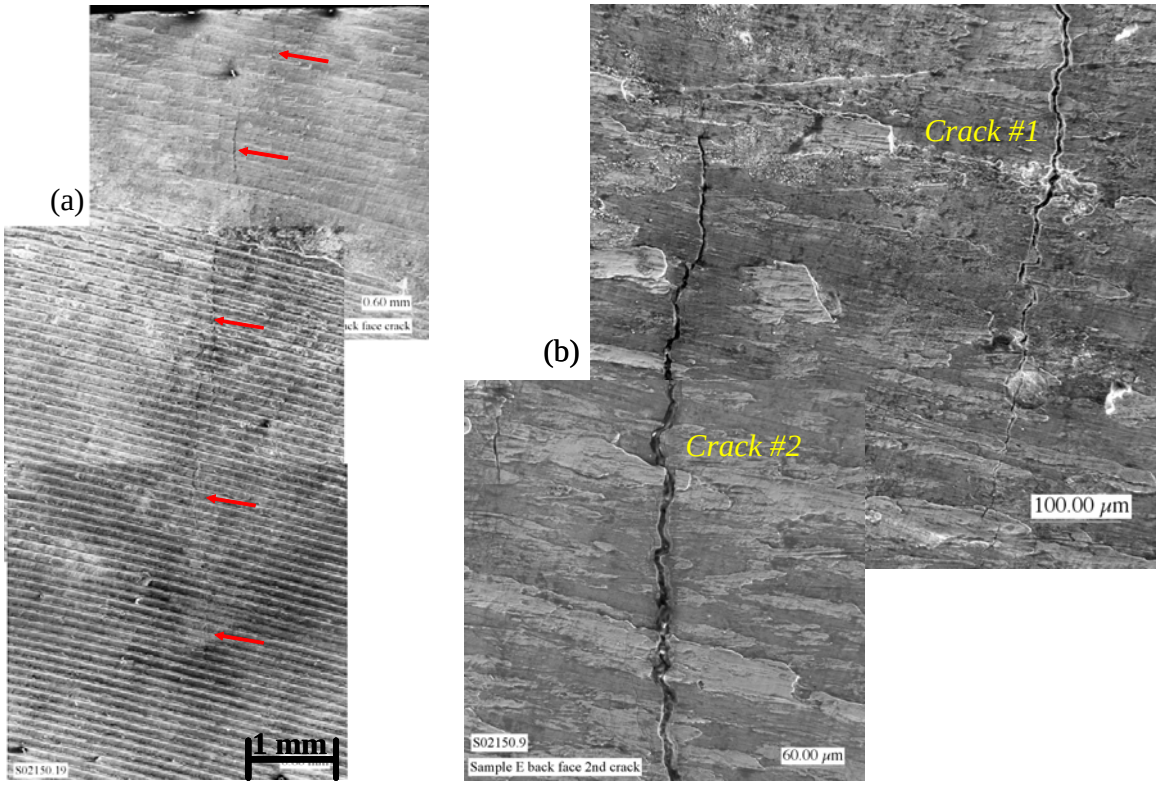

Figure 6.23. Machined Surface and Exit Location for Through-Wall Cracks from Piece E Alloy 182 Weld Metal into Interference-Fit Gap Between Alloy 182 Butter and Alloy 600 Tube. Low-magnification SEM image (a) shows full length and two major cracks, while higher magnification (b) illustrates crack morphologies.

6.5.2 Metallography of Cross-Section Samples

After pieces A, C, and E were cut, each cross-section sample of interest was placed into a mold to create a liquid acrylic resin mount. Each sample mount was marked to identify the bottom side (toward PWR primary water) and ensure that the proper orientation was maintained throughout preparation and characterization. Samples A0, C0, and E0–E3 were not mounted because no cracks were present so no examinations were needed. The mount and sample measured 19 mm in diameter by 12 mm in height. Each mounted sample went through a six-step grinding and polishing process using a Buehler Mini Met Polisher to achieve an adequate surface finish for metallography on each cross section. The process started with grinding with diamond-grit lapping pads at 70, 45, and 15 µm. Approximately 15 minutes were required for each of these initial grinding steps with an applied pressure of 2 lb and a speed of 50 rpm. Polishing required another three-step process using Buehler Mastertex or Texmet 1500 cloth and diamond solution for 9-, 3-, and 1-µm finishes. For each step, the appropriate diamond solution was sprayed onto the cloth to polish the samples. Applied pressure and speed used for polishing were identical to those for grinding. Samples were cleaned with distilled water, and the polishing cloth was changed after each step. After the final 1-µm polishing, the cross-section samples were cleaned and dried for optical metallography in the as-polished condition.

Metallographic characterizations included macros of each sample to document the crack location in the cross section, systematic optical metallographs mapping the entire length of primary and secondary cracks, and selected higher-magnification optical images of the area of interest along the cracks. The whole-sample macros consisted of the entire mounted sample to show direction of the crack(s) within each sample. All the images from pieces A, C, and E were oriented the same way in each image, with the wet-side direction at the top of the image to maintain continuity throughout. Examples of the macro images are shown in Figure 6.24 for samples A2, A3, A4, A5, A7, and A9. Cross-section sample A1 was in the low-alloy steel and did not show any cracks, while sample A10 exhibited only a small crack. Sample thickness can be seen to increase moving from the Alloy 182 butter (A2) near the low-alloy steel to the J-groove weld (A4–A9) toward the Alloy 600 tube.

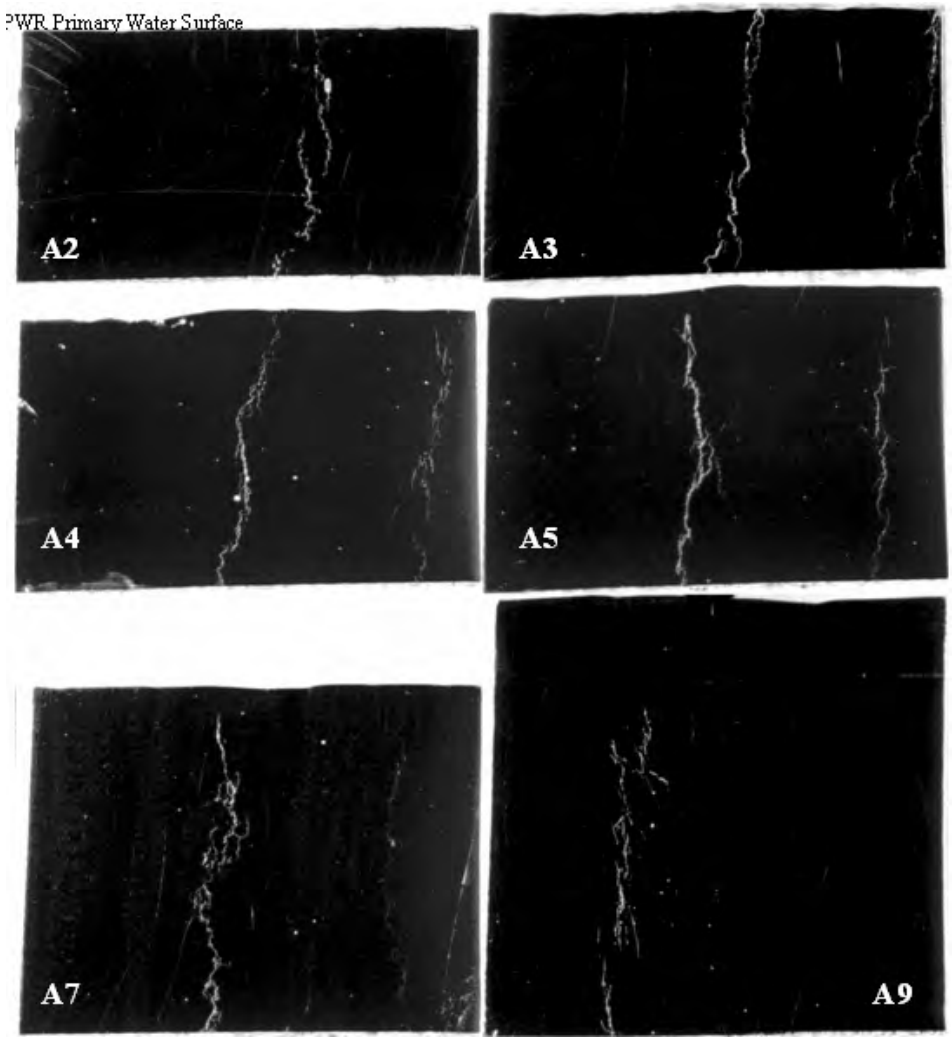

Figure 6.24. Macro Cracks in Several Cross-Section Samples from Piece A Shown Through Photography. Note that PWR primary water surface is now on the top side of these images.

6.5.2.1 Metallography of Piece A Cross Sections

The macro images show extensive cracking through the Alloy 182 weld metal regions with possible initiation sites in cross section A3. A much more detailed evaluation of crack characteristics has been documented by recording systematic images mapping the full range of the cracks in each cross-section sample. Examples of these crack maps are shown for the A cross sections in Figures 6.25, 6.26, and 6.27. The secondary crack present in many of these cross sections also was mapped but will not be presented here. It is sufficient to note that this crack revealed a similar branched morphology.

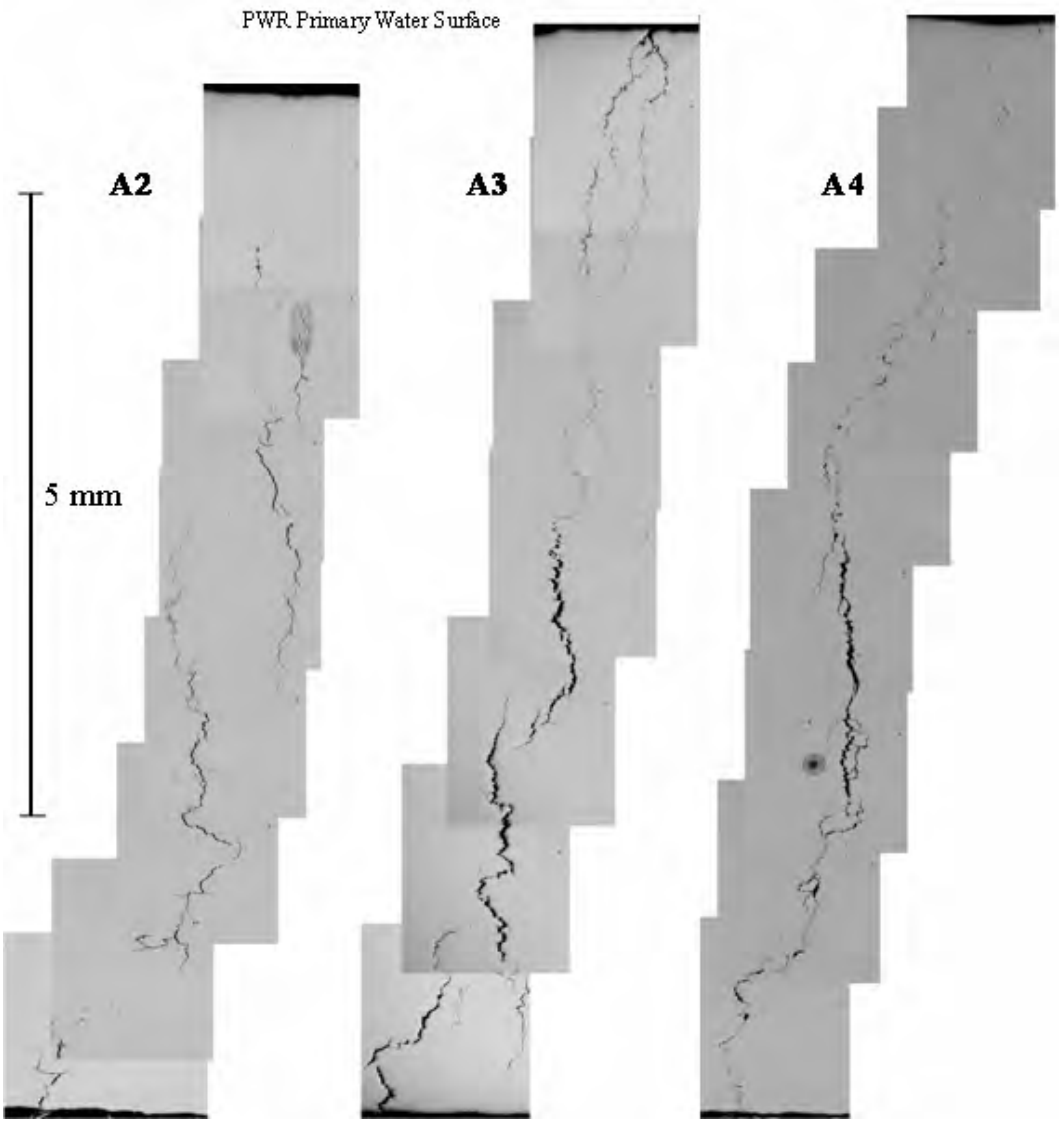

Figure 6.25. Optical Micrographs for A2, A3, and A4 Cross-Section Samples Showing the Main Crack Essentially Running Through Entire Thickness of Each Sample

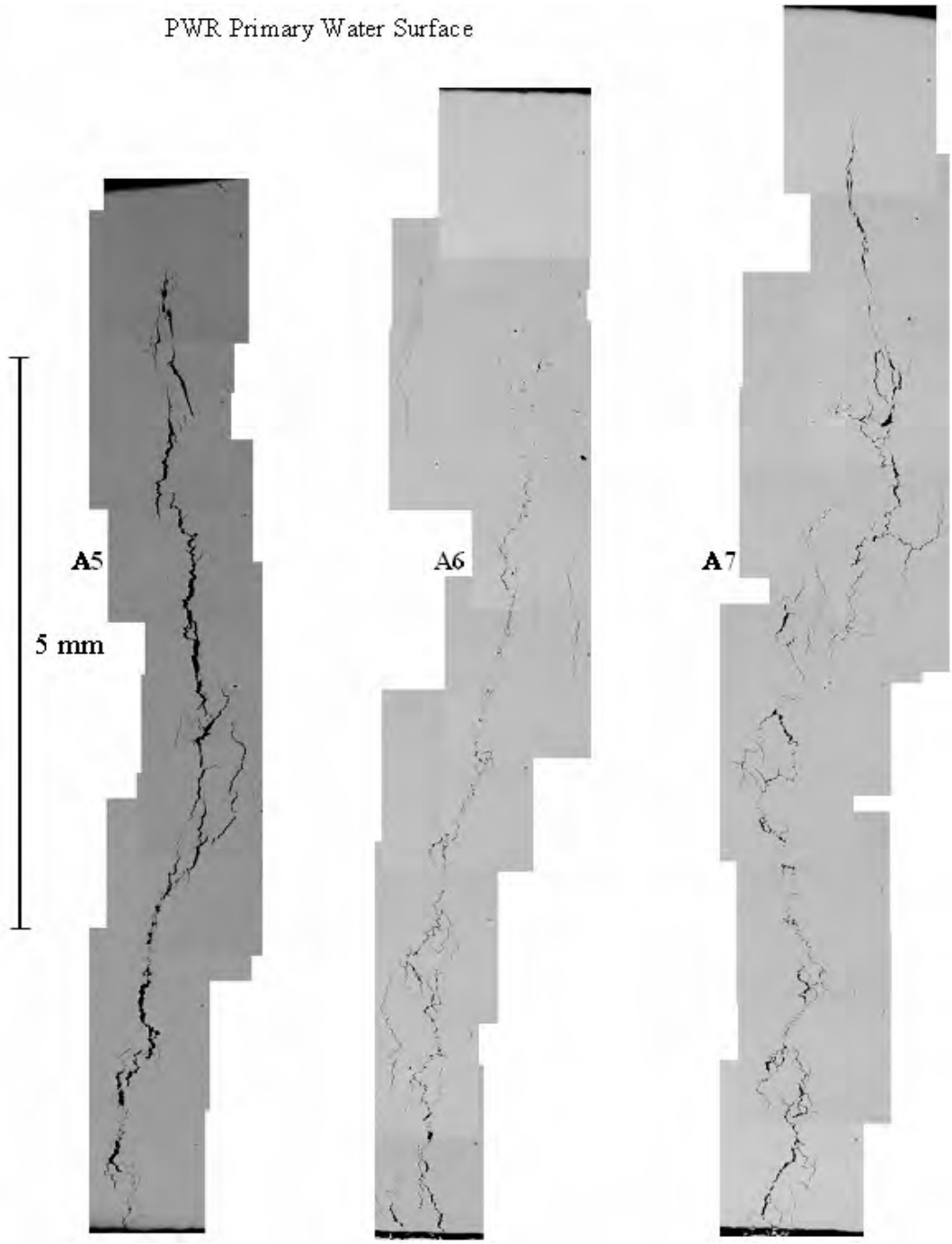

Figure 6.26. Optical Micrographs for A5, A6, and A7 Cross-Section Samples Showing the Main Crack Appearing Below the PWR Primary Water Surface and Through Remaining Thickness of Each Sample

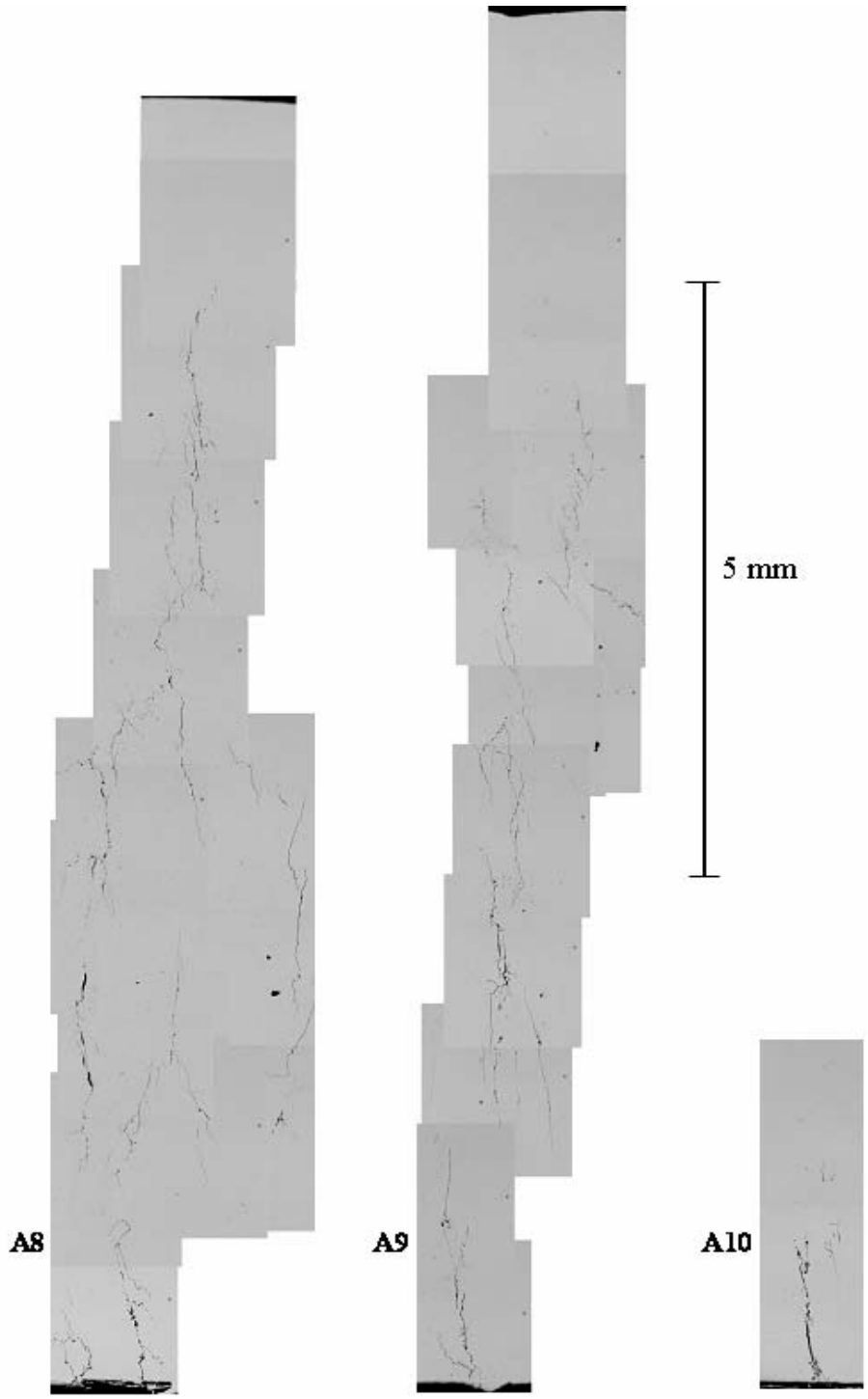

Figure 6.27. Optical Micrographs for A8, A9, and A10 Cross-Section Samples Showing the Main Crack Appearing Farther Below the PWR Primary Water Surface as a Function of Distance from the Crack Initiation Sites in A3

The apparent crack initiation site is near the A3 slice location, as illustrated in the optical micrograph for this cross section in Figure 6.27 and in a higher-magnification SEM image in Figure 6.28. The SEM micrograph suggests a region of damage at the surface near the crack opening. The width of the crack at the surface in the region is ~30 µm, consistent with the SEM examination of the cracks on the piece A primary-water surface presented in Figure 6.20. Crack morphology can be seen as heavily branched immediately below the surface and following convoluted interdendritic or grain boundaries for the most part. The SEM backscatter-electron (BSE) image provides both orientation (grain-to-grain) and compositional contrast. Both can be seen in Figure 6.28, with large grains several hundred micrometers in diameter and finer contrast within grains due to segregation (e.g., manganese and niobium) during final solidification. The heavily branched crack path continues throughout the Alloy 182 weld metal, as illustrated by the tight cracks shown in Figure 6.29. This area is from the mid-depth of the A3 cross section. Similar to the near-surface morphology, the main crack again has split into two separate cracks within this plane and has propagated along parallel interdendritic or grain boundaries. These images from the A3 cross section are representative of the general cracking morphology found within the Alloy 182 weld metal microstructures in nearly all metallographic sections examined.

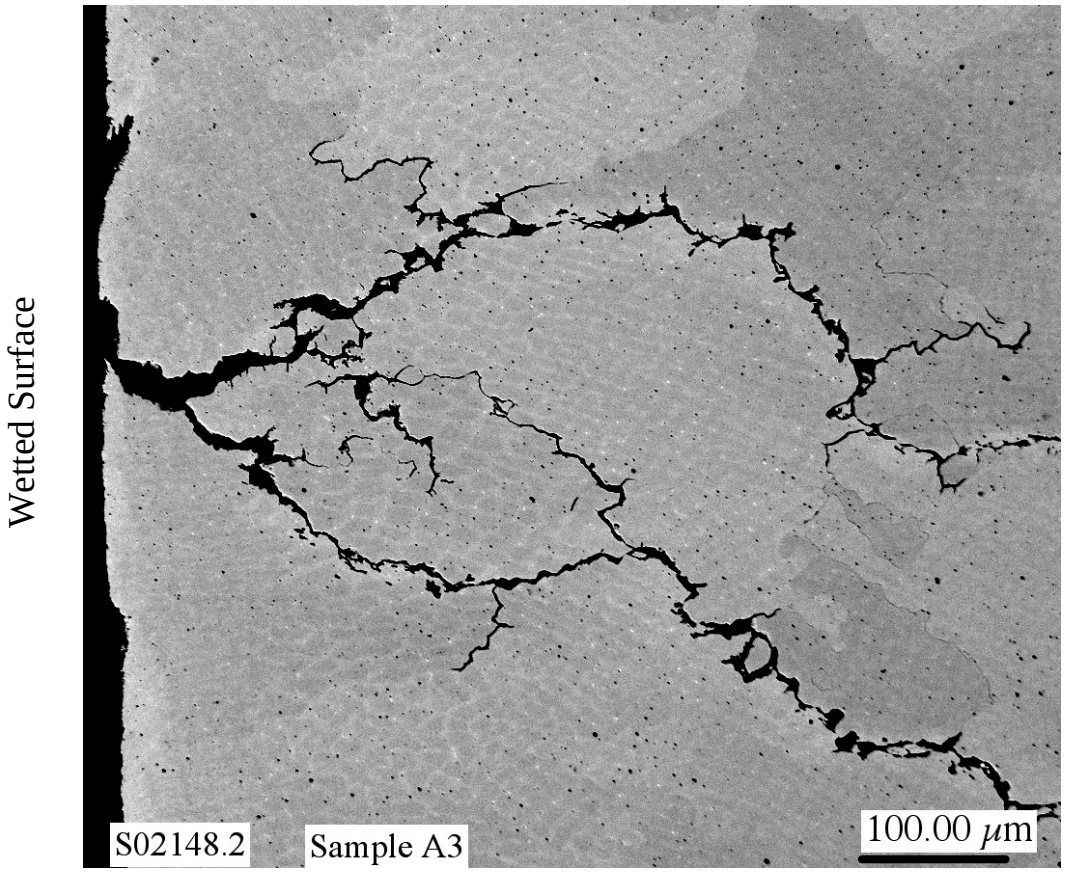

Figure 6.28. Location Where Crack Intersects the PWR Primary-Water Surface in Sample A3 and May Be Near the Initiation Site. Microstructural contrast within individual grains is due to solidification segregation in the Alloy 182 weld metal.

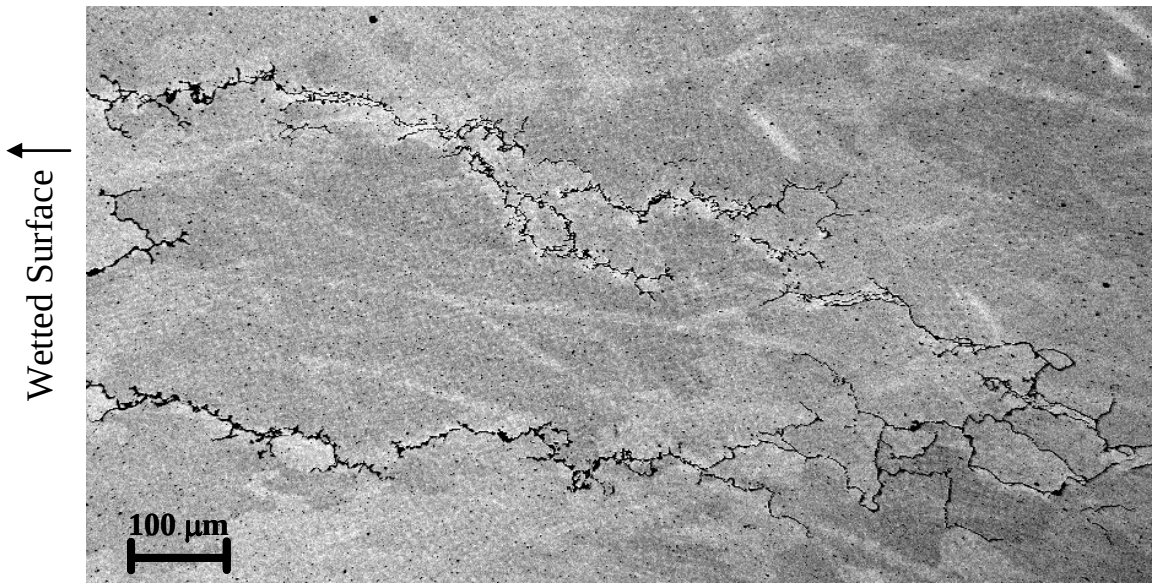

Figure 6.29. Highly Branched Cracks Near Mid-Thickness in Cross-Section Sample A3

After optical and SEM images were recorded on as-polished samples, several samples were given a two-step nital/orthophosphoric etch to highlight weld-metal microstructures. Typical examples are shown in Figure 6.30 for sample A5. The full crack montage in Figure 6.30(a) illustrates that the crack propagates through several different passes of the J-groove weld within the thickness of piece A. In most cases, crack openings appeared to be wider as cracks approached weld pass boundaries (Figure 6.30b). This may reflect the higher stress required to transition to a new set of interdendritic or grain boundaries. Significantly different orientations of the dendritic microstructure can be seen between weld passes. The crack path clearly followed interdendritic or grain boundaries, as documented in Figure 6.30(c). Tight secondary cracks meander along, and end on, the convoluted weld metal boundaries.

6.5.2.2 Metallography of Piece C Cross Sections

The approach for metallographic characterization of the A cross sections was repeated for the C and E cross sections. Cracking was found to extend from the low-alloy steel interface all the way into the Alloy 600 tubing in the C samples, as indicated by the earlier optical examinations (e.g., Figure 6.17) before sectioning. This observation is confirmed in Figures 6.31, 6.32, and 6.33, where crack montages are shown for cross-section slices C1–C4, C5–C7, and C8–C10, respectively. The cracks in sections C1 and C2 end at the low-alloy steel interface with the Alloy 182 butter passes. Scanning electron microscopy micrographs of this region are presented in Figure 6.34, documenting that no propagation occurred into the low-alloy steel. A small pit can be seen, but no significant corrosion of the low-alloy steel.

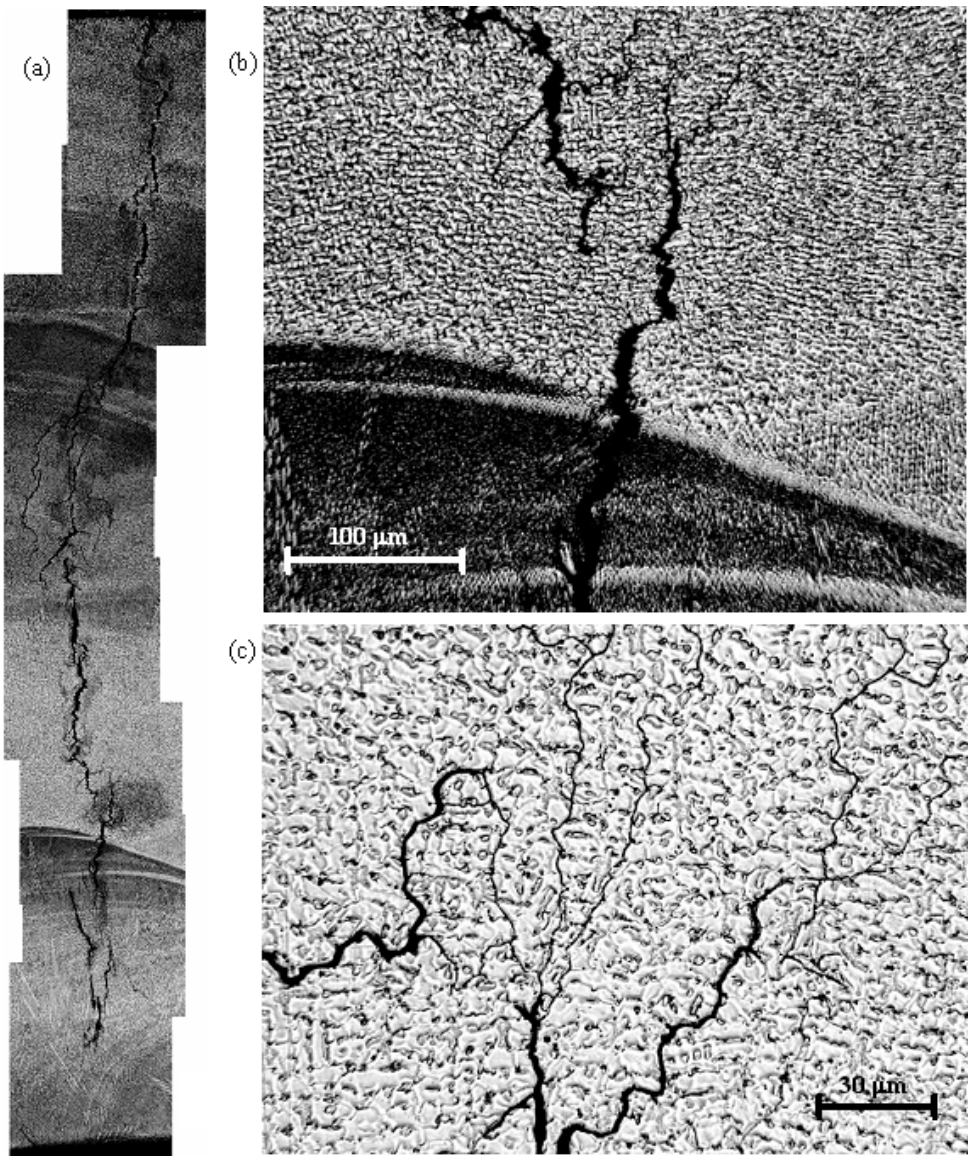

Figure 6.30. Etched Microstructures in A5 Cross-Section Sample: (a) montage showing full length of crack; (b) example of more open crack near/at weld pass interfaces; and (c) example of cracks following convoluted boundaries

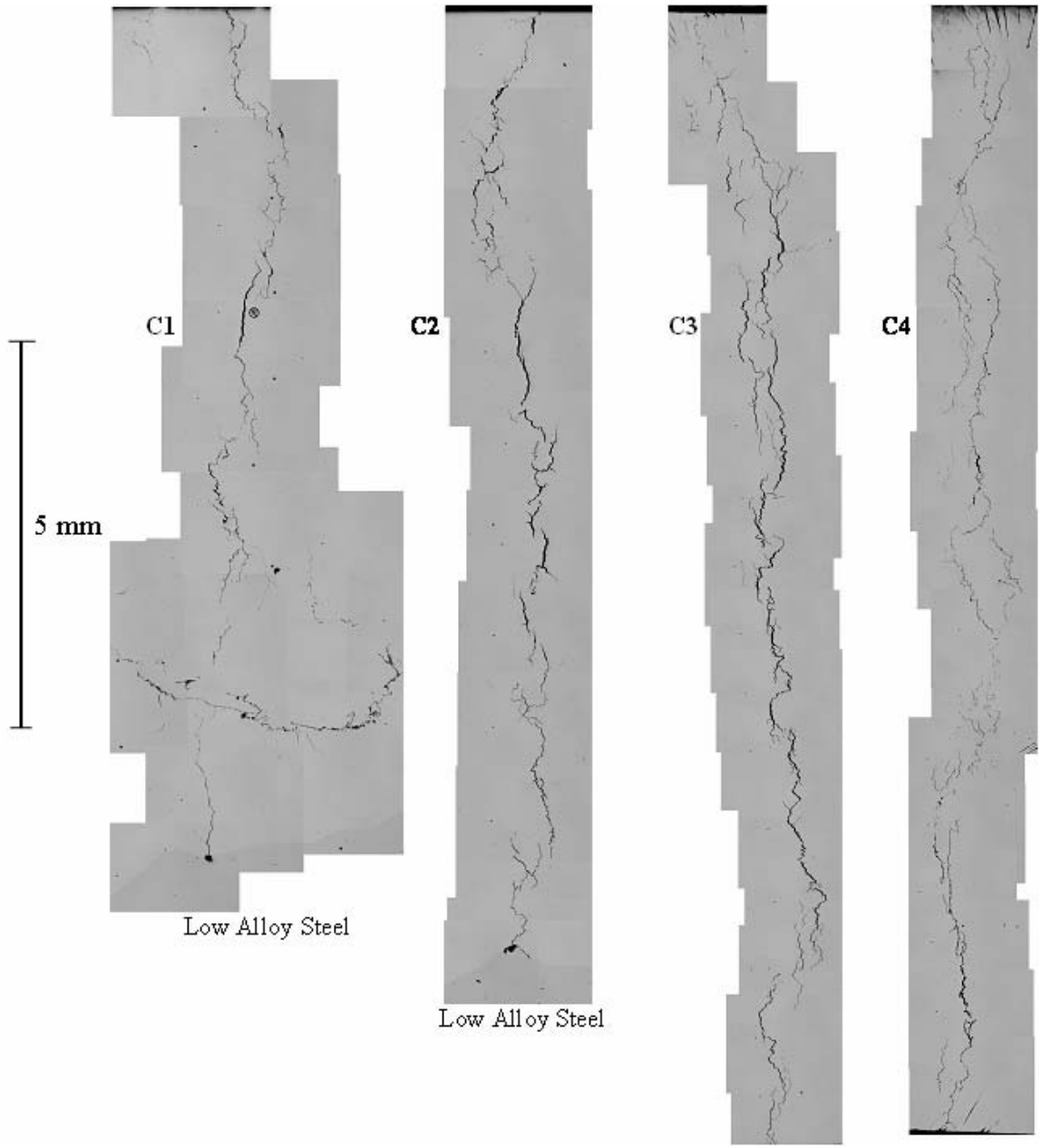

Figure 6.31. C1, C2, C3, and C4 Cross-Section Samples Showing the Main Crack Running to the Low-Alloy Steel Boundary in C1 and C2, While C3 and C4 Show Crack Propagating Through Entire Thickness in Alloy 182 Weld Metal

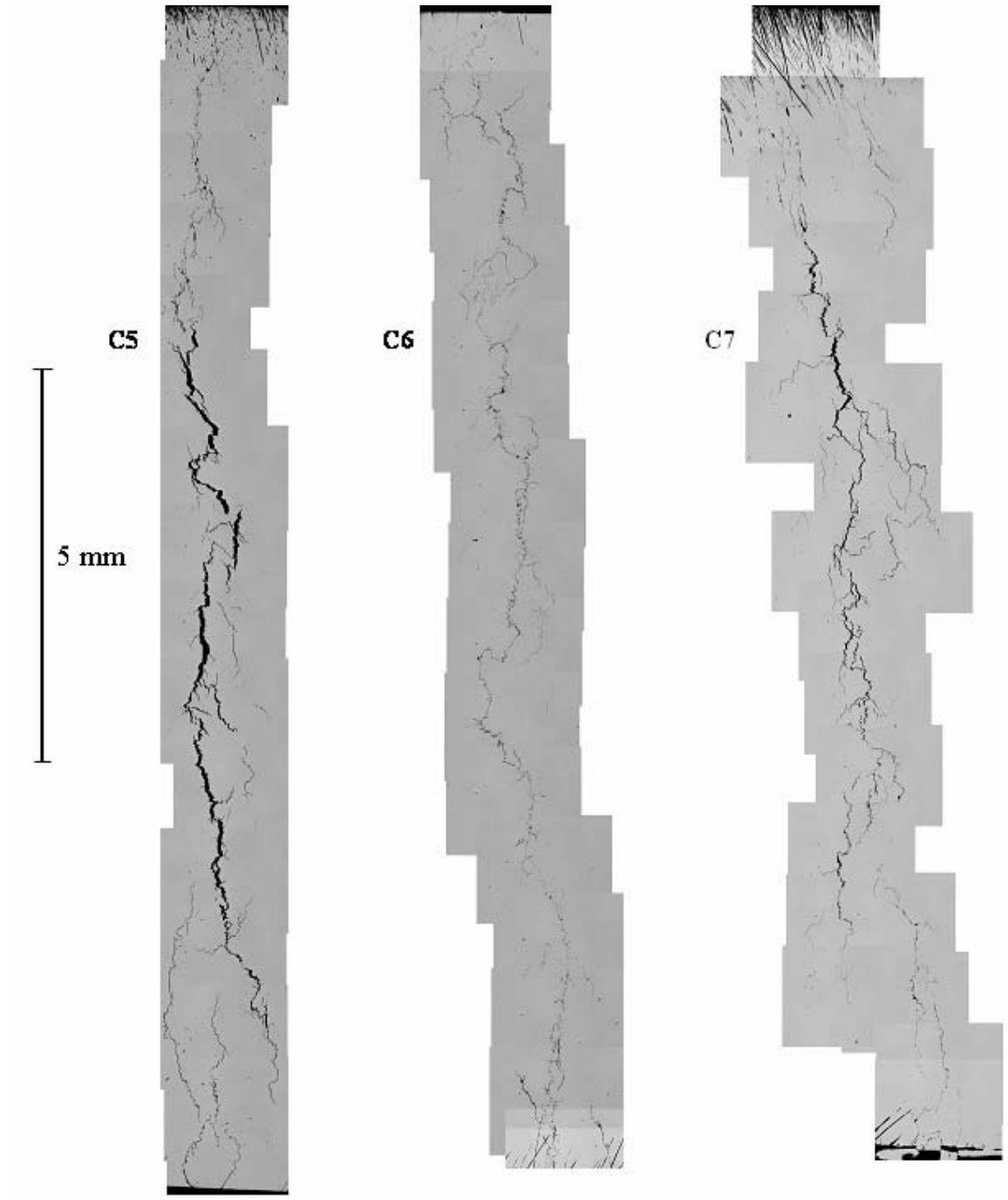

Figure 6.32. C5, C6, and C7 Cross-Section Samples Showing the Main Crack Running Through Entire Thickness for These Locations

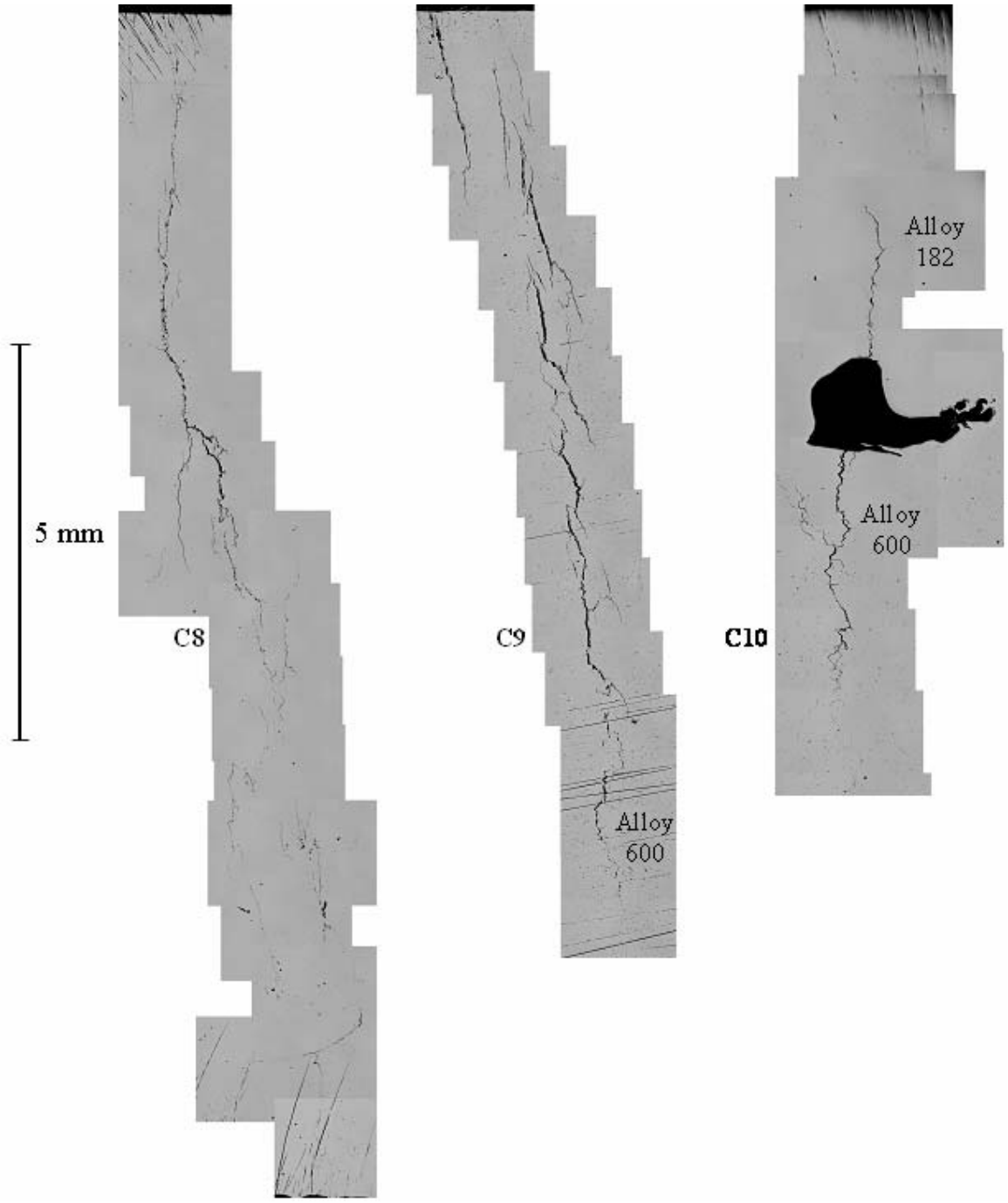

Figure 6.33. C8, C9, and C10 Cross-Section Samples Showing the Main Crack Running Through the Alloy 182 J-Groove Weld into the Alloy 600 Tube. The large hole in the C10 cross section appears to be a weld defect at the alloy fusion line between the Alloy 600 tube and the Alloy 182 weld metal.

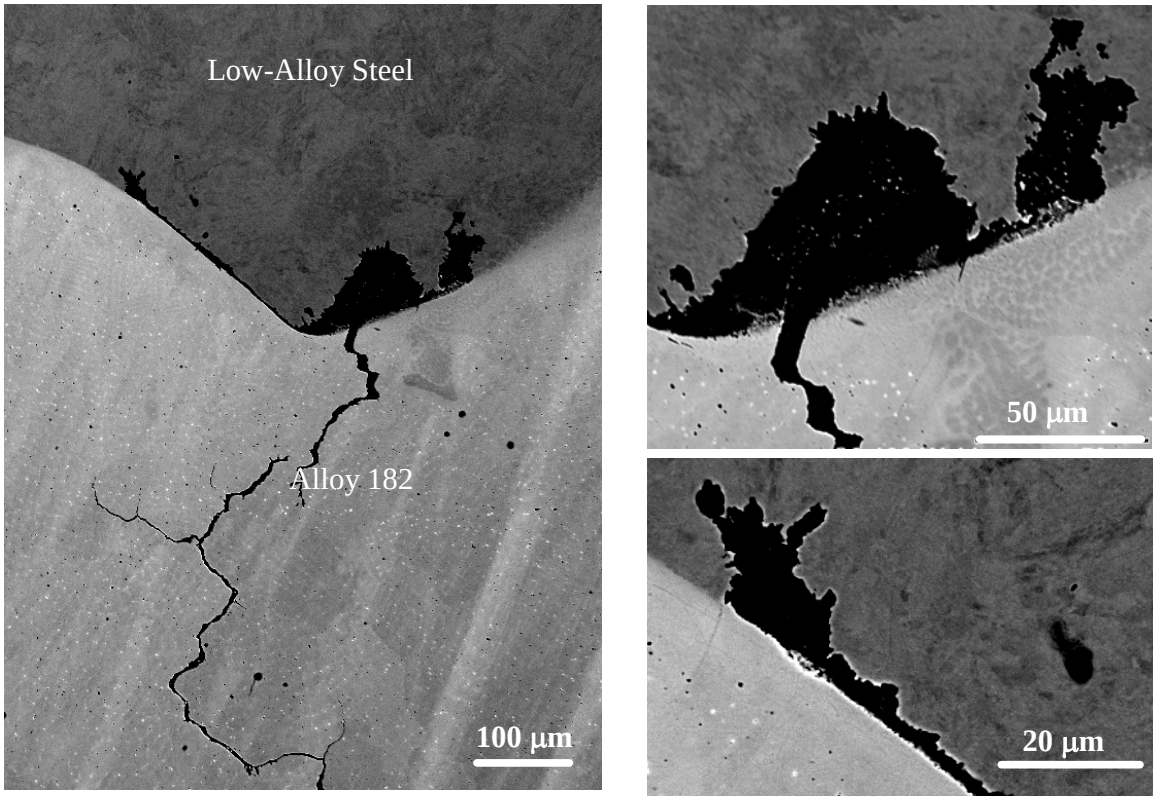

Figure 6.34. Stress Corrosion Crack in Alloy 182 Butter Pass Ending at the Low-Alloy Steel Interface and Creating Small Corrosion Pits

Similar to the microstructures documented for cross-section A5 (Figure 6.30), section C5 also was given an electrolytic etch using nital and orthophosphoric solutions. Although the exposure produced a heavy etch in places, the general microstructural features and the crack path could be recorded as illustrated in Figure 6.35. Once again, the SCC morphology is clearly interdendritic or intergranular following the convoluted boundaries in the Alloy 182 weld metal. Consistent with A5, wider crack openings were typically seen at the weld pass interfaces, with cracks often turning along the interface to find better-oriented boundaries for continued propagation. An example of this behavior is shown in Figures 6.35(b) and (c).

6.5.2.3 Metallography of Piece E Cross Sections

The final sequence of metallographic cross sections for piece E is given in Figure 6.36. This piece is split between the Alloy 182 butter passes and low-alloy steel plate. As a result, cracks are seen in only cross-sections E4 to E8 and propagate in only the Alloy 182 part of the way through the thickness before intersecting the low-alloy steel. Because the adjacent Alloy 600 tube was removed during initial cutting, E8 was the last slice that could be examined. The next sequential observation of the crack is from the exit surface into the interference-fit gap shown in Figure 6.23.

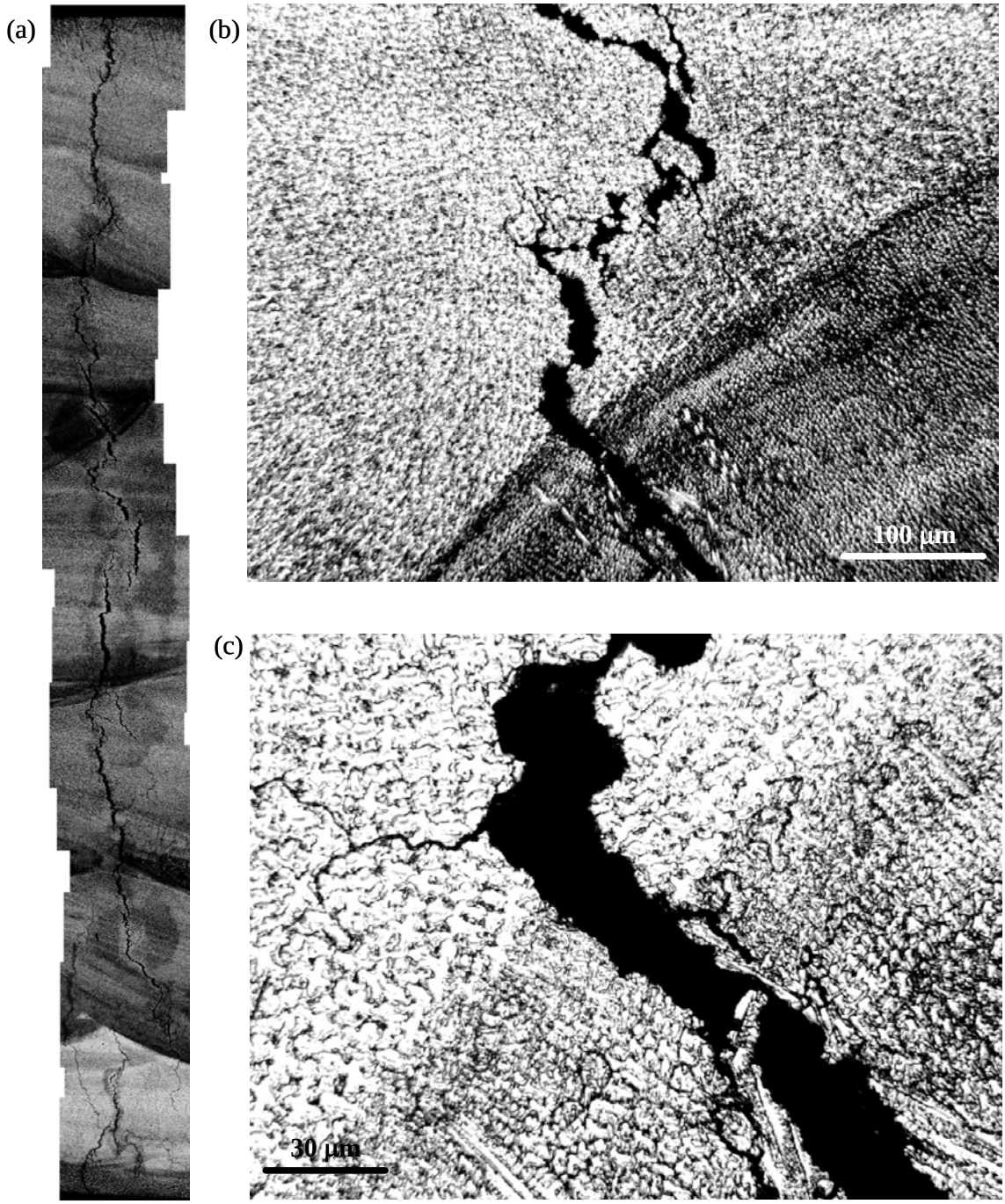

Figure 6.35. Etched C5 Cross-Section Showing Crack Propagating Through Many Alloy 182 Weld Passes

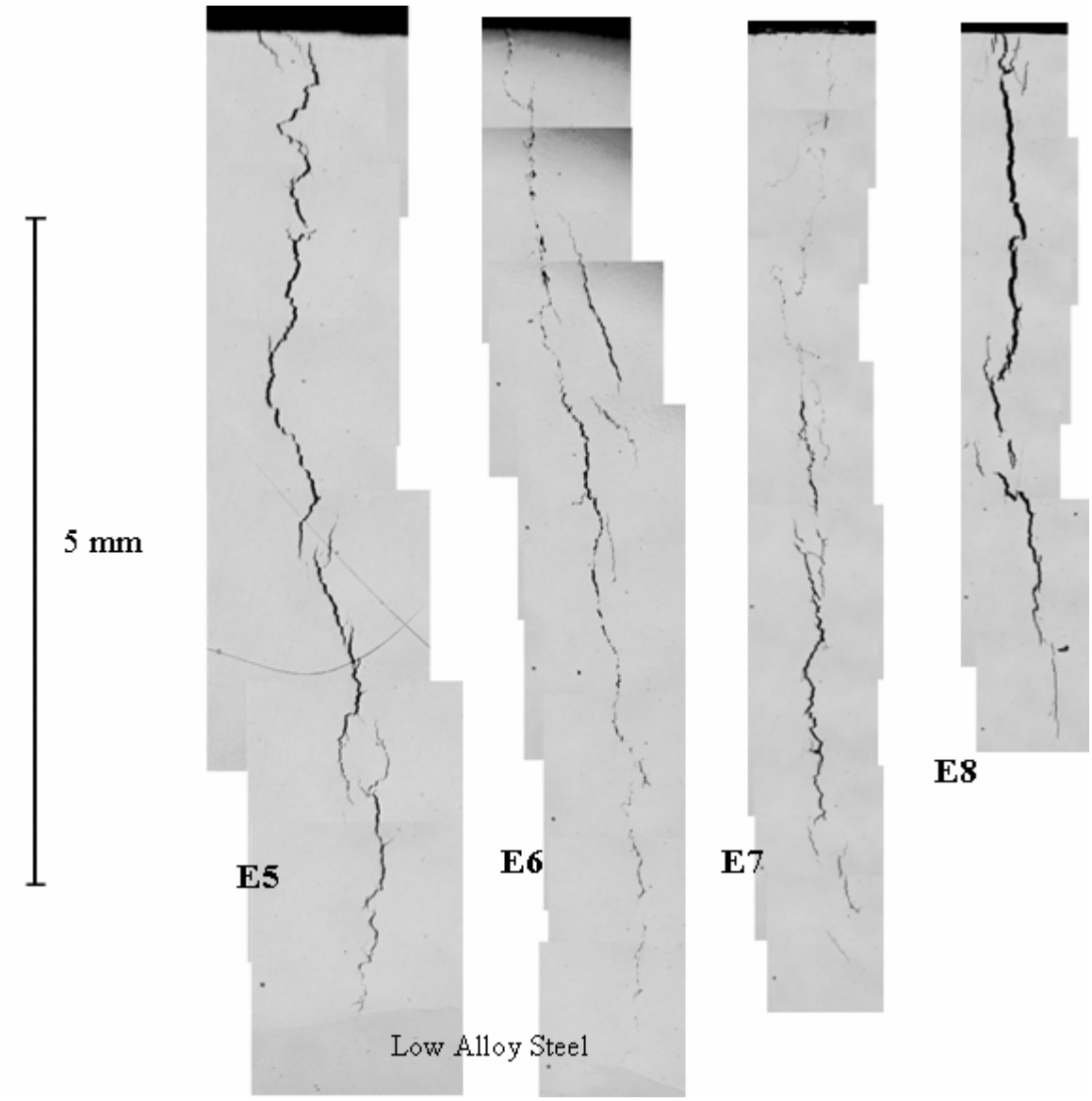

Figure 6.36. E5, E6, E7, and E8 Cross-Section Samples Showing the Main Crack Running to the Low-Alloy Steel Boundary. Only a very small crack was seen in sample E4, and E8 was the closest slice to the gap surface.

6.6 Destructive Evaluation Summary

The cutting of Nozzle 31 Section 2 revealed the through-weld crack to start at 155 degrees on the wetted surface at the weld-buttering interface and end at 135 degrees above the triple point. Cutting this section also revealed two nearby cracks that had penetrated 8 mm into the material.

The metallographic characterization of the serial sections in pieces A, C, and E has effectively mapped the cracks from the their initiation in Alloy 182 weld metal on the PWR primary water surface to their end, either when intersecting with low-alloy steel, entering the Alloy 600 CRDM penetration tube,

or exiting at the interference-fit gap above the J-groove weld. Cracking in Alloy 182 weld metal is interdendritic or intergranular and clearly has propagated due to stress corrosion cracking. No evidence for hot cracking in the weld was observed. Initiation appears to result from SCC near the fusion line between the butter passes and the J-groove weld. Surface damage and defects in the near-surface region may have promoted crack nucleation, but additional examinations will be needed to determine this.

The main crack is observed at a length of ~6 mm on the PWR primary water surface and expands to a lateral length of ~20 mm across the Alloy 182 weld metal within a few millimeters below the surface. At this depth, the crack already has reached the low-alloy steel plate material on one side and remains in the Alloy 182 J-groove weld on the other. Continued SCC propagation of the main crack extended its lateral length to ~25 mm at a depth of ~10 mm, and it eventually reached the Alloy 600 CRDM penetration tube at a depth of ~17 mm in piece C. Limited SCC crack growth (few millimeters) into the Alloy 600 material from the alloy 182 is observed on two C cross-section samples. The extension of the main crack below the PWR primary-water surface finally ends in piece E when it again intersects the low-alloy steel plate at a depth of >30 mm and exits along the interference-fit gap on the side face. The main crack path length from the PWR primary-water surface initiation site to the gap-exit surface is estimated at ~25 mm. Based on laboratory tests in simulated PWR primary water, typical crack-growth rates can range from $\sim 3\times10^{-8}$ to $\sim 3\times10^{-7}$ mm/s for as-welded Alloy 182 at 290 to 320°C. This results in an estimated time of ~2.5 to 25 years for the crack to propagate through-wall after initiation. Because crack initiation normally accounts for some important fraction of life, and through-wall cracking occurred at some time before its full 20-year life, the SCC crack-growth rate experienced in service was probably closer to the high end for measured propagation rates in the laboratory.

The interdendritic and intergranular SCC is highly branched, with tight secondary cracks along connected boundaries typically within a few hundred micrometers of the main crack. Many of these cracks appear to follow orientations nearly perpendicular to the main crack path, suggesting active propagation at somewhat low stresses. In addition to the main SCC crack through all three pieces, a second crack was observed in piece A at a distance of ~5 mm from the main crack. Surface examination and the cross-section samples indicated that this second crack also initiated at the PWR primary-water surface and propagated to a depth of ~10 mm within piece A. Macroscopic examinations suggested that this crack propagated into the adjacent piece B.

An overall image of the rendering that includes pieces A, C, and E is shown in Figure 6.37. One face of the weld section has been left out to allow viewing of the sections. As noted from the metallographic examinations, the crack rapidly expands from the initiation location on the PWR primary-water surface and spreads across the Alloy 182 weld metal reaching the low-alloy steel and Alloy 600. The green line indicates the boundary of the crack in the Alloy 182 weld metal, while the blue line indicates the crack boundary where it arrested at the low-alloy steel interface. Red lines along the crack boundary indicate the points where the crack reaches the Alloy 600 interface and the interference gap (not shown) above the J-groove weld.

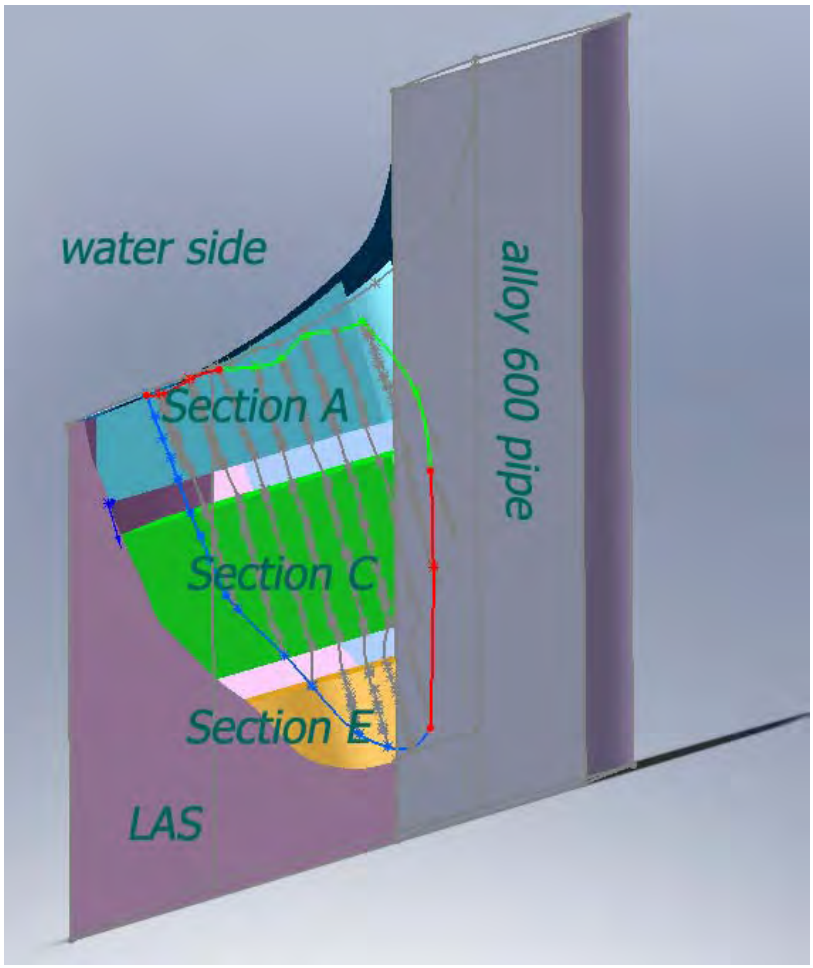

Figure 6.37. Rendering of the Crack Within a Section of the Component Showing the Locations of Sections A, C, and E

Now that the basic framework has been created, much more detail can be built into this rendering to better elucidate the crack morphology through the weldment. Even at this stage, rotating the constructed image allows insights into the through-thickness crack path. For example, a nearly edge-on view of the crack is shown in Figure 6.38. Here it can be seen that the crack meanders during propagation through the weld material, possibly following the residual stress pattern. However, the path is relatively straight overall compared to component dimensions. In a more tilted orientation as shown in Figure 6.39, the small amount of propagation of the crack into the Alloy 600 pipe is more evident. Additional work on this rendering approach and this particular crack example will greatly improve specifics documenting the crack path.

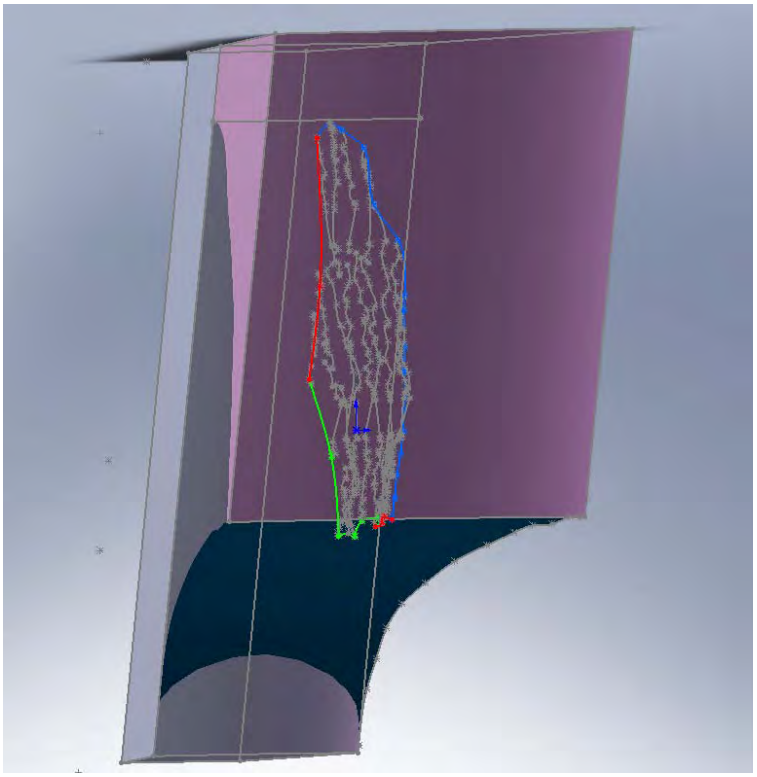

Figure 6.38. Crack Viewed from a Nearly Edge-On Orientation

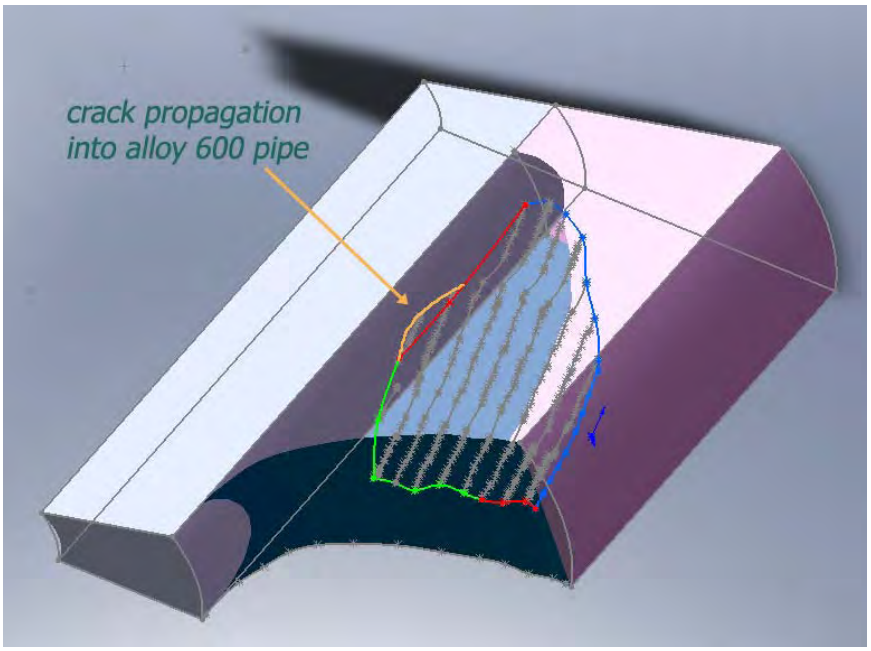

Figure 6.39. Component Section Viewed from a Tilted Orientation Where the Propagation of the Crack into the Alloy 600 Pipe Can Be Seen

7.0 Discussion

The nondestructive and destructive examination results come together to explain why the different NDE techniques worked or did not work, and suggest ways to optimize future inspections of CRDMs and similar product forms. This section describes the NDE responses to the through-weld crack, the physical characteristics that caused these responses, or lack of responses.

7.1 Important Characteristics of the Through-Weld Crack

While many aspects of the through-weld crack were handled in Section 6, this section describes the crack characteristics specifically as they relate to the NDE techniques used to examine the CRDMs. There are three regions with different impacts to NDE detection—the appearance of the crack on the wetted surface, the crack characteristics for the first3 mm, and the profile of the crack as it progresses through the weld. This section focuses on the through-weld crack at 155 degrees.

7.1.1 Crack Surface Characteristics

Scanning electronic microscopy of the wetted surface shows that the crack has a bent and discontinuous profile. Many separate and very tight cracks were found on the weld surface. A 4-mm long (1.6-in.), 20–30 µm (0.0008–0.0012 in.) COD discontinuous crack segment begins at the weld/butter boundary and extends at an angle into the buttering. A tail 2 mm (0.08 in.) long and very tight (too tight for the SEM to measure in many places) extends further into the buttering toward the stainless steel cladding. These features are shown in Figure 7.1. One important feature of the crack at the surface is its discontinuous nature. Even along the 4-mm-long main segment, there are several ligaments of metal crossing the crack. A section of the crack with several connecting ligaments is shown in Figure 7.2.

7.1.2 The First Three Millimeters

As described in Section 6, the crack segments were polished and examined using SEM. The crack has a branching and discontinuous morphology in the through-weld orientation. Images of the crack and a color-coded image showing the various crack segments are shown in Figure 7.3. The first three millimeters show nine separate segments with ligaments between them. All the segments are part of the same crack, but they connect with each other outside the plane shown in the slice.

Also of interest is a detailed look at the crack COD at various points along the crack. Figure 7.4 shows the first 1.5 mm (0.06 in.) of the through-wall crack. Looking close to the surface, one finds several closed points very close to the surface of the crack. While the crack COD is 20–30 µm (0.0008–0.0012 in.), the crack is much tighter—less than a tenth of a millimeter into the weld.

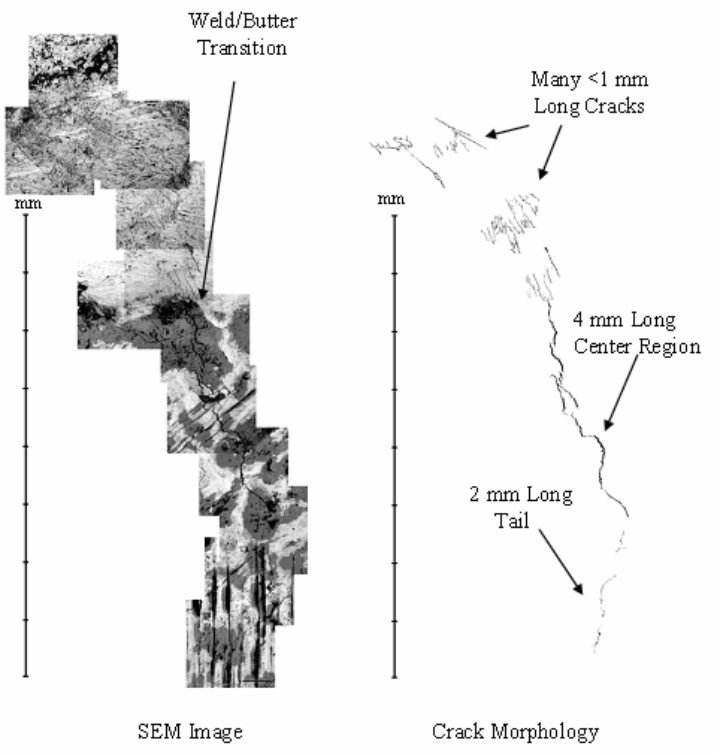

Figure 7.1. Crack Image and Crack Morphology

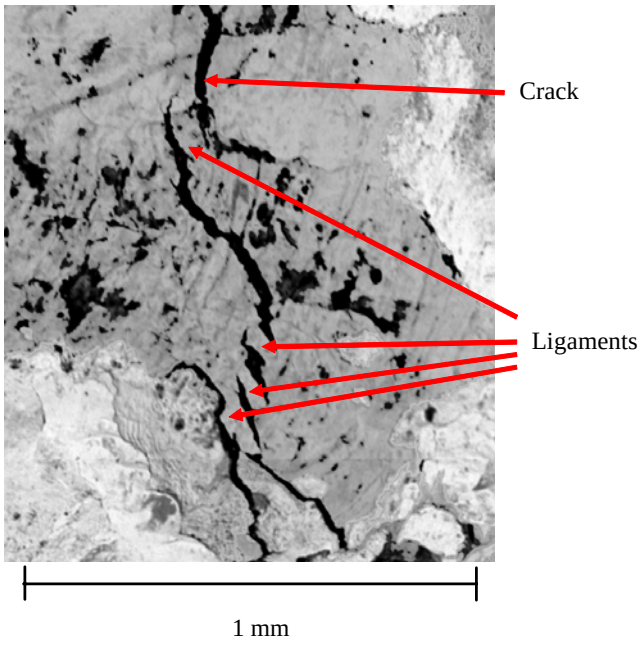

Figure 7.2. Expanded Section of the Crack Showing Ligaments Bridging the Two Sides of the Crack

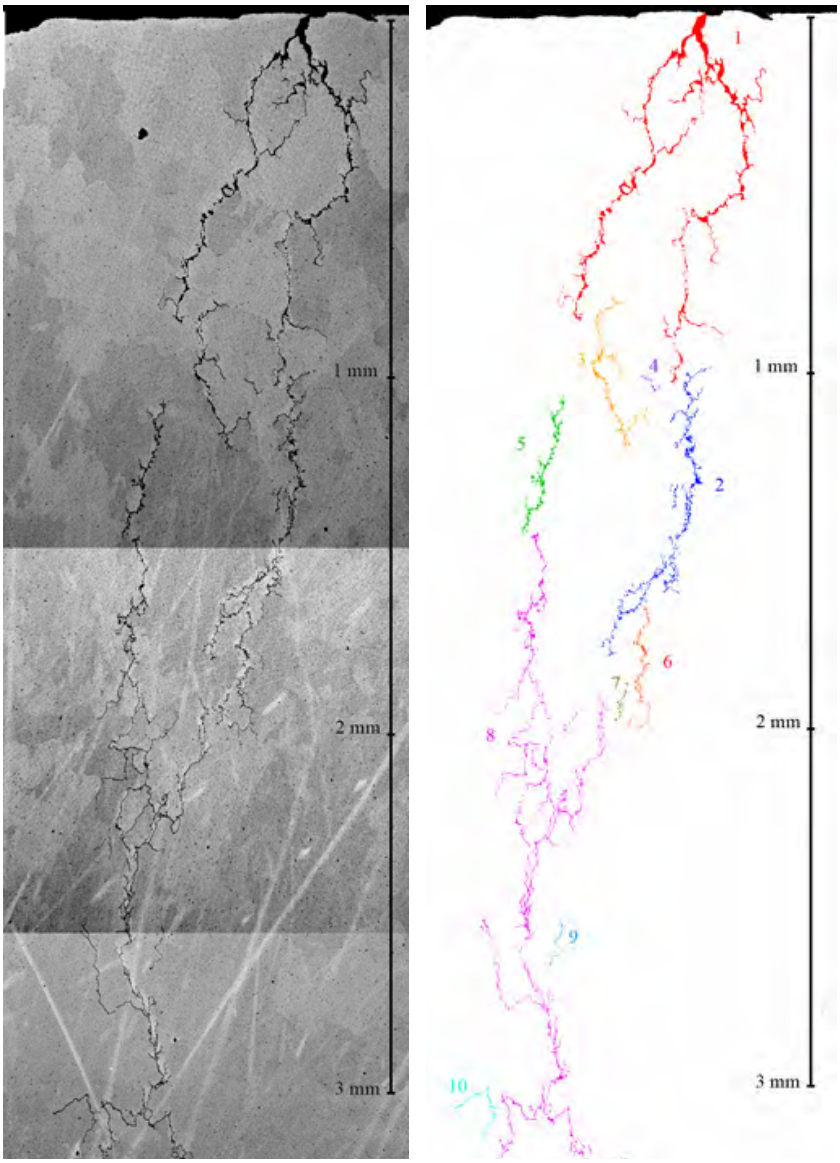

Figure 7.3. Crack Segments. SEM image (left) and color-coded image (right).

Location	COD (μm)
1	10
2	29
3	6
4	2
5	6
6	6
7	2
8	Closed
9	Closed
10	4
11	2
12	9
13	7
14	3
15	2

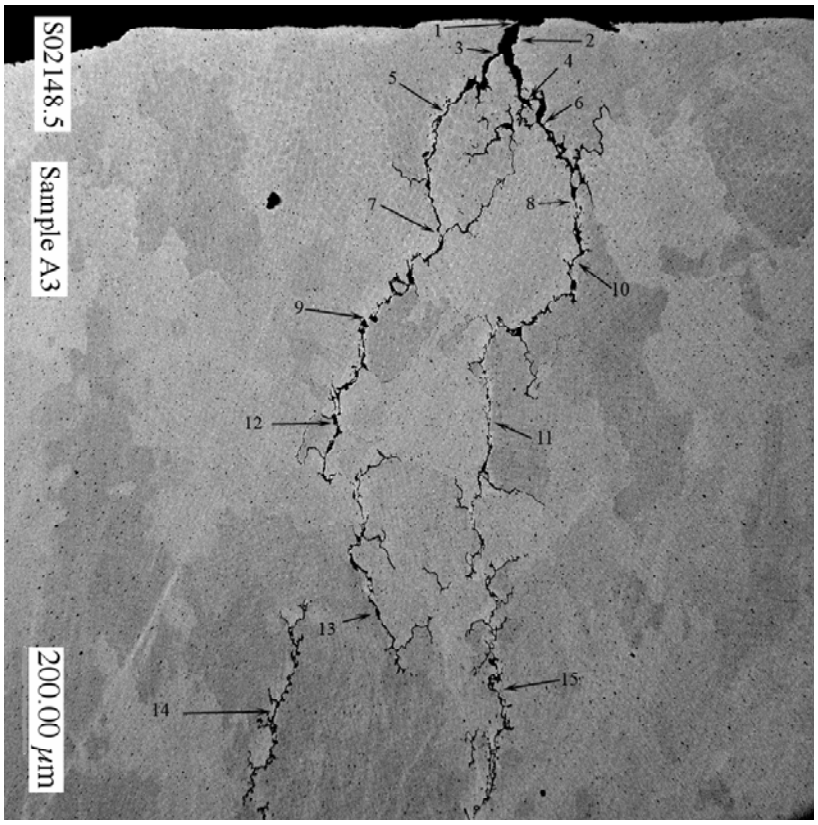

Figure 7.4. Crack CODs at Several Points Close to the Surface

7.1.3 Extent and Exit Point

The crack grew perpendicular to the wetted surface through the weld. The crack begins at 155 degrees on the wetted surface and exits into the annulus at 135 degrees. The crack is oriented axially almost directly, with only a 15-degree shift from a line perpendicular to penetration tube at the cut (8 mm-[0.30 in.-)] deep) and directly perpendicular to the penetration tube at the triple point. Although the crack looks very branched and spread out in the SEM images, it is less than a millimeter across along its length. For any technique looking through the penetration tube, the crack presents a knife's edge to the tube.

The exit into the annulus happens along almost the entire length of the buttering, from above the triple point to the carbon steel. The crack exit into the annulus is 15 μm (0.0006 in.) at its widest point.

7.2 Effects of Crack Morphology on Nondestructive Examination Responses

A re-evaluation of the NDE responses in the context of the known location and morphology of the through-weld flaw is very illuminating. Knowing the location and morphology of a leaking crack essentially "unblinds" the NDE results and allows for a clear discussion of the strengths and weaknesses of each technique.

7.2.1 Time of Flight Diffraction

Time-of-flight diffraction examination was not performed on the J-groove weld, and this work obtained no DE-verified data on the use of TOFD to detect and characterize PWSCC. The TOFD technique could be useful to detect and size PWSCC in the J-groove weld if some development work were done to perform TOFD on this area. The largest barriers to using TOFD on the J-groove weld are the surface conditions, the difficulty of projecting ultrasound through the weld metal, and the geometry around the weld. Significant development work needs to be done before TOFD is usable on the J-groove weld, but it would provide a volumetric verification for ET.

7.2.2 Zero-Degree Ultrasonic Testing

The ultrasonic inspection of the J-groove weld yielded no discernable signal from the through-weld crack. The UT data for the region around 135–155 degrees does show some likely fabrication flaws similar to the fabrication flaws found in the DE, such as in slice C10 Figure 6.33. This lack of signal from the crack is interesting, as the crack is directly against the penetration tube for most of its length. The UT calibrations and the imaging of fabrication flaws in Nozzles 31 and 59 show that the UT can image small defects at the same depth into the weld metal. Even knowing exactly where to look, using the most sensitive frequency at the correct depth (5 MHz) and using high gain, it is not possible to find any significant crack signal. Figure 7.5 shows the 5-MHz results in the cracked area of the J-groove weld. The crack is in an unfavorable orientation, essentially presenting a knife's edge to the beam, which likely accounts for the lack of signal. It was known that the UT inspections would be less sensitive to an axially oriented flaw, and this has been confirmed by these inspections. Performing a UT inspection through the J-groove weld would need to use different angles to be sensitive to the axial cracks present in the weld.

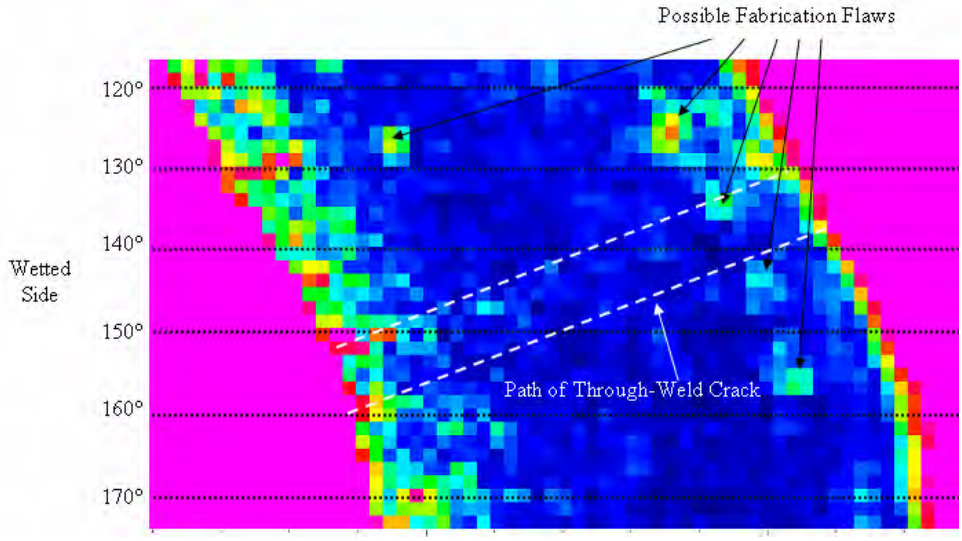

Figure 7.5. 5-MHz Ultrasonic Testing Data for the Cracked Region of the Nozzle 31 J-Groove Weld Metal

7.2.3 Visual Testing via Replication

The results from the visual testing using a replicate as a primary crack detection technique were somewhat disappointing. The replicant material did a very good job of capturing surface features, and the replica imprint also likely includes the cracks. The largest problem that we encountered was our limited ability to discern scratches and innocuous features from cracks. Finding the very tight cracks is complicated by the presence of many larger features. This work used a high-resolution digital camera to investigate the replica, and it is possible that the use of SEM would improve the ability to discriminate between cracks and other features. Using the camera and careful examination of the images found none of the actual cracks, and all indications found using this technique were confirmed as scratches or weld irregularities by ET, PT, and bare-metal VT.

The replicate testing was very useful in following up the ET examinations of the penetration tube in Nozzle 59. The replicate allowed us an alternative examination technique to determine what had caused the ET responses in the tube.

Replicate testing does allow one to examine areas that are otherwise difficult or impossible to examine using conventional VT. We were unable to put the CRDM under a microscope or photograph some areas where the penetration tube interfered with the camera. Also, the replicate did not have the mottled dark-and-bright appearance of the actual piece, making inspection of the replicate somewhat easier than the inspection of the oxidized J-groove weld. With practice and the use of microscopes, replicate techniques could be useful in crack detections, although when using a microscope the inspections will certainly be time-consuming.

One factor that made the replicate testing difficult was that the J-groove weld surface was in the as-welded condition. The lines between the weld passes and the borders of weld beads made many distracting linear indications that may confuse the inspector and camouflage cracks.

7.2.4 Penetrant Testing

The PT performed on the J-groove weld of Nozzle 31 yielded interesting and complex results. The PT results showed conclusively that some cracks were present in the weld, where they were, and that many of the indications found using VT to test the replicate were not cracks. The PT results helped to guide the bare-metal VT testing. Also, the PT result for the crack at 210 degrees was used to set the lower voltage response level used to interpret the ET testing results.

The PT testing did not, however, yield any signal at the site of the through-weld crack. There were three reasonably deep (>8-mm) cracks centered around 150 degrees, yet none of them was detected using PT. This suggests that even very deep PWSCC can be missed by high-sensitivity PT testing. A higher-quality inspection surface may help improve the reliability of the penetrant inspection.

7.2.5 Bare-Metal Visual Testing

The visual testing was not very reliable because the cracks were very tight and the surface of the J-groove weld was mottled and uneven. The region near 0 degrees was difficult to inspect at an optimal angle until the penetration tube was removed, which is not a viable option for ISI. The bare metal visual

was able to confirm the cracks at 200 and 225 degrees, but it was not able to find the through-weld crack at 155 degrees. The cracking near 155 degrees was difficult to image, even in an optical microscope, and images usable for COD determination were really obtainable only using a scanning electron microscope. These results suggest that visual testing in the field would be very difficult and that the detection of tight cracks on an as-welded surface is unlikely to be reliable.

High-magnification optical images of the surface near the crack show that the black oxide and surface features make it difficult to detect the crack with visual techniques. One would expect that a 25-μ-wide crack would be easily visible on a good surface, but the color changes and difficult surface morphology (small dents and apparent grinding marks) effectively mask the crack to direct visual inspection. These surface features also make it difficult to find the crack using replicant techniques such as the Microset replicant. An image of the surface containing the crack is shown in Figure 7.6.

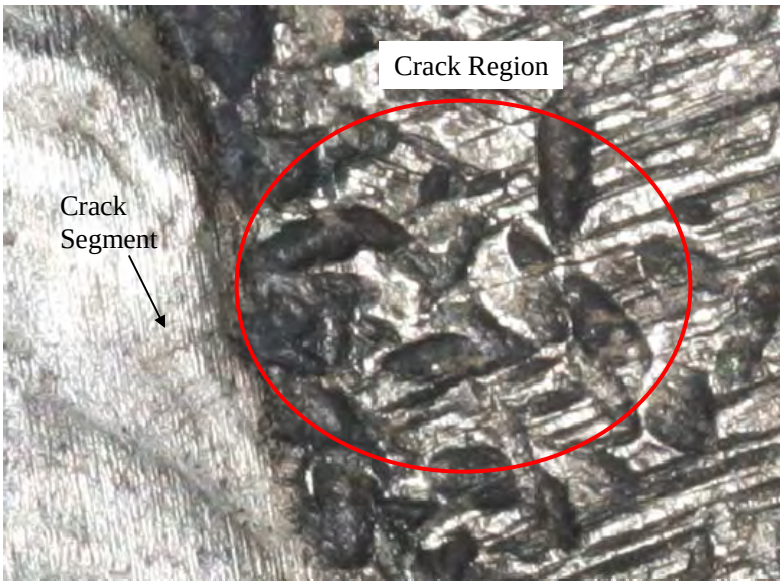

Figure 7.6. Cracked Region with Poor Crack Detection Because of Surface Features and Oxides

It is possible that the reliability of bare metal visual testing would be improved by having a higher-quality inspection surface. The unground as-welded condition was difficult to inspect and provided a large number of distracting indications that can help camouflage a crack.

7.2.6 Eddy Current Testing

ET was the one technique that was able to detect the through-weld crack in the J-groove weld of Nozzle 31, as well as all of the cracks detected using PT and VT. The ET scan of the J-groove weld helped to pinpoint several crack-like indications for further investigation. The ET on the J-groove weld of Nozzle 31 was the most sensitive examination used and yielded the most reliable results.

One interesting result is that the ET response to the through-weld crack (3.1 V) was lower than the responses for some of the shallower cracks (4.1–4.6 V). The discontinuous, segmented nature of the through-weld crack, both on the surface and along the crack's depth, allows for electrical contact between the two crack faces. This electrical contact is the most likely reason for this lower response. This segmented nature reduced the signal by approximately 1–1.5 V, or 25% to 38% of the ET response.

The only drawback of the ET scans was that differential ET used to examine the weld is not able to measure the depth of an indication to detect much of the subsurface extent of the flaw. The differential probes are sensitive to only the first 3 mm and missed the much longer parts of the cracks that were below the surface. The ET scans using the differential probe provided the locations of the crack, but were not able to identify which of the flaws was the leakage path. The determination of which flaw was the through-weld flaw relied on cutting above the triple point with the saw, which is not a feasible ISI technique.

7.3 Integrated Results and Suggestions

Inspecting Alloy 600 and 182 weld metal for PWSCC is a difficult problem because of the complex geometry at the weld, material, the tightness of the cracks, and short length the cracks present at the initiating surface. The three cracks found by DE were all axially oriented, making the volumetric inspections performed through the penetration tube ineffective. The cracks are so tight that VT and PT are of very limited usefulness, as both techniques missed the through-weld flaw.

The only technique that was able to detect the through-weld flaw in the J-groove weld was ET. It would be very helpful to have an additional technique capable of examining the J-groove weld and buttering. If developed, a radially oriented TOFD capable of characterizing axially oriented flaws would possibly be able to verify and depth-size PWSCC in the weld region.

The characterization of the through-weld flaw showed an interesting and important aspect of PWSCC—that the flaws can be very short on the surface and span the width of the weld within a few millimeters. A very deep crack can appear as a very small indication to surface technique such as VT or PT and near-surface techniques such as ET. Penetrant dye testing indications that may be ignored as weld porosity and short, low-voltage ET indications need to be considered important.

As short, low-voltage ET indications are possibly important, work could to be done to use ET to characterize fabrication flaws and noise levels in CRDM welds to prevent false calls based on innocuous indications. A detailed understanding of ET noise levels and common fabrication flaws would be very useful in examining data collected in the field.

8.0 Conclusions

PNNL found, removed, and destructively characterized a through-weld PWSCC crack in the J-groove weld of North Anna 2 CRDM Nozzle 31. Based on the results of the examination, the following conclusions may be drawn:

- Visual testing via replicant and high-resolution photography was ineffective at finding the cracks, as the cracks were very tight and short, and the surface conditions were not conducive to an accurate visual test. It is possible that the replicate would have produced better results if the replicate had been examined using a scanning electron microscope.

- Bare metal visual testing via high-resolution photography was ineffective at finding most of the cracks, as the geometry prevented a complete inspection, the surface conditions were poor, and the cracks were both very short and very tight. The through-weld crack was not clearly visible on the wetted surface of the J-groove weld even when placed in an optical microscope. Bare-metal VT was useful in characterizing the cracks found at 200 and 225 degrees.

- Volumetric inspection of the J-groove weld using zero-degree ultrasound of frequencies ranging from 5 MHz to 500 kHz found many fabrication flaws but was not able to detect the through-weld crack, as the crack was axially oriented and presented almost no surface area to the ultrasonic beam.

- Penetrant testing was ineffective at finding the through-weld crack because the crack was too tight to allow the penetrant dye into the crack in sufficient amounts to produce a visible indication. Penetrant testing was useful in finding other cracks and in following up the visual testing via replicate.

- Eddy current testing was able to detect the through-weld crack, all cracks detected using PT and verified with VT, and others that were detectable only with ET. Eddy current testing was the most useful technique for finding PWSCC on the J-groove weld and showed much higher sensitivity than any of the other techniques.

- It would be very useful for a volumetric technique, such as TOFD, to be developed and deployed on the J-groove weld to verify ET results, as currently only ET provides good sensitivity for inspecting the J-groove weld metal and ET is incapable of depth-sizing flaws.

- A detailed characterization of ET noise levels and ET responses to fabrication flaws in J-groove welds would be helpful in discriminating between the possibly small and low-voltage, service-induced PWSCC and innocuous indications.

9.0 References

Buisine D, F Cattant, J Champredonde, C Pichon, C Benhamou, A Gelpi and M Vaindirlis. 1993. "Stress Corrosion Cracking in the Vessel Closure Head Penetrations of French PWRs." *Sixth International Symposium on Environmental Degradation of Materials in Nuclear Power Systems – Water Reactors*. August 15, 1993. San Diego, California.

Champigny F, C Pages and C Amzallag. 2002. "Vessel Head Penetrations: French Approaches for Maintenance in the PLIM Program." *International Symposium on Nuclear Power Plant Life Management*, IAEA-CN-92/37, November 4–8, 2002, Budapest, Hungary.

Doctor SR, GJ Schuster and MT Anderson. 2004. "Primary Water Stress Corrosion Crack Morphology and Nondestructive Evaluation Reliability." *4th International Conference on NDE in Relation to Structural Integrity for Nuclear and Pressurised Components*. PNNL-SA-43451. December 6–8, 2004. London, United Kingdom.

Ekstrom P and J Wale. 1995. *Crack Characterization for In-service Inspection Planning*. SKI Report 95:70. Swedish Nuclear Power Inspectorate, Stockholm, Sweden.

Embring G and EB Pers-Anderson. 1994. "Investigation of a Weld Defect, Reactor Vessel Head Ringhals " *International Symposium on the Contribution of Materials Investigation to the Resolution of Problems in Pressurized Water Reactors*. September 12–16, 1994. Fontevraud, France.

Faidy C, C Pichon, S Bhandaris and J Vagner. 1994. "Stress Corrosion Cracking in French PWR CRDM Penetrations." *SISSI 94: International Symposium on Structural Integrity*. April 28–29, 1994. Saclay, France.

Lang TA. 2003. "Significant Corrosion of the Davis-Besse Nuclear Reactor Pressure Vessel Head." *ASME Pressure Vessels and Piping Conference*. July 20–24, 2003. Cleveland, Ohio.

MacDonald DE. 1985. *IGSCC Detection in BWR Piping Using the MINAC*. EPRI-NP-3828, Electric Power Research Institute, Palo Alto, California.